DOI:10.15774/PPKE.ITK.2012.004

NEUROMORPHIC MODELING OF REACHING ARM MOVEMENTS

Ph.D. dissertation

Róbert Tibold

Supervisor:
József Laczkó Ph.D.

Péter Pázmány Catholic University
Faculty of Information Technology
Multidisciplinary Technical Sciences Doctoral School

Budapest 2011

DOI:10.15774/PPKE.ITK.2012.004

Any Sufficiently Advanced Technology
Is Indistinguishable From Magic.

By Arthur C. Clarke

“A hatékonyan működő modern technológiát
Nem lehet megkülönböztetni a varázslattól.”

DOI:10.15774/PPKE.ITK.2012.004

Acknowledgments

First and foremost I would like to thank my supervisor and scientific adviser *József Laczkó* for his consistent support, for sharing his concerns and suggestions related to my studies and scientific work. I would also like to express my gratitude to the head of the doctoral school *Prof. Péter Szolgay* and *Profs. Tamás Roska* and *Nyékyné Dr. Judit Gaizler* for the support and the chance to be the member of the doctoral school. The interdisciplinary environment they provided proved to be truly important in the successful conclusion of my PhD studies. I am also thankful to my collaborators *Gábor Fazekas, Györgyi Stefanik* without whom the biomechanical measurements would have never been done in the National Institute for Medical Rehabilitation. I am also very grateful to the members of the team *Tamás Pilissy, Bence Borbély, Péter Katona* working under the leadership of József Laczkó in the Pázmány and Semmelweis University for their useful advice concerning my work and for the valuable meetings.
I am in the same way grateful to my fellow Ph.D students *Éva Bankó, Ádám Fekete, Richard Fiat, László Füredi, Barnabás Hegyi, Zoltán Kárász, András Kiss, László Laki, Csaba Nemes, Tamás Pilissy, Ákos Tar, Dávid Tisza, Gergely Treplán, József Veres, Béla Weiss* for all their assistance and the time we have spent together. I acknowledge the help of *Lívia Adorján, Judit Tihanyi, Vida Tivadarné Katinka* and the staff of the *Registrar's Office, Dean's Office and the Financial Department.*

Last but not least I am tremendously grateful to my *Parents* and *Grandparents* for all their love and support. Finally I would like to thank my darling *Bogi* for all her love, support and patience during my busy days. Without them I could have never managed to succesfully conclude my studies.

DOI:10.15774/PPKE.ITK.2012.004

NEUROMORPHIC MODELING OF REACHING ARM MOVEMENTS

by Róbert Tibold

Abstract

A dynamic, three-dimensional (3D) musculoskeletal model was developed to simulate complex, slightly restricted (prono-supination was not allowed) point-to-point movements (while holding an object) of the entire upper limb containing the shoulder complex under altering external forces manifested in three objects with distinct masses. The model was constructed considering structural and biomechanical aspects of the arm. The outputs of the model were virtually predicted muscle forces capable to generate the desired joint rotations and joint torques. This new approach (predicting muscle activity using measured kinematics of the limb in the 3D space) is planned to support general rehabilitation of movement disorders through the predictive simulation of muscle forces. Literally, activation patterns can be regarded as templates based on the movement of healthy individuals for people with any motor dysfunction. The effect of altering object masses on joint torque profiles was investigated. Joint torque profiles have been found object-invariant through correlation analysis of joint torques predicted under distinct object conditions. Elbow and shoulder joint torque profiles predicted by the model are invariant to changes of the mass of the object held in the hand. The range but not the shape of the torque-time curve depended on the object in the hand. This may reflect the existence of a general movement pattern.

Variances of hand position (endpoint), joint configuration and muscle activities (measured EMG, muscle force) were calculated to analyze the stability of the studied movement. Ratios of movement variances observed in two conditions (load versus without load) showed no differences for hand position and arm configuration variances. Virtual muscle force variances for all muscles except deltoid posterior and EMG variances for 4 muscles increased significantly by moving with the load. The greatly increased variances in muscle activity did not imply equally high increments in kinematic variances. As a conclusion of the stability analysis the enhanced muscle cooperation helps to stabilize the movement at the kinematic level through synergies when a load is added.

DOI:10.15774/PPKE.ITK.2012.004

TABLE OF CONTENTS

DOI:10.15774/PPKE.ITK.2012.004

LIST OF ABBREVIATIONS

Abbreviation	Concept
2D	2 dimensional
3D	3 dimensional
3DAA	3D angular acceleration
AA	Angulus acromialis
AC	Acromion
AI	Angulus inferior
BI	Biceps
BII	Biceps insertion
BIO	Biceps origin
CNS	Central nervous system
CoM	Center of mass
CRI	Coracobrachialis insertion
CRO	Coracobrachialis origin
DA	Deltoid-anterior
DOF	Degrees of freedom
DP	Deltoid-posterior
EL	Epycondilus lateralis
EMG	Electromyogramm
EP	Endpoint
ES	Electrical stimulation
FES	Functional electrical stimulation
ia	Index of architecture
JC	Joint configuration
MA	Moment arm
MoI	Moment of inertia
NaN	Not a number
NIMR	National Institute for Medical Rehabilitation
PD	Putting-down

DOI:10.15774/PPKE.ITK.2012.004

RMS	Root mean square
RS	Processus styloideus radii
SCI	Spinal cord injury
sEMG	Surface electromyography
SD	standard deviation
TR	Triceps
TRI	Triceps insertion
TRO	Triceps origin
TS	Trigonum spinae
UCM	uncontrolled manifold
usMA	ultrasonic-movement analyzer
UP	lifting
US	Processus styloideus ulnae

DOI:10.15774/PPKE.ITK.2012.004

LIST OF FIGURES

Chapter II

Chapter III

DOI:10.15774/PPKE.ITK.2012.004

Chapter IV

Chapter V

Chapter VI

DOI:10.15774/PPKE.ITK.2012.004

DOI:10.15774/PPKE.ITK.2012.004

Chapter I

INTRODUCTION

I.1. Preface

In everyday running life there are many situations in which people can be injured seriously thus becoming spinal cord injured (SCI) patients or suffer from the symptoms of diseases which effect different movement functions like controlling or executing a given movement. Such movement disorders - without further details - are Parkinson's Disease [1-4] caused by the malfunctioning of the basal ganglia and/or the dopaminerg system; dystonia as a neurological movement disorder where oscillating muscle contractions result in twisting and uncontrolled repetitive movements with abnormal postures [5], [6]; multiple sclerosis in which the nerves of the central nervous system (CNS) (brain and spinal cord) degenerate as a result of inflammation of the nerves [7-10]. Another serious disorder of the brain is the stroke in which the individual rapidly loses some of his brain functions due to disturbance or damage of the blood supply. In many cases of stroke the motor cortex of the brain is highly affected. In such cases the individual cannot move the limb(s) on one side of the body (hemiplegia, hemiparesis). In more serious cases when the brainstem is involved in the stroke the abilities of the patient for sensing and balancing may be reduced or totally lost.

Hence, for current science of motion it would be a great deal to help people overcoming their serious movement dysfunctions whether it is caused by an accident or neural disease.

In SCI patients in both paraplegics (caused by the injury or the illness of the thoracic area of the spinal cord - normal movement functions of the neck, hand and thorax are usually not effected) and tetraplegics (caused by the injury or the disease of the cervical area of the spinal cord – all limbs under the neck are effected) functional electrical stimulation (FES) has been recently used to restore lost motor functions and muscle strength of the leg muscles partially [11-17]. Muscle forces have been studied by the famous Hungarian born nobel laurate biologist Albert Szentgyorgyi, who studied submolecular processes and suggested further study of muscle activities at the level of electrons and electricity [18]. Since then, engineering methods and modeling procedures have been developed

DOI:10.15774/PPKE.ITK.2012.004

and gave us a chance for fine artificial regulation of muscle activities by well designed electrical activity patterns.

FES driven cycling offers paraplegics the possibility of muscle and cardiovascular training as well as the chance for independent locomotion [19]. In the study of Szecsi, three different muscles (gluteus maximus, quadriceps, hamstring) were stimulated on both legs by an 8-channel electrical stimulator applying bipolar electrodes. Based on the measurements of cycling of healthy subjects it was found that at higher gear the muscles spanning the ankle joint had to generate more torque so as to maintain a given cycling speed [11], [20]. Beside SCI patients FES cycling has been applied in patients with multiple sclerosis by Szecsi *et al.*, [21]. In the studies applying FES during cycling muscle activities were generated as a function of the pedal angle [11], [22]. Here, a challenging task was to find the proper timing course of stimulating the knee flexor or extensor muscle at appropriate time instants.

For upper limb movements the Freehand system [23], [24] is an implanted FES device for restoration of lateral and palmar grasps following C5 or C6 tetraplegia. Naito *et al.*, [25] presented an FES method to stimulate the biceps brachii so as to perform supination of the forearm.

However, FES has its own limits. Namely, a number of personalized anthropometric parameters, neural and biomechanical features (muscle geometry, muscle action lines with acting muscle forces) of the particular limb are not taken into account in generating stimulation patterns.

If the results of accurate 3D modeling of the above written features were applied in the generation of activity patterns it might increase the effectiveness of rehabilitation techniques.

No information has been found so far whether FES based on (3D) modeling of the human arm would be applied in general rehabilitation procedures of the whole upper limb containing the shoulder complex.

The usefulness of 3D modeling of different motor tasks in the generation of activation patterns has been revealed by many studies so far [26-36]. Furthermore, a virtual 3D model of the upper limb consisting of 4 segments (the humerus, the ulna, the radius and the hand) and personalized muscle geometries using parameters introduced by Zajac [37]

DOI:10.15774/PPKE.ITK.2012.004

was developed for getting accurate biomechanical analysis of the arm [38]. Dynamic, EMG (electromyogramm) driven methods are used for predicting muscle forces in single and multi joint movements [39] and for estimating the corrective changes in muscle activation patterns needed for a stroke patient to walk [39], [40].
Other 3D biomechanical models are applied during robot assisted rehabilitation to enhance the functionality of therapeutic robot treatment for stroke limb injury [41-43].

Unfortunately current rehabilitation methods are not capable of fully restoring the previously lost motor functions. For instance according to statistics from the United States 50% of individuals suffered from a stroke may have paralysis on one side of their body after the rehabilitation procedure [44].

In summary, it is really desirable to either improve the efficiency of the rehabilitation techniques applied or to develop brand new methods based on both personal anthropometric and neuro-biomechanical parameters of the patient using 3D modeling approaches.
Graphic based multidimensional computer models were developed to discern motor activity patterns of musculoskeletal systems [45], [46]. Furthermore, a general framework was introduced in a neuro-mechanical transducer model to determine possible muscle forces and firing frequencies of flexor and extensor motoneuron pools during voluntary limb movements [47-49].

In motor control when dealing with the 3D modeling of different limb movements on the one hand a complex 3D inverse kinematic problem must be solved to obtain muscle forces needed to reach a selected point in the space while on the other hand the muscle redundancy must be taken into account as well. Muscle redundancy - having more muscles than mechanical degrees of freedom (DOF) - has long been a central problem in biomechanics and neural control. The issue in this context is how muscle coordination patterns are derived by the CNS from a theoretically infinite set of possibilities. In other words any given motor task might be performed in an infinite different manner without having any restriction on the selection of proper muscles being activated. In this sense an optimal solution has to be found by the CNS for selecting a proper combination of muscle activity patterns applied during movement execution.

DOI:10.15774/PPKE.ITK.2012.004

The infinite number of solutions for a given arm movement task is the major issue, since a human limb has generally more joints and around each joint the human body has much more spanning muscles than necessary [4], [50]. There have been two major approaches to the problem of muscle redundancy so far. The first approach is the elimination of the redundant degrees of freedom [51]. The second approach follows the findings of Gelfand *et al.*, [52] who suggests that all elements within a redundant motor system are always involved in solving the motor tasks. This means that no degrees of freedom are eliminated.

It is still an important question to consider which solutions are chosen by the human motor control to solve a given motor task. There are approaches based on optimization techniques as optimization of smoothness [53], [54] or minimization of torques [55], [56] while other methods employ statistical approaches based on the fact that the participating muscles can work together in different ways.
This concept is called muscle synergies and was studied generally by Bernstein [51] and in particular for arm movements by Latash [57]; Prilutsky [58]; Domkin *et al*. [59], [60].
Despite the fact that the muscle synergy problem was introduced more than forty years ago, it is still not obvious what is controlled by the central nervous system and how it chooses controlling strategies especially under altering conditions. These types of motor control issues have been recently investigated in different studies for multi-finger quick force production [61] and for different limb postures [62-64].

In the dissertation a new, fully 3D biomechanical model, containing personalized segment and muscle geometry of the entire upper limb is presented based on the neuro-mechanical framework introduced by Laczkó *et al*. [47], [65]. As a result of this, activation patterns for general rehabilitation (muscle forces, joint torque) have been revealed during the execution of complex upper limb motor tasks (lifting and putting-down an object from a certain place to another one).

Besides, the effect of altering object conditions on motor control levels has also been studied by analyzing the variances of measured (endpoint of the upper limb, joint configuration, muscle activity) and simulated (muscle force) parameters resulted by the above mentioned biomechanical model. Here, different levels of the motor apparatus

DOI:10.15774/PPKE.ITK.2012.004

such as the end point of a limb, the joint configuration defined by the set of joint angles, muscle activities and muscle forces are regarded as motor control levels.

It has been found that if the individual held a heavier object in his hand then the stabilization of the outer descriptors (the endpoint of the arm, joint configuration) was the consequence of an enhanced cooperation of the inner descriptors (muscle activity).

I.2. Motivation and Aims

At the beginning of this chapter it was shown that there are various ways how a healthy individual might become a patient having a kind of a movement disorder. It has also been mentioned that the possibility of being handicapped after rehabilitation procedure is relatively high (50%) [44].
Thus the most important aim of the research was to find out how muscles of the upper limb acted and cooperated while they were producing muscle forces so that they can be reproduced artificially by the application of modern rehabilitation techniques.

All in all, the future purpose is to define personalized stimulation patterns for FES applied on stroke patients suffering from hemiplegia. However, the generation of FES patterns and the development of new control methods for improving the efficacy of current upper limb rehabilitation methods are not the scope of the thesis. Here, a biomechanical approach for determining joint torques; muscle forces exerted by the prime arm movers and the variability of the activity of different parts of the motor apparatus are investigated under specific conditions.
In order to do that based on the measurements of healthy individuals, who performed reaching and grasping arm movements, a 3D biomechanical model of the entire upper limb was developed containing the geometry of 3D limb segments (with shoulder complex); the location of 3D muscle attachment sites and the anatomical/biomechanical structure of 4 muscles.
The outputs of the musculoskeletal model are the magnitude of predicted 3D force and torque vectors; the direction of the 3D force and joint torque vectors.

DOI:10.15774/PPKE.ITK.2012.004

In the future the relations between predicted muscle forces and neural activities are planned to be revealed in order to generate muscle activation patterns taking into account the personal characteristics of the patients.

I.3. Framework of the Dissertation

In Chapter 2, an overview on the materials and methods used in the measurement series that had been performed in the National Institute for Medical Rehabilitation is presented. Furthermore, elementary data processing; the steps of the model development (determination of 3D angular acceleration (3DAA), moment of inertia (MoI), moment arm (MA), gravitational torque, joint torque and muscle force); calculation of variances observed at different levels of motor control and statistical tools applied are described here as well. The most important part and the core of the dissertation can be found here: the prediction of 3D muscle forces from measured joint coordinates.

In Chapter 3, the results and important findings of the simulation method are summarized. The invariant nature of the predicted torque profiles under specific conditions is revealed and the framework for displaying personalized muscle and limb geometries is introduced.

In Chapter 4, the results of the variance analysis at four motor control levels (endpoint of the upper limb, joint configuration, muscle activity, muscle force) are described to show how these levels were affected by a heavier object while it had been held in the hand of the actual subject.

In Chapter 5, new scientific results and possible applications in form of theses are provided.

In Chapter 6, appendices concerning the variances of motor control levels are depicted for all individuals participated in the biomechanical measurements.

DOI:10.15774/PPKE.ITK.2012.004

Chapter II

MATERIALS AND METHODS

II.1. Subjects, Instrumentation, Measurement and Data Processing

A daily executed reaching arm movement task performed by healthy individuals was measured. Twenty individuals (aged 21-25; mean±SD.: 21.1±1.9), 14 men and 6 women with no upper extremity complaints, voluntarily participated in the study at the National Institute for Medical Rehabilitation (NIMR) in Budakeszi, Hungary.

Movements were investigated by the ultrasonic-movement analyzer (usMA) ZEBRIS CMS 70P (Zebris Medical GMBH,Germany) [66], [67]. Eight ultrasonic markers and four bipolar surface EMG (sEMG) electrodes were used. Seven markers (Figure 2.2, Table 2.1) were placed on the participant and one as a reference point placed on the object being moved. 3D coordinates of the markers and muscle activities were recorded simultaneously for the 4 main arm muscles: biceps (BI), triceps (TR), deltoid anterior (DA) and deltoid posterior (DP).

The total sampling rate of the usMA was 200 Hz. The sampling rate of one marker was 25 Hz because the ultrasound sensor of the system senses the 8 markers serially. The sampling frequency of the sEMG was 1000 Hz. The different sampling rates were synchronized by the manufacturer.

After the markers and the sEMG electrodes had been placed on the individual, the measurement was started without having a learning phase.

II.1.1. Measurement of Kinematics and EMG – Movement Description

The individual sat in front of a 2-level-computer desk. The difference between the heights of the two levels of the desk was 20 cm (70 cm and 90 cm above the floor). The upper level was approximately at shoulder level. The distance between the chair and the desk was given by the maximum stretch of the elbow. The external angle of the elbow (the angle of the forearm in respect to the elongation of the upper arm) was required to be about 10-15 degrees. The angular stretch was measured with a protractor.

DOI:10.15774/PPKE.ITK.2012.004

The motor task was executed under three conditions corresponding to three objects with different masses:

1) a 0.06 kg light CD case (CD)
2) a 1 kg object (O1)
3) a 2 kg object (O2)

Object masses were chosen taking into account the limits (pronosupination was not allowed while the palm was facing backward) of the studied movement on obtainable joint torques.
The shapes of the objects were the same to avoid the effects of different extrinsic and intrinsic object properties [68].

The actual object was placed on the lower level of the desk. In the starting position the arm of the individual was hanging alongside the body and the palm was facing backwards. This posture was chosen because hemiplegic patients hold their lower arm in that way and the 3D arm movement model presented in the dissertation is planned to be used mostly in the case of hemiplegics to define artificial stimulation patterns for their upper limb muscles.

The measured movement was divided into 3 phases (Figure 2.1):

a) **lifting phase:** The individual was instructed to lift his arm from the initial position to reach and grasp the object on the lower level of the desk and had to lift it. After that he had to place the object onto the upper level and finally release it and move the arm back to the initial hanging position.

b) **pause:** In the second phase, the arm remained in the hanging position taking a short pause (2-5sec).

c) **putting-down phase:** In this phase, the individual had to lift his arm to reach the object on the upper level of the desk, grasp it and then put it back down to the lower level, release the object and move the arm back to the starting position again.

DOI:10.15774/PPKE.ITK.2012.004

The entire task was repeated ten times: 10 lifting and 10 putting-down trials were recorded under each condition. Individuals had one-minute pause between series of trials with different conditions. The effect of fatigue was not investigated and the influence of it was blocked by selecting the execution order of the different objects randomly. Instructions on the speed of movement execution were not given. The average movement execution time was 7.5 s ± 1.3 s (mean ± SD). Revealing the difference (if there were any) between females and males was not the scope of the study.

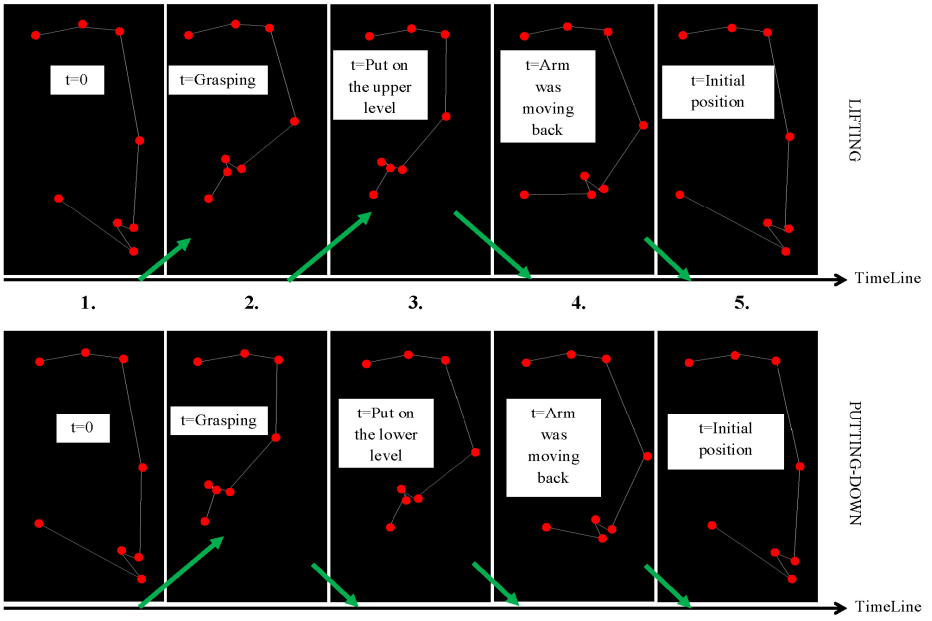

Figure 2.1. Stick figure of the measured movement represented by the Zebris (Zebris CMS 70P, Zebris Medical GMBH, Germany)interface.

Upper panel: A lifting phase is presented from the initial position (t=0; the arm was hanging alongside the body) through grasping and lifting (to the upper level) the object to moving back the limb again to the initial position.

Lower panel: A putting-down phase is presented from the initial position (t=0) through grasping and putting-down (to the lower level) the object to moving back the limb again to the initial position.

The green arrows show how the vertical direction was changing during the execution of the motor task.

DOI:10.15774/PPKE.ITK.2012.004

II.1.2. Data Processing

II.1.2.1. Kinematic Data Processing

In the first and the third phases of the movement task the object was moved upwards or downwards, respectively (Figure 2.1). During these phases 3D coordinates of 7 anatomical points of the arm, a point of the object (Figure 2.2, panel A) and muscle activities of 4 arm muscles were recorded (Figure 2.2, panel B, Table 2.1).

Kinematic data was divided into two parts according to the measured lifting and putting-down phases.

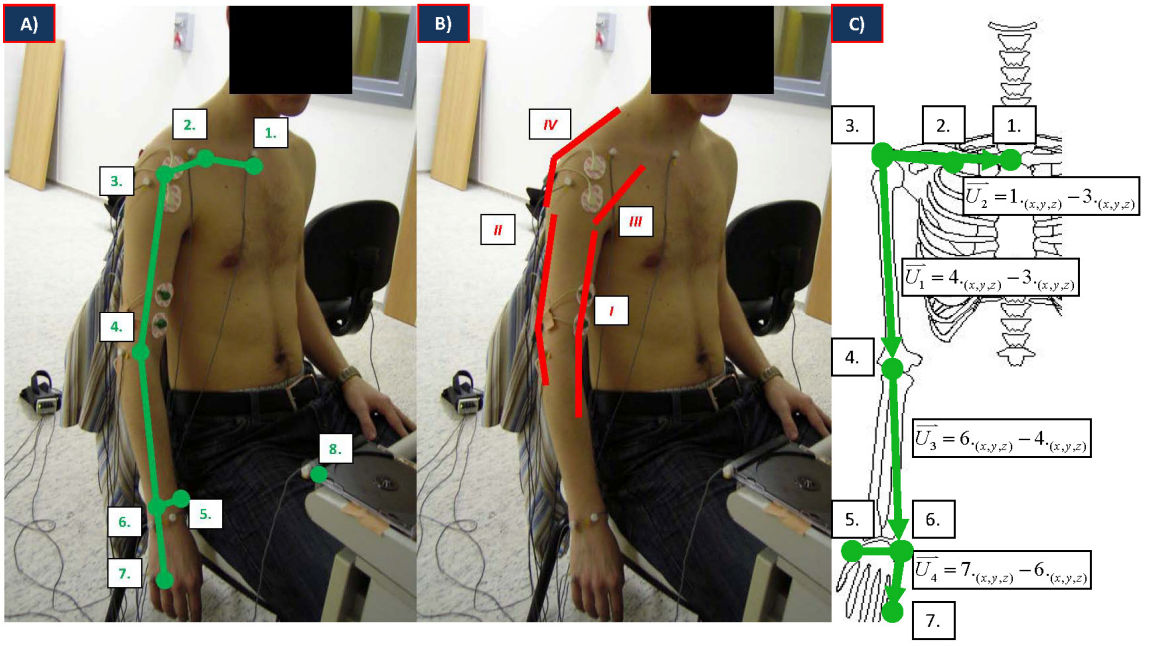

Figure 2.2. A) Ultrasound markers placed on seven anatomical landmarks (Table 2.1, MARKER CHANNEL 1-7) and on the actual object (Table 2.1, MARKER CHANNEL 8) moved by the individual. B) The activity of 4 arm muscles (Table 2.1, EMG CHANNEL I-IV) was measured by bipolar surface EMG electrodes. C) $\overrightarrow{U_i}$ *vectors are segment vectors representing the clavicle (*$\overrightarrow{U_2}$*); the upper arm (*$\overrightarrow{U_1}$*); the lower arm (*$\overrightarrow{U_3}$*) and the hand(*$\overrightarrow{U_4}$*) used in data processing and in modeling. Green lines sign the personalized limb geometry applied during the measurements and modeling (panels A and C) while the red ones (panel B) denote the measured and modeled muscle geometry.*

DOI:10.15774/PPKE.ITK.2012.004

Three dimensional inter-segmental joint angles were computed in the shoulder, elbow and wrist joints. The inter-segmental joint angle in the elbow is the internal angle between (Figure 2.3) the upper segment vector and lower segment vector ($\overrightarrow{U_1}$ and $\overrightarrow{U_3}$); in the shoulder it is the angle between the clavicle vector and the upper segment vector ($\overrightarrow{U_2}$ and $\overrightarrow{U_1}$); while in the wrist it is the angle between the lower segment vector and hand vector ($\overrightarrow{U_3}$ and $\overrightarrow{U_4}$). The instantaneous joint configuration (JC) is represented by the set of these three joint angles.

TABLE 2.1.
ULTRASONIC MARKER AND EMG CONFIGURATION

MARKER CHANNEL		EMG CHANNEL	
1	Proximal Clavicle	I	Biceps (BI)
2	AC joint	II	Triceps (TR)
3	Proximal Humerus	III	Deltoid Anterior (DA)
4	Distal Humerus	IV	Deltoid Posterior (DP)
5	Distal Ulna		
6	Distal Radius		
7	Little finger Proximal Metacarp		
8	Object point		

Note. In the left column the names of seven bony landmarks (1-7) marked by ultrasound markers (Figure 2.2, panel A) are summarized. In the right column the names of muscles (Figure 2.2, panel B) that activities were recorded are presented.
For detailed anatomical description of bony landmarks (1-7) and muscles (I-IV) see Szentágothai and Réthelyi[69], [70].
Remark: MARKER CHANNEL 8 was assigned to the object moved by the individual.

DOI:10.15774/PPKE.ITK.2012.004

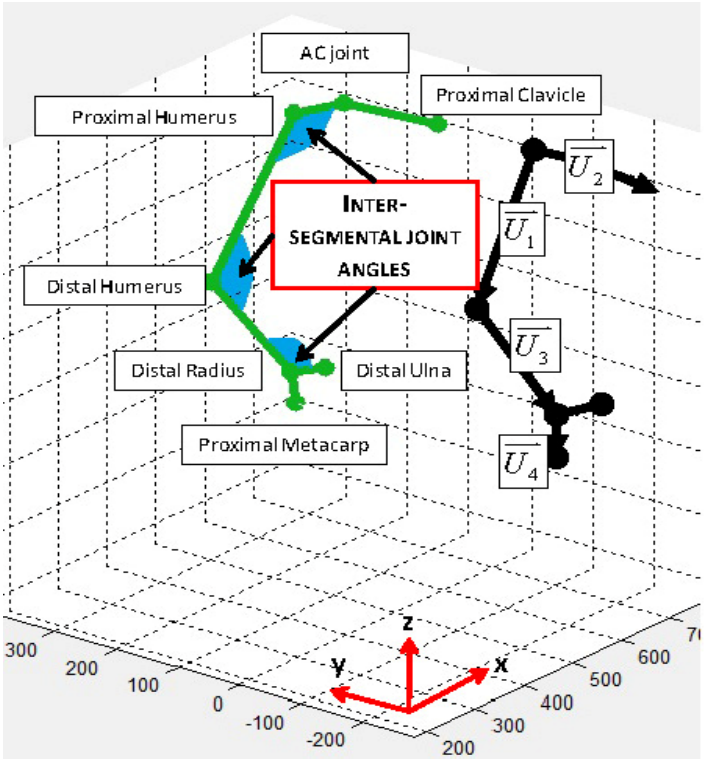

Figure 2.3. The computed inter-segmental joint angles (green stick figure, blue joint angels) and segment vectors (black stick figure; $\overrightarrow{U_i}$ vectors were composed according to Figure 2.2, panel C) used during data processing in the global coordinate system. The x-axis is horizontal in the frontal plane directed outward from the body, the y-axis is horizontal in the sagittal plane directed forward, and the z-axis is perpendicular to the x-y plane directed upwards. The upper arm segment vector ($\overrightarrow{U_1}$) pointed from the shoulder joint (Proximal Humerus) to the elbow joint (Distal Humerus); the clavicle vector ($\overrightarrow{U_2}$) pointed from the shoulder joint to the thorax (Proximal Clavicle); the lower arm vector ($\overrightarrow{U_3}$) pointed from the elbow joint to the wrist (Distal Radius) and the hand vector ($\overrightarrow{U_4}$) pointed from the wrist (Distal Radius) to the base of the little finger (Proximal Metacarp).

All kinematic data were linearly interpolated because at some time instants “not a number” (NaN) 3D coordinate values were recorded as a result of ultrasound sensing error. After interpolation time normalization was performed by the SPLINE built-in function of the MATLAB (The MathWorks Inc., Natick, MA, USA) to allow trial alignment within the same movement phases and object conditions (Figure 2.4).

DOI:10.15774/PPKE.ITK.2012.004

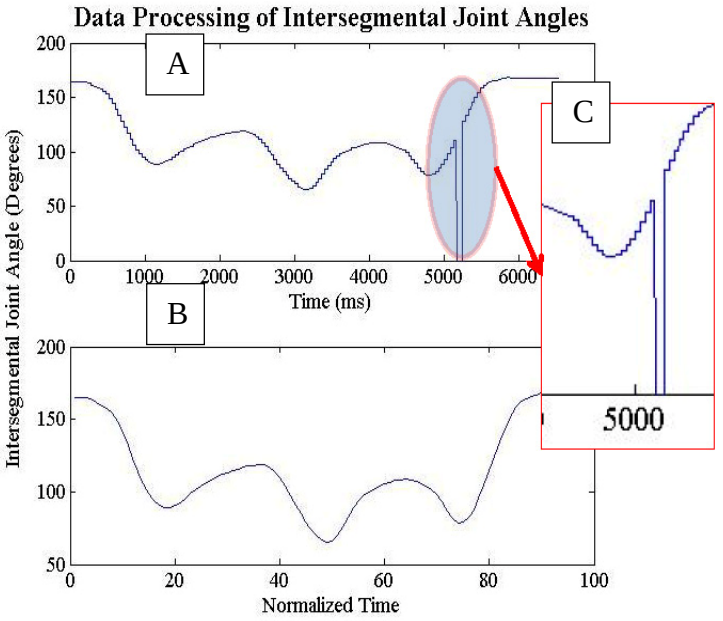

Figure 2.4. A) Raw elbow joint angular changes with a split (signed by the blue circle). B) Linearly interpolated and time normalized elbow joint angular changes. Time normalization was performed by using the spline built-in MATLAB function. C) A short time split in raw elbow joint angle.
The same data processing method was applied for the shoulder and wrist joint angles (Figure 2.3, green stick figure).

II.1.2.2. EMG Data Processing

EMG data were processed for both the lifting and putting-down phases considering all four muscles.

First, sEMG data were filtered as is commonly used in kinesiological electromiography [71-74]. Frequencies below 50 Hz and above 450 Hz were cut off by the MATLAB built-in function (4^{th} order Butterworth band-pass filter) and the root mean square (RMS) of the smoothed signals were extracted. For smoothed sEMG signals (Figure 2.5) the same time normalization was applied as in kinematics.

DOI:10.15774/PPKE.ITK.2012.004

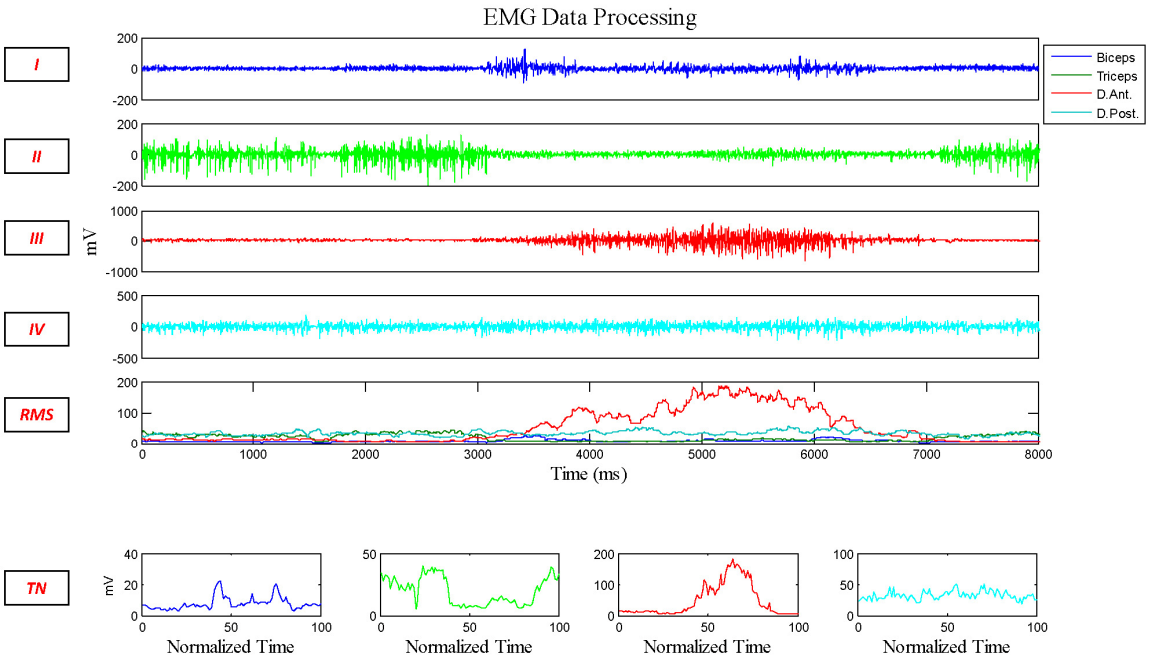

Figure 2.5. I-IV) Raw muscle activities measured by bipolar surface electrodes at 1000 Hz sampling rate for the biceps (blue), triceps (green), deltoid anterior (red), deltoid posterior (light blue). RMS) Butterworth and RMS filtered EMGs of the same muscles. Filtration was solved by applying 50 – 450 Hz bandpass Butterworth filter and RMS. TN) Time normalized EMGs.

II.2. Prediction of Muscle Forces from Joint Coordinates

II.2.1. Prediction of Muscle Forces

A general 3D musculoskeletal upper limb model is presented. The model applies the same coordinate system which is used by the usMA (Figure 2.3). The x-axis is horizontal in the frontal plane directed outward from the body. The y-axis is horizontal in the sagittal plane directed forward while the z-axis is perpendicular to the x-y plane directed upward. Primary input parameters of the model are measured 3D coordinates of anatomical landmarks (Table 2.1, MARKER CHANNEL 1-7). The time courses of inter-segmental joint angles were computed from these coordinates (Figure 2.3). Secondary input parameters of the model were arm segment masses, segment lengths estimated from the height and body mass according to Zatsiorsky [75]. Muscle forces were determined based on muscle moment arms, angular accelerations, moment of inertias of

DOI:10.15774/PPKE.ITK.2012.004

all arm segments and gravitational torque. If only one muscle is active at a time *t*, than the torque generated by this muscle in the joint is computed as the difference of the total torque and the gravitational torque [47], [48]:

$$\overrightarrow{F_m(t)} \times \overrightarrow{R_m(t)} = \overrightarrow{\beta(t)} \cdot {}^{(\mathbf{joint})}I\,(t) - \overrightarrow{T_{g(\mathbf{joint})}(t)} \tag{2.1}$$

where $\overrightarrow{F_m(t)}$ vector is the force generated by the muscle, $\overrightarrow{R_m(t)}$ is the moment arm vector of the muscle, $\overrightarrow{\beta(t)}$ is the angular acceleration vector of the joint spanned by the muscle, ${}^{(\mathbf{joint})}I\,(t)$ is the moment of inertia, $\overrightarrow{T_{g(\mathbf{joint})}(t)}$ is the gravitational torque vector due to the rotated body part. Depending on the direction of the required torque either the flexor or the extensor muscle group should be activated at each instant for an artificial control of the joint torque. Such virtual muscle forces eliciting torque in the joint were predicted for the 4 arm muscles separately (BI, TR, DA, DP) at each time step during the desired movement.

II.2.2. Definition of Segment and Muscle Geometry

II.2.2.1. Definition of Segment Geometry

Using recorded 3D coordinates of 7 anatomical landmarks (Figure 2.2, panel A, Table 2.1) 4 different 3D segment vectors were defined representing the clavicle ($\overrightarrow{U_2}$); the upper arm ($\overrightarrow{U_1}$); the forearm ($\overrightarrow{U_3}$) and the hand ($\overrightarrow{U_4}$) (Figure 2.2, panel C, Figure 2.3).

II.2.2.2. Definition of Muscle Geometry

In the simulation approach muscle attachment sites – either the origin or the insertion – were assumed as three dimensional points on the surface of the given bone segment. A muscle is represented by its midline that connects its insertion and origin on two different segments. To build an accurate muscle geometry "via points" ($ViaP_{x,y,z}$) – which are certain 3D points located on the bisectrix vector of the joint spanned by the

DOI:10.15774/PPKE.ITK.2012.004

investigated muscle – were defined to build up the connection between the specific muscle origin and insertion located in different planes. In general, the 3D coordinates of the muscle attachments for the studied muscles were computed in 2 major steps. In the first step a virtual subject was created (next subsection) with virtual body parameters (segment length) based on the study using fresh cadavers by Veeger *et al*. [76]. In the study of Veeger *et al.* [76] muscle attachments were originated for the whole upper limb by disarticulating first the arm from the thorax and then by using the 3Space^{TM} system [77] to collect three dimensional position and orientation data of the muscle attachment sites in different postures. On the one hand by using the data provided by Veeger *et al.* [76] muscle origin and insertion points are located on the midline of the bone segment and on the other hand accurate locations of muscle attachments are available only for the initial position (the arm was hanging alongside the body) of the measured movement. To avoid this, in the second step origin and insertion direction vectors were obtained (Figure 2.7). To get the spatial locations of the investigated muscle attachments for the entire movement and not only for the initial position the rotation method of Rodrigues was applied to rotate the direction vectors by a certain rotation angle.

Muscle Geometry – Creation of the Virtual Subject

In the study of Veeger *et al.* [76] the disarticulated upper extremity was mounted on a measuring board and markers of the 3Space^{TM} measurement system were placed on the humerus (EL – epycondilus lateralis), ulna (US – processus styloideus ulnae) and radius (RS - processus styloideus radii). To get the position and orientation of the scapula the Angulus Acromialis (AA), the Angulus Inferior (AI), the Trigonum Spinae (TS) and the Acromion (AC) were marked as well. The global reference frame of these measurements had the z-axis pointing upward, the x-axis was parallel to the surface of the measuring board pointing to the lateral side of the specimen, and the y-axis pointing from the posterior surface to the anterior surface of the scapula. The spine of the scapula was approximately parallel to the x-axis. This global coordinate system was the same used in the biomechanical measurements described previously. Based on the 3D coordinates given in the study of Veeger *et al.* [76] (Table 2.2) the virtual subject was obtained (Figure 2.6).

DOI:10.15774/PPKE.ITK.2012.004

TABLE 2.2.
3D COORDINATES OF THE VIRTUAL SUBJECT

Joint/muscle attachment	x	y	z
AC	252.9	12.8	409.6
EL	307.5	-11.3	51.8
US	322.1	68	-216
BIO (origin)	237	18.1	381.8
BII (insertion)	287.4	19.2	0.6
TRO (origin)	239.7	19.6	345.3
TRI (insertion)	259.5	-35.3	50.8
DO (deltoid origin)	242.7	55.4	393.3
DI (deltoid insertion)	257.2	6.4	207

Note. 3D coordinates published by Veeger et al. [76]. *The global coordinate system applied by Veeger et al. was the same as presented in Figure 2.3. Here, AC represents the AC joint (ultrasound marker 2 in the measurement, according to Figure 2.2, panel A), EL is the elbow joint (ultrasound marker 4 in the measurement according to Figure 2.2, panel A) and US is the wrist (ultrasound marker 6 in the measurement according to Figure 2.2, panel A).BIO is the biceps origin, BII is the biceps insertion, TRO is the origin of the triceps, TRI is the insertion of the triceps, DO is the origin of the deltoid muscles, DI is the insertion of the deltoid muscles. Although the deltoid anterior and posterior muscles were discerned, the insertion and origin of the two parts of these muscles were overlapping* [78].

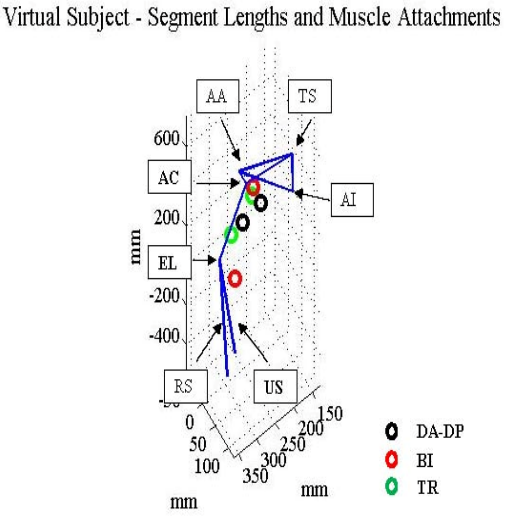

Figure 2.6. Virtual subject based on cadaveric measurements of Veeger [76]. *Anatomical sites denoted by bold are taken into account in the model (AC,EL,US,DA-DP,BI,TR). AC, AA, TS, AI define the geometry of the scapula although it was omitted from the study. The clavicle was not part of the study of Veeger. Based on the measurements done in the NIMR the clavicle was added to the virtual subject with a mean segment length.*

DOI:10.15774/PPKE.ITK.2012.004

Since the clavicle had been omitted from the study of Veeger *et al.* [76] the mean clavicle length was composed by using the measurements that had been acquired in the NIMR. For each individual the length of the clavicle was determined by calculating the length of the three dimensional clavicle vector ($\overrightarrow{U_2}$). After this the average clavicle length of all participants was taken. To know the length of the clavicle was a must because the origins of the biceps (longer head of the biceps muscle) and the deltoid are located on this segment.

Muscle Geometry – Computation of Spatial Muscle Attachments

Using the segment and muscle parameters of the virtual subject (Figure 2.6, Table 2.2) the muscle attachment vectors ($\overrightarrow{BIO_t}$ – biceps origin, $\overrightarrow{BII_t}$ – biceps insertion, $\overrightarrow{TRO_t}$ – triceps origin, $\overrightarrow{TRI_t}$ – triceps insertion, $\overrightarrow{DO_t}$ – deltoid origin, $\overrightarrow{DI_t}$ – deltoid insertion at each time (t) step) were composed pointing from the joint that was the center of rotation to the certain muscle attachment (Figure 2.7).

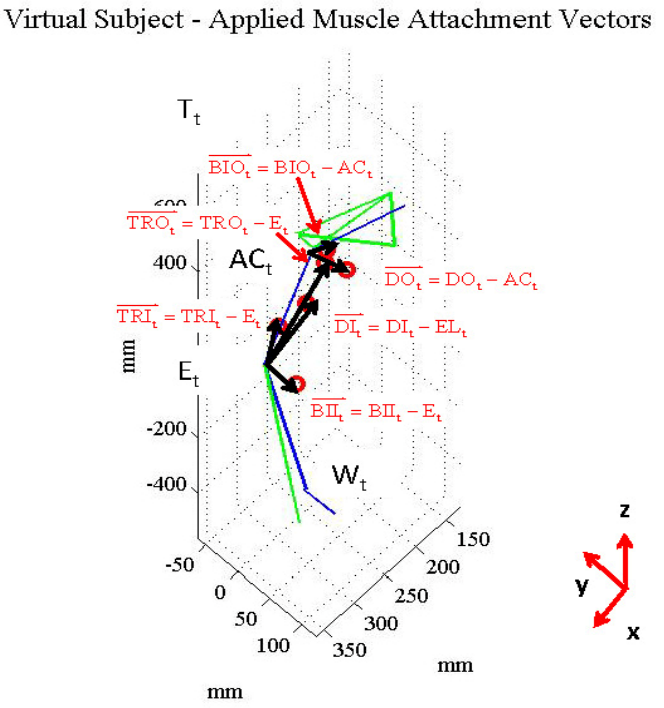

Figure 2.7. Muscle attachment vectors ($\overrightarrow{BII_t}, \overrightarrow{BIO_t}, \overrightarrow{TRI_t}, \overrightarrow{TRO_t}, \overrightarrow{DI_t}, \overrightarrow{DO_t}$). Vectors represented by black are muscle attachment vectors at a certain time step (t) pointing from the joint that is the center of rotation of the segment containing the specific muscle attachment. Green lines are segments omitted from the model; Blue lines are segments taken into account in the model.

DOI:10.15774/PPKE.ITK.2012.004

The endpoint of muscle attachment vectors were then projected onto the midline of the bone segment. The length of the projected muscle attachment vectors were obtained for the initial time instant (t=0) of the measured movement. Using the length of the projected muscle attachment vectors and the length of the midline of the segment the ratio was composed for the virtual subject representing the relation of the muscle attachment vectors to the segment vectors containing the specific attachment. As a result, the spatial location of muscle attachments on the midline of the segment was obtained for the initial position (the arm was hanging alongside the body).

Muscle attachments located on the surface of the bone were originated for the whole movement time interval by using the rotation formula of Rodrigues which is a general tool for rotating a certain vector in the 3D space around an arbitrary rotation axis (z is a unit vector of $z \in R^3$) by a given angle of rotation (θ).

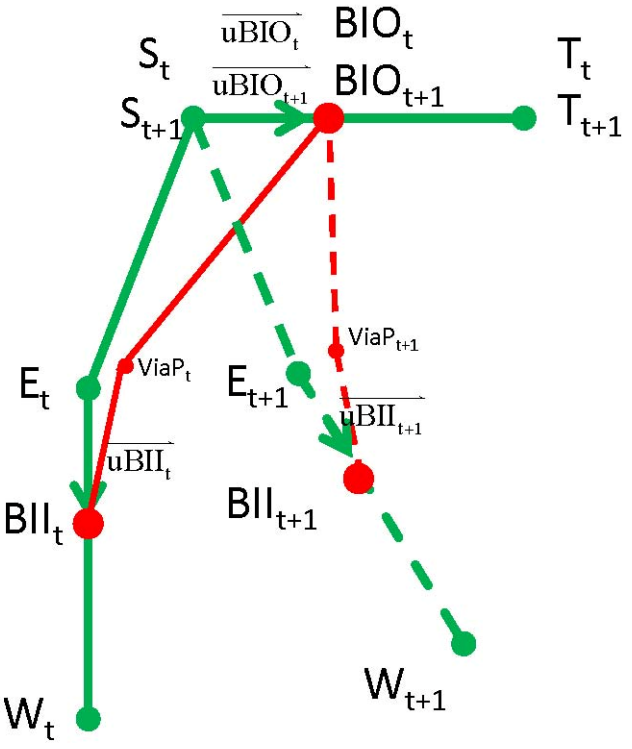

Figure 2.8. Anatomical landmarks (T – thorax; S – shoulder; E – elbow; W - wrist); muscle attachments of the biceps (BIO - origin; BII - insertion); unit muscle attachment vectors ($\overrightarrow{uBII}, \overrightarrow{uBIO},$) used in the rotation method of Rodrigues during the calculation of the biceps attachments located on the surface of the bone are presented at two successive time instants (t and t+1). The rotation method was applied to determine muscle insertions and origins for not only the initial position (t=0) but for the whole movement interval as well.

DOI:10.15774/PPKE.ITK.2012.004

Initial (t=0) muscle insertion and origin points were calculated as written above [79]. Equations (2.2) - (2.5) were applied to calculate biceps insertion and origin at each time step (Figure 2.8).

$$\overrightarrow{\mathrm{uBII}_{t+1}} = \overrightarrow{\mathrm{uBII}_t}\cos\Theta_{(e)t} + (z_t \times \overrightarrow{\mathrm{uBII}_t})\sin\Theta_{(e)t} + z_t z_t^T \cdot \overrightarrow{\mathrm{uBII}_t} \cdot (1-\cos\Theta_{(e)t})) \tag{2.2}$$

In equation (2.2) the unit muscle attachment vector ($\overrightarrow{\mathrm{uBII}_t}$) at time t was rotated about the elbow rotation axis (z_t) determined by the cross product of the two adjacent segments (in this case the upper segment and lower segment) by $\Theta_{(e)t}$ angle of elbow rotation in order to determine the unit muscle attachment vector ($\overrightarrow{\mathrm{uBII}_{t+1}}$) at time t+1.

$$\Theta_{(e)t} = \alpha(E_{t+1}) - \alpha(E_t) \tag{2.3}$$

In (2.3) the angle of elbow rotation ($\Theta_{(e)t}$) was determined by subtracting the inter-segmental joint angle of the elbow at time t ($\alpha(E_t)$) from the inter-segmental elbow joint angle at time t+1 ($\alpha(E_{t+1})$).

$$\overrightarrow{\mathrm{BII}_{t+1}E_{t+1}} = \left\|\mathrm{BII}_{t+1} - E_{t+1}\right\| \cdot \overrightarrow{\mathrm{uBII}_{t+1}} \tag{2.4}$$

In (2.4) the muscle attachment vector ($\overrightarrow{\mathrm{BII}_{t+1}E_{t+1}}$) pointing from the elbow joint (E_{t+1}) to the biceps insertion (BII_{t+1}) at time t+1 was computed by multiplying the unit muscle attachment vector of the biceps insertion ($\overrightarrow{\mathrm{uBII}_{t+1}}$) at t+1 by the length of the muscle attachment vector ($\left\|\mathrm{BII}_{t+1} - E_{t+1}\right\|$) at time t+1.

To compute the spatial coordinates of the biceps insertion ($\mathrm{OnBoneSurf\_BII}_{t+1}$) at time t+1 located on the surface of the lower limb segment, the elbow joint coordinates (E_{t+1}) at t+1 were added to the muscle attachment vector ($\overrightarrow{\mathrm{BII}_{t+1}E_{t+1}}$) at time t+1 (Equation 2.5).

$$\mathrm{OnBoneSurf\_BII}_{t+1} = \overrightarrow{\mathrm{BII}_{t+1}E_{t+1}} + E_{t+1} \tag{2.5}$$

DOI:10.15774/PPKE.ITK.2012.004

The same method as written above (Equations 2.2 – 2.5) was applied for calculating the attachments (Figure 2.9) of the triceps; deltoid anterior; deltoid posterior by replacing the rotation axis; the rotated unit vector and the angle of rotation to proper ones related to the specific muscle.

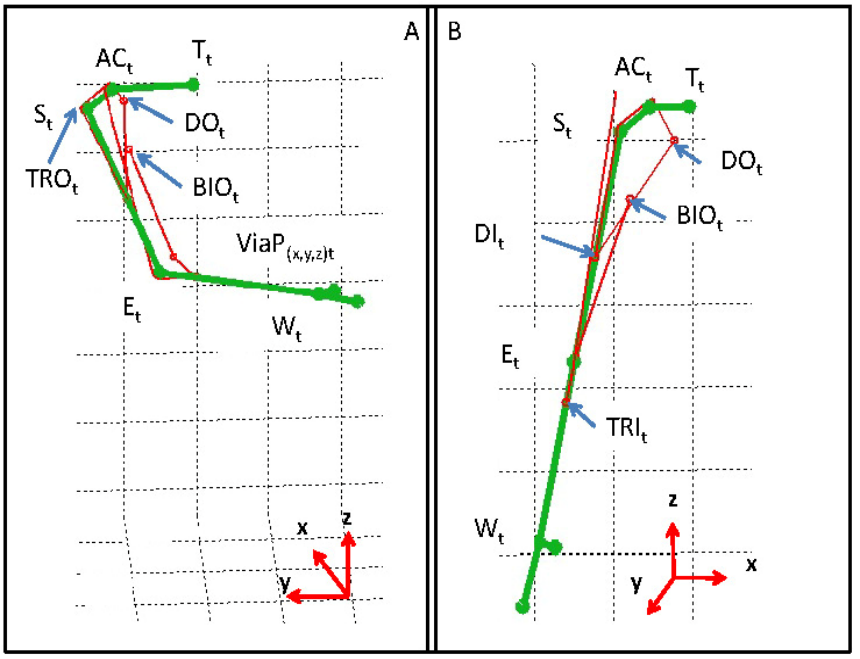

Figure 2.9. In panel A) and B) 3D muscle attachments are presented for the biceps (BIO_t), the triceps (TRO_t, TRI_t) and deltoid (DO_t, DI_t) muscles. The insertion of the biceps (BII_t) was covered by either the lower segment or the triceps in both spatial view (in panel A and B). Red lines represent the midline of muscles; green lines represent the midline of bones.

Note: The insertion and origin of the DA and DP are considered to be overlapped [78], [80].

II.2.2.3. Calculation of the Angular Acceleration

Angular acceleration - also called rotational acceleration - is in general a quantitative expression of the change in angular velocity that a spinning object undergoes per unit time. The angular acceleration ($\overrightarrow{\beta(t)}$) is a vector quantity, consisting of a magnitude component and the direction of the vector component. Generally, the direction of the angular acceleration vector is perpendicular to the plane in which the rotation takes place. If the increase in angular velocity appears clockwise with respect to an observer, then the angular acceleration vector points away from the observer. If the increase in angular velocity appears counterclockwise, then the angular acceleration vector points

DOI:10.15774/PPKE.ITK.2012.004

toward the observer. Thus, the angular acceleration vector does not necessarily point in the same direction as the angular velocity vector especially not in the 3D space.

Consider a car travelling forward along a highway at an increasing speed. The 3D angular acceleration vectors for all tires point toward the left along the lines containing the wheel axles (axis of rotation). If the car stops accelerating and maintain a constant velocity the 3D angular acceleration vectors break off. If the car goes forward at a decreasing speed, the vectors reverse their directions, and point toward the right along the lines containing the wheel axles.

Theoretically, if the car is put into reverse and increases velocity going backwards, the 3D angular acceleration (3DAA) vectors point toward the right along the axis of rotation. If the backward velocity is constant, the 3D angular acceleration vectors disappear and obviously if the backward velocity decreases, the 3D angular acceleration vectors point toward the left along the axis of rotation of the wheels.

The magnitude of the angular acceleration vector ($\beta(t)$) is directly proportional to the rate of change of the angular velocity and it is calculated by the second time derivative of the inter-segmental joint angle ($\alpha_{joint}(t)$) of the specific joint.

$$\beta(t) = \frac{d^2\alpha_{joint}(t)}{dt^2} \tag{2.6}$$

The direction of $\overrightarrow{\beta(t)}$ is perpendicular to the plane of rotation defined by two adjacent segments. The right side of this plane is assigned by the cross product of the unit vector pointing from the joint to the direction of the distal limb segment and the unit vector pointing from the joint to the direction of the proximal one. If its scalar product with a particular vector is positive then that vector is directed to the right of the plane. According to the car analogy if $\alpha_{joint}(t)$ was decreasing (flexion) at a magnitude of $\beta(t) > 0$ (Figure 2.10, case a)) then the angular acceleration vector pointed toward the left of the plane of rotation. In this case the speed of the flexion was decreasing.

During flexion at a magnitude of $\beta(t) < 0$ (Figure 2.10, case c)) the angular acceleration vector pointed toward the right of the plane, while the speed of the flexion was increasing. Note that flexion was associated with negative angular velocity and its speed was the absolute value of the angular velocity.

DOI:10.15774/PPKE.ITK.2012.004

If $\alpha_{joint}(t)$ was increasing (extension) at $\beta(t) < 0$ (Figure 2.10, case b)) then the acceleration vector pointed toward the right of the rotation plane while during extension at $\beta(t) > 0$ (Figure 2.10, case d)) it pointed toward the left of that plane. Angular changes at constant velocity were not observed.

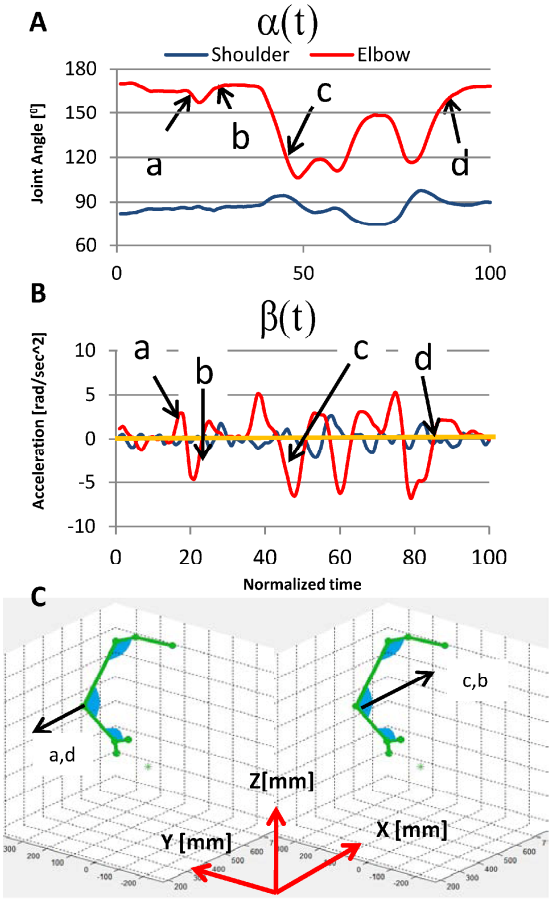

Figure 2.10. The direction of the angular acceleration vector in the 3D space. Considering how the joint angle was changing (increasing-decreasing joint angle) - panel A – and the rate of change of the joint velocity (acceleration) - panel B - the direction of the angular acceleration vector coincide with 4 cases assigned by a-d presented in panel C. In a) decreasing elbow angle at decreasing speed; b) increasing elbow angle at increasing speed; c) decreasing elbow angle at increasing speed; d) increasing elbow angle at decreasing speed are presented. The same is true for the shoulder joint. Filtration during the calculation of the magnitude of the angular acceleration was solved by applying moving average.

II.2.2.4. Determination of the Moment Arm

The moment arm (MA) vector is perpendicular to the line of action of the muscle and it points from the muscle action line to the axis of rotation.

DOI:10.15774/PPKE.ITK.2012.004

The moment arm calculation method in the shoulder extensor is presented in (Figure 2.11) and is written in equations (2.7) – (2.8). Theoretical moment arms for the other muscles are also shown in (Figure 2.11) signed by black vectors. Furthermore, in the elbow and in the shoulder joints muscle pulleys were defined. The diameter of these muscle pulleys were set to 10 mm. The effect of the muscle pulleys occur if the magnitude of the MA vector is equal to the pulley radius and the muscle line touches the curve of the pulley. In such a state the MA vector is directed from the point where the muscle reaches the curve of the pulley to the center of rotation. However, such muscle geometries were not present during the simulation.

As it was written above, a muscle was represented by its "midline" that connected its attachment sites in two segments via a given point ("via point"). The geometry of the muscle was provided as two lines originating on the proximal $O(t)_{x,y,z}$ and distal $I(t)_{x,y,z}$ segments respectively and were connected at the via point $ViaP(t)_{x,y,z}$. The via point was on the bisectrix vector $\overrightarrow{F(t)}$ of the joint angle.

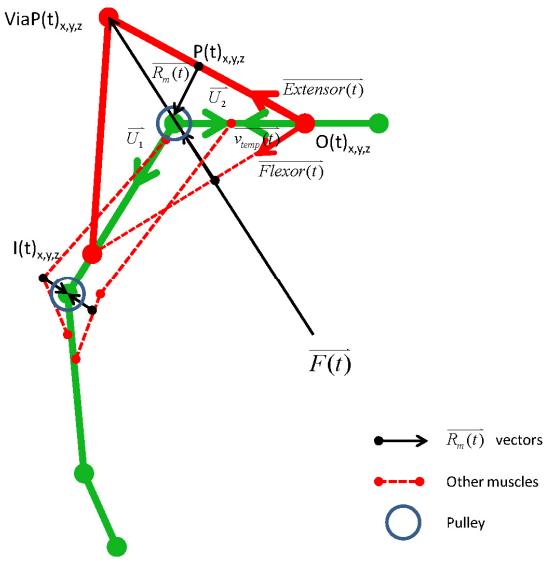

Figure 2.11. Origin and insertion points ($O(t)_{x,y,z}$ and $I(t)_{x,y,z}$); auxiliary vectors ($\overrightarrow{F(t)}$, $\overrightarrow{Extensor(t)}$); segment vectors($\overrightarrow{U_1}$, $\overrightarrow{U_2}$) used in the computation of the DP moment arm. Black vectors denote the muscle moment arm vectors for the investigated muscles at specific muscle geometries (dashed red lines). Blue circles are muscle pulleys. The diameter of these muscle pulleys were set to 10 mm. The effect of the muscle pulleys would occur if the magnitude of the MA vector was equal to the pulley radius and the muscle line touched the curve of the pulley. In such a state the MA vector would be directed from the point where the muscle touched the pulley curve to the center of rotation. Such muscle geometries were not present during the simulation.

DOI:10.15774/PPKE.ITK.2012.004

If the distance of Via$P(t)_{x,y,z}$ and $I(t)_{x,y,z}$ was greater than the distance of the via point and $O(t)_{x,y,z}$ then point $P(t)_{x,y,z}$ was determined as:

$$P(t)_{x,y,z} = (\overrightarrow{\text{Extensor}(t)} \cdot \text{dot}(\overrightarrow{v_{temp}(t)}, \overrightarrow{\text{Extensor}(t)})) + O(t)_{x,y,z} \quad (2.7)$$

Given $J(t)_{x,y,z}$ as the measured 3D coordinates of the joint spanned by the investigated muscle then:

$$\overrightarrow{R_m(t)} = J(t)_{x,y,z} - P(t)_{x,y,z} \quad (2.8)$$

In equation (2.8) S_t as shoulder joint coordinates, E_t as elbow joint coordinates and W_t as wrist joint coordinates at time t were assigned to $J(t)_{x,y,z}$.

The similar algorithm as presented above was used for calculating the moment arm vector of the shoulder flexor using the unit vector ($\overrightarrow{Flexor(t)}$) pointing along the midline of the flexor muscle. An obvious fact is that the geometry of the biceps is similar to the geometry of the triceps although the previous one is an extensor while the latter one is a flexor muscle with completely different functions (Figure 2.11).

II.2.2.5. Definition of the Moment of Inertial Properties

In classical mechanics, moment of inertia (MoI) or rotational inertia is the measure of the resistance of an object to changes to its rotation. It is the inertia of a rotating body with respect to its rotation. The moment of inertia of a certain object about a given axis describes how difficult it is to change its angular motion about the given axis. Therefore, it encompasses not just the overall mass of the object, but how far each bit of mass is from the axis. Thus, the farther the bit of mass of the object is, the more rotational inertia the object has and therefore the more force is required to change its rotation rate.

A good example is to consider two discs (A, B) made of the same material with equal mass. Disc A is larger in diameter but it is thinner than disc B. Hence, it requires more force to accelerate disc A (to change its angular velocity) because its mass is distributed

DOI:10.15774/PPKE.ITK.2012.004

farther from its axis of rotation. In that case disc A has a larger moment of inertia than disc B. From this example it can be figured out that the moment of inertia of an object changes with the change of its shape. There is a good example in sport sciences to prove this fact when for instance figure skaters begin a spin with arms outstretched providing a striking. If they pull in their arms, they will reduce their moment of inertia resulting a faster spin about their axis of rotation.

In general the moment of inertia has two different forms. A scalar form used if the axis of rotation is well defined and a more general tensor form that does not require the axis of rotation to be specified. In the presented model the axis of rotation of all segments are specified by taking the cross product of two adjacent unit segment vectors thus the scalar form of MoI was taken for the entire upper limb. To determine the MoI for all the rotated body parts of the arm a general property of the scalar MoI form was used. Namely, the moment of inertia of a given body is additive. That is, if the body can be decomposed into several constituent parts, then the moment of inertia of the whole body about a given axis is equal to the sum of moments of inertia of all parts around the same axis. According to the so-called parallel axis theorem the MoI of an object about the rotation axis going through its center of mass is the minimum MoI for an axis in that direction in space and furthermore the MoI about any parallel axis to that axis through the center of mass was given by:

$$I_{parallel} = I_{cm} + Md^2 \tag{2.9}$$

where I_{cm} is the moment of inertia about the center of mass, M is the mass of the segment, d is the distance between the axis through the center of mass and the parallel axis through the rotation center.

Arm segments were considered as uniform cylinders with different thickness. The moment of inertia about the center of mass of the rotated segment is:

$$\underset{center}{I}^{(segment)} = \frac{1}{4}Mr^2 + \frac{1}{12}ML^2 \tag{2.10}$$

The moment of inertia around the end of the rotated segment is:

DOI:10.15774/PPKE.ITK.2012.004

$$\underset{end}{\overset{(segment)}{I}} = \frac{1}{4}Mr^2 + \frac{1}{3}ML^2 \tag{2.11}$$

where r is the radius, L is the length of the segment. The length of the upper segment, lower segment, hand segment was originated by the length of the segment vectors (Figure 2.2, panel C) respectively. The radius values of the same bone segments were set to be r_u=0.05 m, r_l=0.04 m, r_h=0.04 m where u, l, h denote the upper segment, lower segment, hand segment respectively.

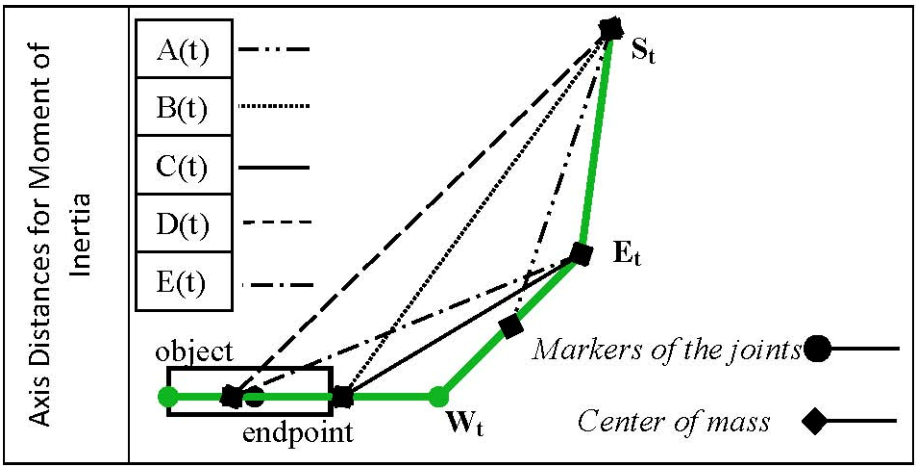

Figure 2.12. Distances between the center of mass of particular upper limb segments and the rotation centers (in the shoulder and elbow joints) used in the MoI calculation method. Green lines are the segments of the arm. S_t – shoulder; E_t – elbow; W_t – wrist are anatomical landmarks while the little finger Proximal Metacarp (Table 2.1, MARKER CHANNEL 7) is denoted as the endpoint.

In summary, the moment of inertia of the rotated upper limb around the shoulder if the object was not in the hand is defined by:

$$\overset{(S)}{I}(t) = \underset{end}{\overset{(U)}{I}} + \underset{center}{\overset{(L)}{I}} + M_L A^2(t) + \underset{center}{\overset{(H)}{I}} + M_H B^2(t) \tag{2.12}$$

where (U), (L) and (H) refer to the upper arm, lower arm and the hand respectively, $A(t)$ is the distance between the rotation axis of the shoulder and the center of mass of the lower arm, $B(t)$ is the distance between the rotational axis of the shoulder and the center of mass of the hand (Figure 2.12).

DOI:10.15774/PPKE.ITK.2012.004

Moment of inertia around the elbow joint when the load was not held is calculated as follows:

$$I^{(E)}(t) = I^{(L)}_{end} + I^{(H)}_{center} + M_H C^2(t) \tag{2.13}$$

where $C(t)$ is given by the distance between the rotation axis of the elbow and the center of mass of the hand (Figure 2.12).

In equations (2.10) – (2.11) the moment of inertia of elementary limb segments considered as uniform cylinders are given. In equations (2.12) – (2.13) the moment of inertia of all segments rotated around the shoulder and the moment of inertia of the lower segment and the hand rotated about the elbow joint are determined respectively taken the fact into account that in both cases the object to be moved was not the part of the kinematic chain since it was not in the hand of the individual.

In order to get the moment of inertial properties of the entire kinematic chain - when the object was added - first the detection of the duration of the holding the object time intervals had to be found for each subject individually for all trials.

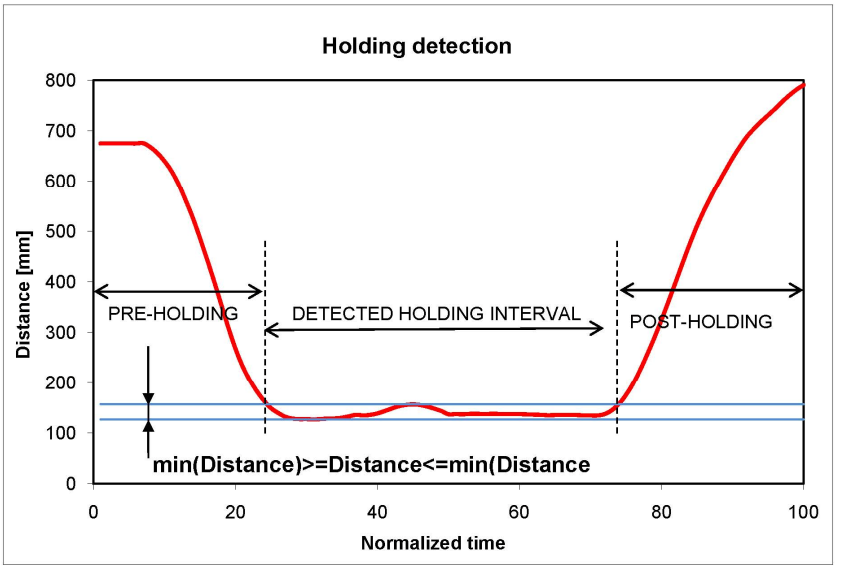

Figure 2.13. Detection of the holding periods for all trials. The threshold was assessed as the minimal distance between the markers (Table 2.1, MARKER CHANNEL) number 7 (marker on the Proximal Metacarp) and 8 (marker on the object moved by the individual) plus 25 mm to avoid measuring inaccuracy. Variation in holding time period was handled by the time normalization of each detected holding.

DOI:10.15774/PPKE.ITK.2012.004

The detection was done by using the distance between the marker placed on the little finger (Figure 2.2, panel A, marker 7) and the marker on the actual object (Figure 2.2, panel A, marker 8). Holding time interval within a trial was started if the distance between the base of the little finger and the object was smaller than a threshold. The threshold was assessed during the trial as the minimal distance between the two markers (Figure 2.2, panel A, markers 7 and 8) plus 25 mm to avoid any measuring inaccuracy (Figure 2.13). Holding was considered to be finished if the distance was greater than the threshold after detecting the start of a holding time interval. The duration of detected holding intervals were highly varied either across trials or across individuals. For further analysis time normalization of each holding period was performed.

The object was considered as a solid cylinder (a disc) and its moment of inertia was calculated by:

$$I^{(object)} = \frac{1}{2} M_{object} r_{object}^2 \tag{2.14}$$

where M_{object} is the mass of the object and r_{object} is the distance of its center of mass from the rotation center. According to the measurements, three different M_{object} conditions were defined. Therefore in the three cases M_{object} was set to be equal to 0.06, 1, 2 according to the mass of the actual object respectively. The radius of all objects was set to be equal to 0.06 m.

If the object was in the hand then the moment of inertia for the whole kinematic chain was calculated as the sum of (2.12) and (2.14) plus the square of the distance between the center of mass of the object and the rotation center (Figure 2.12, D(t)) multiplied by the mass of the object while for the rotation of the elbow and the hand $I^{(E)}(t)$ was calculated as the sum of (2.13) and (2.14) plus the square of the distance between the center of mass of the object and the rotation center (Figure 2.12, E(t)) multiplied by the mass of the object.

II.2.2.6. Gravitational Torque

Gravity is a natural phenomenon by which physical bodies are attract with a force proportional to their mass. Thus, if we would like the presented musculoskeletal model to

DOI:10.15774/PPKE.ITK.2012.004

be used under terrestrial conditions then the effect of the gravity must be taken into account. According to equation (2.1) the gravitational torque vector ($\overrightarrow{T_{g(\mathbf{joint})}(t)}$) is subtracted in each time step from the torque generated by the given joint. The magnitude of the gravitational torque vector was computed by multiplying the magnitude of the gravitational force vector (Figure 2.14, vectors signed by red dashed line) pointing from the center of mass (CoM) of the rotated segments to the ground by the magnitude of the gravitational moment arm (Figure 2.14, black dashed lines). The magnitude of the gravitational torque vectors are given by the equations (2.15) and (2.16) for the shoulder and elbow joints respectively.

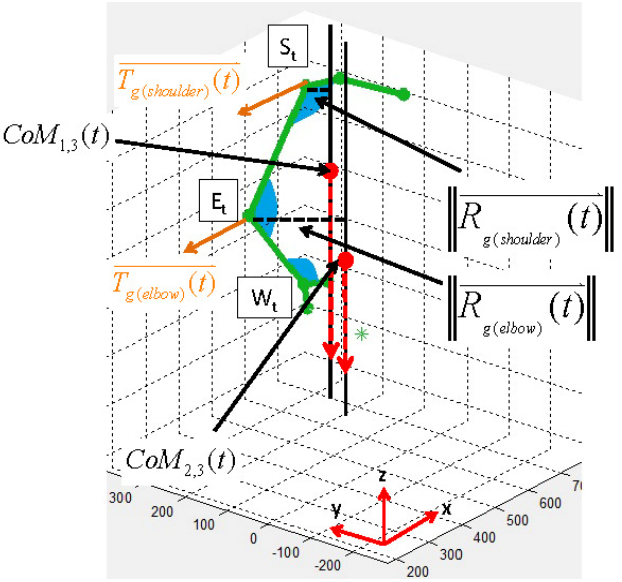

Figure 2.14. Schematic figure for representing the direction (perpendicular to the gravitational force) of the gravitational torque (orange vectors) vectors. The magnitude of the gravitational torque vectors are computed by multiplying the magnitude of the gravitational moment arm vectors ($\left\|\overrightarrow{R_{g(\mathbf{joint})}(t)}\right\|$) by the magnitude of the gravitational force vectors ($\left\|\overrightarrow{F_{g(\mathbf{joint})}(t)}\right\|$), (Equations (2.15-2.16)). The magnitude of the gravitational moment arm vector is assigned by black dashed lines while the gravitational force is signed by the vectors drawn by red dashed lines pointing from the center of mass ($CoM_{i,j}$) of the rotated part of the arm. Here, i and j are variables between $1 \leq (i,j) \leq 3$ numbering the three different segments (upper arm, lower arm and hand respectively). CoM_{13} is the center of mass of all upper limb segments rotated around the shoulder joint, while CoM_{23} defines the CoM of the lower arm and hand segments rotated about the elbow joint.

DOI:10.15774/PPKE.ITK.2012.004

$$\left\|\overrightarrow{T_{g(shoulder)}(t)}\right\| = \left\|\overrightarrow{R_{g(shoulder)}(t)}\right\| \cdot \left\|\overrightarrow{F_{g(shoulder)}(t)}\right\| \tag{2.15}$$

$$\left\|\overrightarrow{T_{g(elbow)}(t)}\right\| = \left\|\overrightarrow{R_{g(elbow)}(t)}\right\| \cdot \left\|\overrightarrow{F_{g(elbow)}(t)}\right\| \tag{2.16}$$

The direction of the gravitational torque was perpendicular to the force caused by the gravity and it pointed from the rotation center along the x axis in the negative direction (Figure 2.14, orange vectors). To determine the magnitude of the gravitational moment arm (Figure 2.14, black dashed lines) of the rotated body segments first the center of mass of the segments was given by:

$$CoM_{i,j}(t) = \frac{1}{M}\sum_{i=1}^{j} m_i s_i(t) \tag{2.17}$$

Here, i and j indexes are variables between $1 \leq (i,j) \leq 3$ numbering the three different segments (upper arm, lower arm and hand respectively) used in the model. Thus, CoM_{13} is the center of mass of all upper limb segments rotated around the shoulder joint, while CoM_{23} defines the CoM of the lower arm and hand segments rotated about the elbow joint. Furthermore, M refers to the sum of the segment masses (m_i) while $s_i(t)$ assigns the 3D coordinates of the CoMs of the individual segments located on the half of the particular segment. In this context the gravitational moment arm was the length of the perpendicular projection of the shoulder and elbow joints to the line going through CoM_{13} or CoM_{23} respectively which were parallel to the z axis.

$$\left\|\overrightarrow{F_{g(shoulder)}(t)}\right\| = \sum_{i=1}^{3} m_i g \tag{2.18}$$

$$\left\|\overrightarrow{F_{g(elbow)}(t)}\right\| = \sum_{i=2}^{3} m_i g \tag{2.19}$$

In equations (2.18) – (2.19) the calculations of the magnitude of the gravitational force vectors for the shoulder and elbow joints are written respectively.

DOI:10.15774/PPKE.ITK.2012.004

II.2.2.7. Defining Biomechanical Properties

Muscle fibers generate tension through the action of actin and myosin cross-bridge cycling. While under tension, the muscle may lengthen, shorten or remain at the same length. Voluntary muscle contraction is controlled by the central nervous system. Voluntary muscle contraction occurs as a result of conscious effort originating in the brain. If the goal (for instance a movement to execute) is known for the CNS it makes a plan to execute the desired movement. This plan is referred as the motor command. The brain sends the motor command to the spinal cord in the form of action potentials, through the nervous system to the motor neuron that innervates several muscle fibers. The α-moto neuron located in the ventral horn of the spinal cord generates action potentials and send them to the innervated muscle fibers. The stimulated muscle fibers then exert a contraction and the muscle force required to generate the desired torque is exerted. The amount of the force exerted by the muscle fibers primarily depends on the stimulation frequencies and the characteristics of particular muscle fibers composing the muscle itself. Such characteristics are the force-length relationship and the force velocity relationship.

The previous one also called the length-tension curve relates the strength of an isometric contraction to the length of the muscle at which the contraction occurs. In general, muscles operate at highest active force when close to an ideal length (often their resting length). When stretched or shortened beyond this, whether due to the action of the muscle itself or by an outside force, the maximum active force decreases [81]. This decrease is minimal for small deviations, but the force decreases rapidly as the length deviates further from the ideal. As a result, in most biological systems, the range of muscle contraction will remain on the peak of the length-tension curve, in order to maximize contraction force. Due to the presence of elastic proteins within a muscle (such as titin), as the muscle is stretched beyond a given length, there is an entirely passive force, which opposes lengthening.

The latter one, the speed at which a muscle changes length also affects the force a muscle can exert. Force declines in a hyperbolic way relative to the isometric force as the shortening velocity increases, reaching zero at some maximum velocity. The reverse holds true for when the muscle is stretched. The force increases above isometric maximum, until finally reaches an absolute maximum. This fact has strong effects for the rate at which muscles can perform mechanical work. Since power is equal to force

DOI:10.15774/PPKE.ITK.2012.004

multiplied by the velocity, the muscle generates no power at either isometric force (due to zero velocity) or maximal velocity (due to zero force). Instead, the optimal shortening velocity for power generation is approximately one-third of maximum shortening velocity.

Both fundamental biomechanical properties of muscles have several biomechanical consequences including limiting running speed, strength, and jumping distance and height. The force–length relationship is built in the presented model which uses exponential equations for generating the active and passive force-length characteristics based on data adopted from the literature.

Active-Passive Force-Length Relation

In 1938 among others Hill [81] proved that the force a muscle can exert is given by the sum of the active force ($F_a(l)$) and passive force ($F_p(l)$).

$F_a(l)$ is the force generated by the muscle compartment while $F_p(l)$ is resulted by connective tissues and tendons attaching the muscle to the bone surface. The biomechanical function determines how the active and passive components of the exerted force acted during the investigated movement using only computed muscle length determined by the personalized muscle geometry presented in the above subsections. Active and passive force components of the biceps (BI), triceps (TR), deltoid anterior and posterior (DA, DP) were determined separately.

Muscle length for each time instant was computed by using previously determined 3D muscle attachments originated on bone surfaces.

Active and passive characteristics of muscles were determined based on the following studies [82-85].

According to Woittiez *et al*., [82], [83] the unique characteristics of a muscle structure can be represented by the index of architecture (ia). It is calculated as the ratio of a single muscle fiber length to muscle belly length. Muscle belly length is defined as the distance between the proximal and distal tendon of the selected muscle.

Active and passive force-length relationships were characterized by the following exponential equations:

DOI:10.15774/PPKE.ITK.2012.004

$$F_a(\varepsilon, ia) = \exp\left(-\left(\frac{(\varepsilon+1)^{0.96343*(1-1/ia)}-1}{0.35327*(1-ia)}\right)^2\right) \tag{2.20}$$

$$F_p(\varepsilon, ia) = 0.0195*\exp\left(\left(2.933+\frac{4.911}{ia}\right)*\varepsilon\right) \tag{2.21}$$

where $F_a(\varepsilon,ia)$ is the normalized muscle tension; $F_p(\varepsilon,ia)$ is the normalized passive muscle force. ε is the muscle strain computed as $(L(t)-L_o)/L_o$. Here $L(t)$ denotes the muscle length at an arbitrary time instant and L_o is the optimum muscle length where the muscle is able to generate the peak force.

L_o were set as follows:

$$L_o = \min(L_a) + \left(\frac{\max(L_a)-\min(L_a)}{2}\right) \tag{2.22}$$

In this context L_a denotes the anatomical limits of muscle length of the investigated muscle. Thus, in order to compute the optimum muscle length of the certain muscle first the anatomical minimum ($\min(L_a)$) and maximum ($\max(L_a)$) muscle length must be determined using the given muscle geometry of the actual individual. In order to determine the anatomical muscle limits of the biceps and the triceps the elbow joint must be either fully outstretched or fully extended. In the previous case the inter-segmental joint angle of the elbow is about 180^o while in the latter one the inter-segmental elbow angle reaches approximately 20^o. The problem is that such angular postures were not reached by either of the participated individuals. Hence, the previously presented rotation method of Rodrigues was applied to virtually produce the mentioned maximum and minimum angular ranges.

In the case of the elbow joint the lower arm segment vector was rotated around the axis of rotation (the cross product of the lower segment and the upper arm segment vectors) until the inter-segmental joint angle reached the desired posture. If the desired posture

DOI:10.15774/PPKE.ITK.2012.004

was reached the length of the muscle was obtained considering the given muscle geometry. Using this method, in the fully extended elbow joint the maximum and minimum anatomical length of the biceps and the triceps were determined respectively while at the fully extended elbow posture the minimum and maximum biceps and triceps lengths were computed. In the case of the shoulder anatomical minimum and maximum muscle lengths were assumed to be equal to the minimum and maximum muscle lengths achieved by the shoulder muscles.

TABLE 2.3.
INDEX OF ARCHITECTURE VALUES ADOPTED FROM THE LITERATURE

	BI	**TR**	**DA-DP**
ia	0.67	0.39	0.7

Note. Index of architecture is the unique measure of muscles with different structures [82], [83]. *It is calculated as the ratio of a single muscle fiber length to muscle belly length. Ia. was used to define the active ($F_a(\varepsilon, ia)$) and passive force ($F_p(\varepsilon, ia)$) as the function of muscle strain according to equations (2.20)-(2.21) respectively.*

Index of architecture values of all investigated muscles were adopted from the literature (Table 2.3). BI ia was determined from Chang *et al*. [85]; TR ia was applied according to Friden and Lieber [86]. DA and DP index of architectures were set to be equal [87] because these two different parts of the deltoid muscle are pretty similar and strap-like [78], [80]. Index of architecture values are summarized in (Table 2.3). Using ia parameters and equations (2.20) – (2.22) the following biomechanical muscle characteristics were established.

DOI:10.15774/PPKE.ITK.2012.004

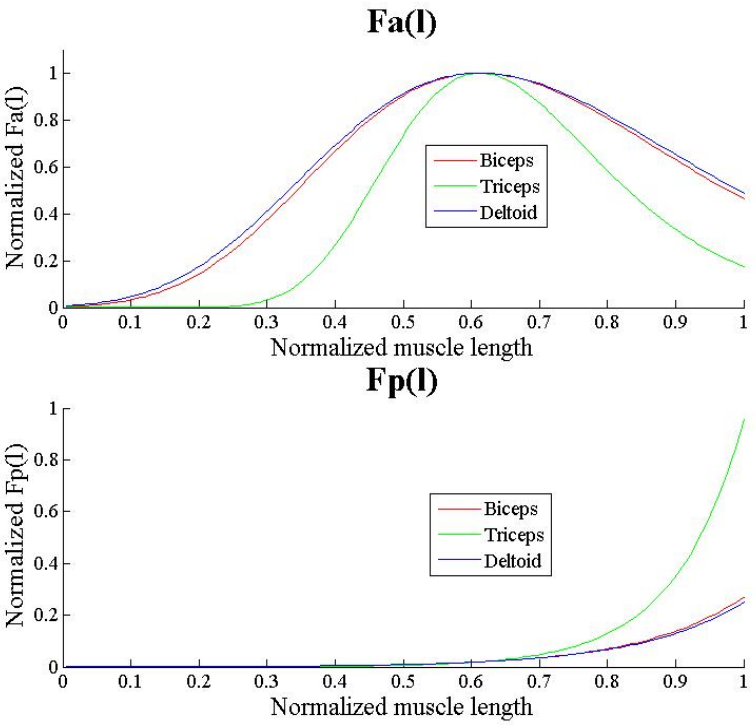

Figure 2.15. Normalized active (Fa(l)) and passive force (Fp(l))length relations for the investigated muscles. Note that in the case of the deltoid muscle the two different compartments (DA, DP) of the muscle were regarded to have the same structure.

Figure 2.16 summarizes the major steps of the development of the presented biomechanical model in the form of a block diagram.

DOI:10.15774/PPKE.ITK.2012.004

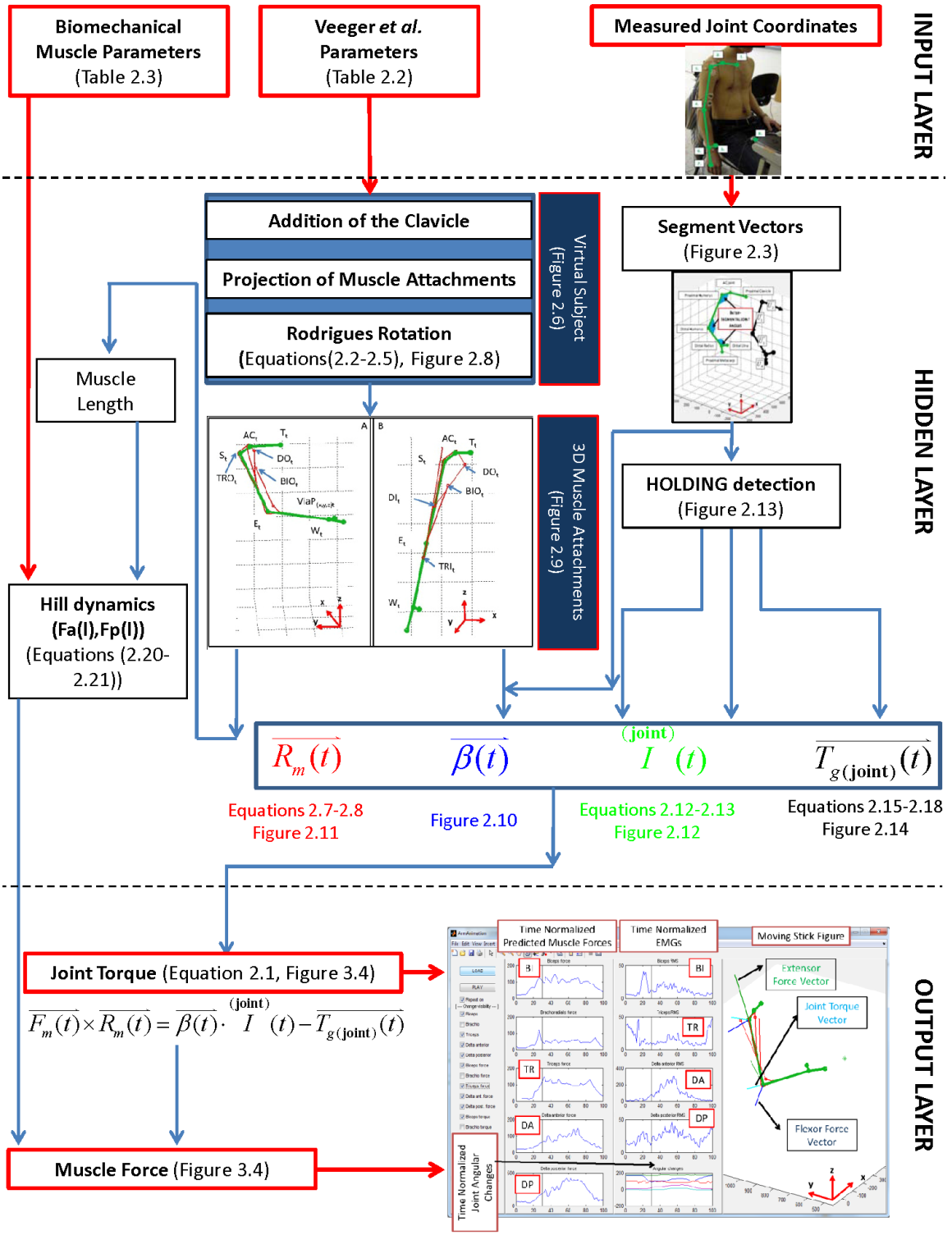

Figure 2.16. Block diagram of the joint torque and muscle force calculation method presented in this subsection. Input parameters of the model were 1) measured joint coordinates 2) muscle attachment parameters published by Veeger et al. [76] *3) biomechanical parameters of muscles (index of architecture, active ($F_a(l)$) and passive force ($F_p(l)$) length relations). In the hidden layer personalized segment geometry (segment vectors); personalized muscle geometry (3D muscle attachments located on the surface of the bone) were defined. Output parameters were joint torque of the shoulder and the elbow; muscle force of the biceps (BI), triceps (TR), deltoid anterior (DA) and deltoid posterior (DP).*

DOI:10.15774/PPKE.ITK.2012.004

II.3. Variance Analysis of Motor Control Levels

To study how particular motor control levels are affected under changing conditions (different object masses) variance analysis of kinematics and muscle activities were performed for the individuals (N=20; aged 21-25; mean±SD.: 21.1±1.9) participated in the biomechanical study summarized in this chapter. In the analysis 4 different motor control levels were discerned:

1) endpoint of the limb (EP)
2) joint configuration (JC)
3) surface electromyogramm (EMG)
4) predicted muscle forces (FORCE)

The variance analysis contained only two object conditions corresponding to the lightest (CD case; 0.06 kg) and the heaviest (O2; 2 kg) object masses.

II.3.1. Calculation of Variances of Motor Control Levels

The stability of the movement can be represented by calculating variances where the variance is used as the measure of how far a set of numbers are spread out from each other or in other words it describes how far the numbers lie from the mean (expected value). The calculation of the variance is given by:

$$\sigma^2 = Var(X) = E\left[\left(X-\mu\right)^2\right] = E\left[X^2\right] - \left(E\left[X\right]\right)^2 \tag{2.23}$$

If the variance of random variables, for instance muscle forces, is high than in the sense of motor control the exerted force differs from the average in a higher manner since the muscle force values lies far from the mean muscle forces.

Time normalized ($1 \le t \le 100$) variances of ten repetitively executed trials were calculated for the two conditions: 1) without load (CD case; 0.06 kg) 2) with load (O2; 2 kg) during lifting (UP) and putting-down (PD). In both object conditions the variances were computed for:

DOI:10.15774/PPKE.ITK.2012.004

A) the whole time interval of the lifting and putting-down,
B) the interval while the object was held in the hand (the holding)

for the above mentioned motor control levels such as the endpoint of the limb (EP) and joint configuration (JC) as kinematic levels and measured EMG and predicted muscle forces regarded as muscle activity levels.
As a consequence of the holding time interval every measured trial was divided into 3 time intervals (Figure 2.13). The first part was the time elapsed from movement initiation to the instant when the hand reached the object. This is the so-called pre-holding period. The second period was the time interval in which the object was held in the hand (holding) while the third part started when the individual released the object and ended when the arm was replaced to its initial position. This was the post-holding period.

The variance of the endpoint is determined by using the measured spatial coordinates of the ultrasonic marker placed on the little finger Proximal Metacarp (Figure 2.2, panel A, Table 2.1, [70]). Endpoint variances were determined as the sum of separately computed variances of the 3 coordinates of the endpoint position.

$$c_i = \left[c_{xi}; c_{yi}; c_{zi} \right] \tag{2.24}$$

First an EP vector (equation 2.24) was created by using the x,y,z coordinates (c_{xi},c_{yi},c_{zi} respectively) of marker 7. Here, i denotes the serial number of the actual trial. Since each condition was measured ten times in both lifting and putting-down i has a minimum value of 1 and a maximum value of n where n denotes the maximum number of the trials (n =10).

$$\bar{c} = \left[\frac{\sum_{i=1}^{n} c_{xi}}{n-1}; \frac{\sum_{i=1}^{n} c_{yi}}{n-1}; \frac{\sum_{i=1}^{n} c_{zi}}{n-1} \right] \tag{2.25}$$

In the next step by using the EP vector (c_i) the average EP vector ($\bar{c}$) was obtained based on all measured trials in both lifting and putting-down.

DOI:10.15774/PPKE.ITK.2012.004

$$\sigma_{EP}^2 = \frac{\sum_{i=1}^{n}\left(\bar{c} - c_i\right)^2}{n-1} \tag{2.26}$$

Finally, the square deviation of the endpoint coordinates was computed based on equation (2.26).

Joint configuration variances (arm configuration variances) were obtained as the sum of separately computed joint angle variances. To determine the variance under different object conditions for the joint configuration, first α_i JC vector was obtained by using the shoulder inter-segmental joint angle $\alpha_{(\text{Shoulder})i}$ (the joint angle determined by $\overrightarrow{U_1}$ and $\overrightarrow{U_2}$ segment vectors); elbow inter-segmental joint angle $\alpha_{(\text{Elbow})i}$ (the joint angle computed from the $\overrightarrow{U_1}$ and $\overrightarrow{U_3}$ segment vectors) and the inter-segmental joint angle in the wrist $\alpha_{(\text{Wrist})i}$ (defined by $\overrightarrow{U_3}$ and $\overrightarrow{U_4}$ segment vectors) where i assigns the number of the actual trial.

$$\alpha_i = \left[\alpha_{(Shoulder)i}; \alpha_{(Elbow)i}; \alpha_{(Wrist)i}\right] \tag{2.27}$$

By using the JC vector (α_i) an average JC vector ($\bar{\alpha}$) was composed based on equation (2.28).

$$\bar{\alpha} = \left[\frac{\sum_{i=1}^{n}\alpha_{(Shoulder)i}}{n-1}; \frac{\sum_{i=1}^{n}\alpha_{(Elbow)i}}{n-1}; \frac{\sum_{i=1}^{n}\alpha_{(Wrist)i}}{n-1}\right] \tag{2.28}$$

The variance of the JC (σ_{JC}^2) was then originated as the sum of squares of the difference of the mean JC vector ($\bar{\alpha}$) and the actual JC vector (α_i) divided by n-1.

$$\sigma_{JC}^2 = \frac{\sum_{i=1}^{n}\left(\bar{\alpha} - \alpha_i\right)^2}{n-1} \tag{2.29}$$

DOI:10.15774/PPKE.ITK.2012.004

The variance for muscle activities either EMGs or predicted muscle forces were computed for each investigated muscle separately in order to present any change in muscle activation levels.

$$\overline{EMG} = \frac{\sum_{i=1}^{n} EMG_i}{n-1} \tag{2.30}$$

$$\sigma_{EMG}^2 = \frac{\sum_{i=1}^{n} \left(\overline{EMG} - EMG_i \right)^2}{n-1} \tag{2.31}$$

$$\overline{FORCE} = \frac{\sum_{i=1}^{n} FORCE_i}{n-1} \tag{2.32}$$

$$\sigma_{FORCE}^2 = \frac{\sum_{i=1}^{n} \left(\overline{FORCE} - FORCE_i \right)^2}{n-1} \tag{2.33}$$

Using equations (2.30) and (2.32) the mean vectors of the EMG ($\overline{EMG}$) and predicted muscle forces ($\overline{FORCE}$) were generated respectively. In equations (2.31) and (2.33) the variance of the measured surface EMGs and the muscle forces were determined for the BI, TR, DA, and DP muscles.

In A) the above summarized variance calculation methods were applied to compute variances as a function of normalized time resulting column vectors with the length of 100 for all the twenty individuals. Thus the variances at each percentage of total movement time were computed for each individual separately.

In B) variance calculation methods were only applied for detected and time normalized holding periods (t=35) resulting column vectors with the length of 35 for all the twenty individuals. The length of the time normalized holding periods was chosen by taking into account that holding time lasted approximately the one-third of the entire movement time. Since, the entire movement time was 100% the holding time was regarded as 35%.

DOI:10.15774/PPKE.ITK.2012.004

Variance vectors in both A) and B) were averaged across normalized time and then assigned to the actual object condition during both lifting and putting-down for the twenty participated individuals separately.

The data structure created in the variance analysis is presented in (Figure 2.17) in the case of the endpoint either for the whole movement execution time (Figure 2.17, case B)) or for time normalized holding periods (Figure 2.17, case C-D)). The same data processing method was applied for all motor control levels.

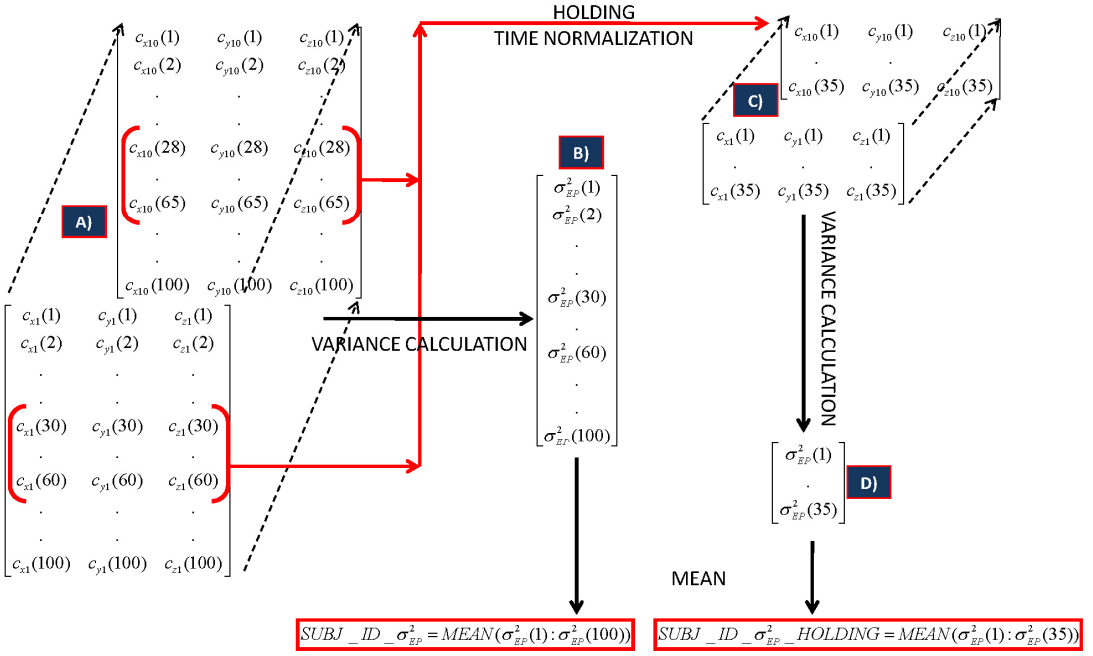

Figure 2.17. Schematic view of the creation of variance data structures in the case of the endpoint (EP) for the whole movement time interval (case B)) and for detected holding periods (case C-D)). In the most left block (A) time normalized 3D coordinates of the endpoint (Table 2.1, MARKER CHANNEL 7) are presented. First, variance calculation of the whole movement interval was performed. As a result, a column vector containing the variance of the EP at each percentage of total movement time was generated (B). Red blocks in (A) are detected holding time intervals. In the second step, a block of detected holding time intervals (C) was generated for all trials. Finally, as a result of variance calculation a column vector (D) containing the variances of the endpoint during holding was generated. Using (B) and (D) the mean of endpoint variances was obtained as a function of normalized time.

The same data processing method is applied for all the discerned motor control levels. As a result, the motor variances of an individual are represented by 1.) the mean variances across the whole movement time 2.) by the mean variances across the holding time interval.

DOI:10.15774/PPKE.ITK.2012.004

II.3.2. Computation of the Ratios of Mean Variances

The question is whether the effect of the object with distinct masses held in the hand is different on motor variances at particular motor control levels? Thus, during the analysis only the variances obtained in the holding period were taken into account.

In order to investigate this, first the mean variances for all individuals were obtained for all controlling levels concerning both object conditions during lifting and putting-down as well. Then the mean variance across holding with load (O2) was divided by the mean variance across holding without load (CD) for both kinematic variances and muscle activity variances for each individual separately (ratios within subjects). If the ratio is smaller for a certain motor control level than 1 than the central control of the nervous system tends to stabilize the movement better under O2 than under CD conditions. Variance ratios ((meanO2/meanCD)), (Figure 2.18) across all individuals (ratios between subjects) were generated by dividing the mean O2 (meanO2) variance across individuals by the mean CD (meanCD) variance across all individuals.

II.3.3. Statistical Analysis – Repeated Measures ANOVA

Variances of kinematic data, measured EMGs and predicted muscle forces observed during the entire movement and during holding were analyzed by performing a two-way repeated-measures ANOVA (Figure 2.18) with $p<0.05$ significance level. The effect of load conditions (CD, O2) were processed as within-group factors by using repeated measured ANOVAs executed for all investigated level of control (endpoint, joint configuration, EMGs, predicted muscle forces). At muscle levels the effect of the external load was analyzed for each muscle separately. Lifting and putting-down were investigated independently from each other. The block diagram of the variance calculation method is presented in Figure 2.18.

In summary, endpoint of the limb, joint configuration, EMG, muscle force parameters were regarded as the input layer of the variance calculation method. In the variance layer, the variances of ten trials for each condition (UP, DOWN, CD, O2) were composed based on the processes presented in Figure 2.17. In the statistical layer the mean variances for all individuals were computed. Using the mean variances of movements performed with the O2 and the mean variances of movements executed with the CD the ratio (meanO2/meanCD) was generated. Based on the mean variances across participants

DOI:10.15774/PPKE.ITK.2012.004

between and within subjects standard deviations were obtained and compared to each other. Statistical investigations were made by using repeated measures ANOVA at $p<0.05$ significance level.

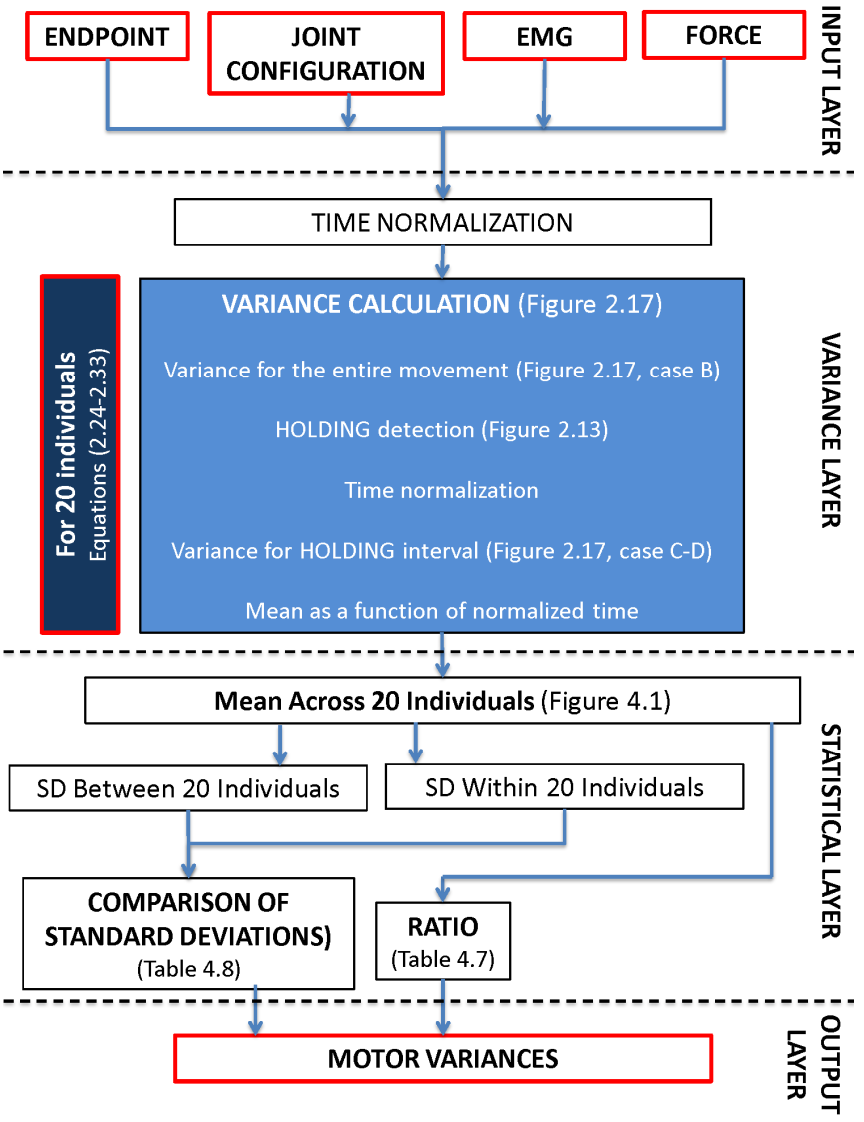

Figure 2.18. The block diagram of the variance analysis method used to demonstrate the effect of altering object conditions on motor control levels (endpoint, joint configuration, EMG, muscle force). These parameters were regarded as the input layer of the variance calculation method. In the variance layer, the variances of ten trials for each condition (UP, DOWN, CD, O2) were composed based on the processes presented in Figure 2.17. In the statistical layer the mean variances for all individuals were computed. Using the mean variances of movements performed with the O2 and the mean variances of movements executed with CD the ratio (meanO2/meanCD) was generated. Based on the mean variances across participants between and within subjects standard deviations were obtained and compared to each other. Statistical investigations were made by using repeated measures ANOVA at $p<0.05$ significance level.

DOI:10.15774/PPKE.ITK.2012.004

Chapter III

PREDICTION OF MUSCLE FORCES FROM JOINT COORDINATES

III.1. Introduction

Functional electrical stimulation is a rehabilitation technology that can restore some degree of motor function in individuals who have sustained a spinal cord injury or stroke. The effective application of FES in the rehabilitation of both the lower and the upper limbs was summarized in the preface, although the development of FES control methods are not in the scope of the dissertation.

However, by extending the electrical stimulation methods with 3D simulation results of muscle forces based on particular muscle and segment characteristics would improve the effectiveness of the rehabilitation procedure.

No information have been found so far whether FES applied together with 3D biomechanical modeling would be applied for the entire upper extremity. This is caused by the high complexity of the shoulder girdle which makes the number of DOF increased resulting a more complex methodology.

Whole upper limb models ([26], [27], [88-91] or partial studies [29-31], [34], [92] have been described over the past decades. These models were mostly developed to study the static effects of muscles and joint torques. Other models include dynamic control of Hill type muscles [93], [94]. A general issue with dynamic models is that the correctness of these models was only verified under simple limb movements (elbow flexion-extension; pronation-supination; shoulder abduction-adduction) in restricted planes.

Another virtual 3D model of the arm consisting of 4 segments (the humerus, the ulna, the radius and the hand) and personalized muscle geometries using parameters published by Zajac [95] and Zajac and Gordon [37] were developed for getting accurate biomechanical analysis by Pennestri *et al*. [38].

EMG driven models are used for predicting muscle forces in single and multi joint movements and for estimating the corrective changes in muscle activation patterns needed for stroke patients to walk [40].

DOI:10.15774/PPKE.ITK.2012.004

These approaches gave some insight into human limb coordination. Further 3D biomechanical models are applied in robot assisted rehabilitation of after stroke limb injury [41], [96].

All in all it would be desirable to 1) improve the efficiency of rehabilitation techniques or 2) to develop new methods using 3D muscle force simulation approaches based on both individual anthropometric and neuro-biomechanical limb properties. Simulation models for two dimensional (2D) movements have been developed to discern motor activity patterns of musculoskeletal systems [45], [46]. 2D inverse kinematic problem was studied in a neuro-mechanical transducer model that computes possible muscle forces and firing frequencies of flexor and extensor motoneuron pools during voluntary limb movements [48].
The model and the predicted muscle forces and joint torques presented in this dissertation are based on both 3D kinematic properties and electrical muscle activities of the upper limb. Furthermore, the prediction of muscle forces and joint torques was done for a slightly restricted (avoiding pronation-supination), complex point to point movement with objects having distinct masses in the hand.

Principally, in this chapter the results and important findings of the simulation method are summarized. The invariant nature of the predicted torque profiles under specific conditions is revealed and the framework for displaying personalized muscle and limb geometries is introduced.

III.2. Results

In the previous chapter a new method for predicting 3D muscle force vectors were presented to generate the torque to establish the required joint angular changes in the shoulder and elbow joints during the execution of point to point upper limb movements under altering load conditions only using previously measured 3D coordinates of 7 anatomical landmarks (Figure 2.2, panels A and C).
The force a muscle can exert was determined by using the equation (2.1.) for the cases when only one muscle was activated at a given time instant. The presented model was simulated on healthy individuals (N=20) by using the measured joint coordinates as the inputs of the model. The outputs (without details) are the magnitude of predicted 3D

DOI:10.15774/PPKE.ITK.2012.004

force (Figure 3.1) and torque vectors (Figure 3.2); the direction of the 3D muscle force (Figure 3.4) and joint torque vectors (Figure 3.4) for all object conditions (CD, O1, O2) in both directions (LIFTING, PUTTING DOWN). Mean torque profiles (magnitude of torque as the function of time) of all trials were generated within each individual for the three object conditions during lifting and putting-down separately for both the entire and the holding movement periods. Ten trials of each individual were averaged. The mean muscle force of one representative subject for the whole movement time and the mean joint torque profiles for holding are shown in Figure 3.1, Figure 3.2 respectively.

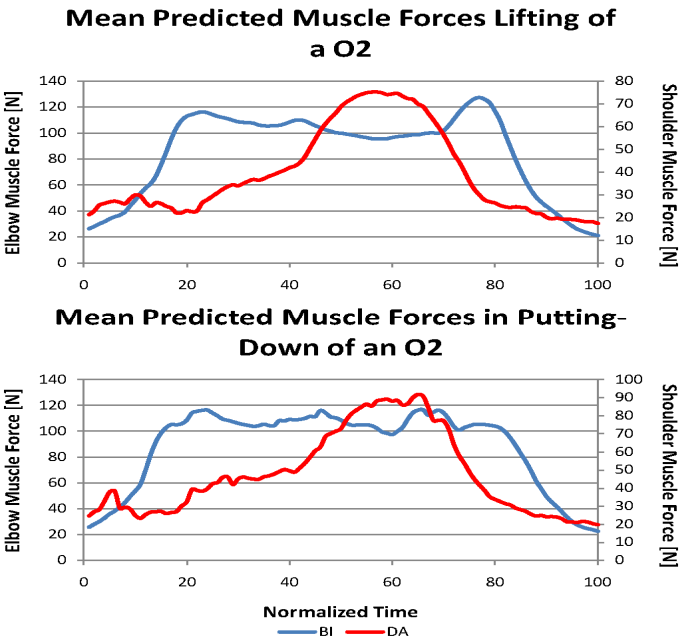

Figure 3.1. Mean muscle force magnitudes as the function of normalized time are depicted for one representative individual. 10 trials of lifting with O2 (upper panel) and 10 trials of putting-down with O2 (lower panel) were averaged.

DOI:10.15774/PPKE.ITK.2012.004

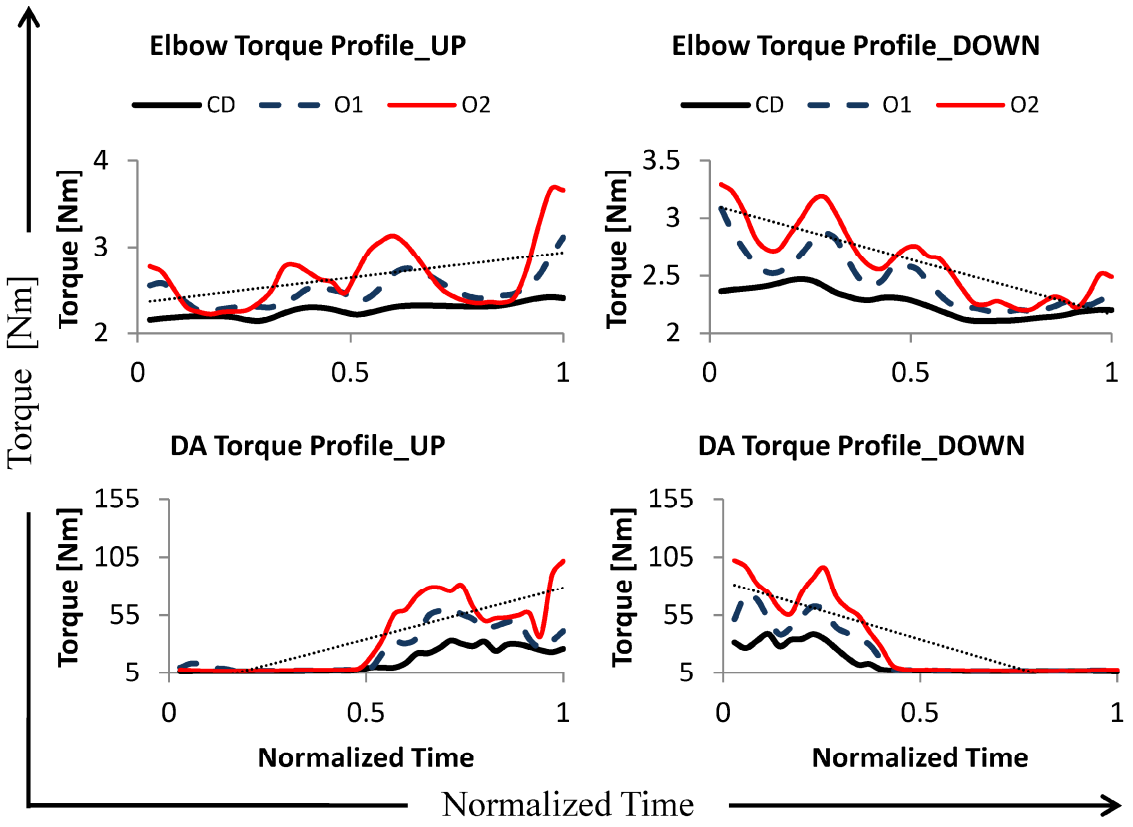

Figure 3.2. Mean predicted torque profiles of ten trials in each object conditions (CD, O1, O2) for both movement directions (UP, DOWN) observed during holding time interval (the period during which the subject was holding the object) for one representative individual (number 1). Dotted lines (linear regression fit) sign the linear increasing or decreasing tendency of the torque during lifting and putting-down respectively. Only the range but not the shape of the torque-time curve depended on the mass of the object held in the hand. The magnitude of joint torques was larger for heavier objects than for the lightest one in both joints. The invariance of the shape is supported by the correlation coefficients performed for all conditions (considering all movement directions and object masses) in both joints (shoulder and elbow) summarized in Table 3.1.

To present the effect of changing object conditions on mean torque profiles correlation analysis was performed for the holding time intervals (Table 3.1). The strongest (**$0.77 \leq r \leq 0.99$**) Pearson's coefficients were observed when comparing the linear relation between O1 and O2 torque curves. Weaker ($0.35 \leq r \leq 0.98$) but still strong linear correlation was present between CD and O1 torque profiles while the weakest ($0.12 \leq r \leq 0.96$) correlation was found between CD and O2 conditions. Because mean correlation coefficients are higher than 0.58 in all object conditions for both directions indicating high linear connection between separate conditions, the torque profile is considered to be object invariant for both directions (Table 3.1).

DOI:10.15774/PPKE.ITK.2012.004

TABLE 5.1.
PEARSON'S R-VALUES OF ALL SUBJECTS FOR THE ELBOW AND SHOULDER JOINT TORQUES OBSERVED DURING HOLDING CONSIDERING ALL OBJECT CONDITIONS.

SUBJID	ELBOW TORQUE						SHOULDER TORQUE					
	UP			DOWN			UP			DOWN		
	CD-O1	CD-O2	O1-O2	CD-O1	CD-O2	O1-O2	CD-O1	CD-O2	O1-O2	CD-O1	CD-O2	O1-O2
1	0.71	0.58	**0.85**	0.89	0.87	**0.97**	0.69	0.79	**0.9**	**0.91**	0.77	0.8
2	0.69	0.51	**0.88**	0.9	0.82	**0.95**	0.75	0.87	**0.9**	0.92	0.87	**0.95**
3	0.89	0.74	**0.92**	0.89	0.87	**0.9**	0.98	0.97	**0.99**	0.95	0.9	**0.97**
4	0.63	0.55	**0.86**	0.87	0.83	**0.94**	0.51	0.71	**0.87**	0.9	0.84	**0.98**
5	0.83	0.66	**0.88**	0.66	0.76	**0.89**	0.79	**0.93**	0.73	**0.97**	0.86	0.87
6	0.86	0.72	**0.91**	0.55	0.72	**0.92**	0.88	0.81	**0.93**	0.92	0.91	**0.97**
7	0.67	0.62	**0.86**	0.97	0.96	**0.98**	0.45	0.5	**0.8**	0.95	0.94	**0.99**
8	0.85	0.74	**0.92**	0.95	0.94	**0.97**	0.82	0.76	**0.83**	0.9	0.75	**0.98**
9	-0.3	-0.01	**0.87**	0.4	**0.72**	-0.08	0.35	0.12	**0.86**	**0.87**	0.75	0.79
10	0.44	0.37	**0.86**	0.9	0.87	**0.97**	0.75	0.74	**0.89**	0.79	0.72	**0.94**
11	0.64	0.58	**0.85**	0.81	0.7	**0.82**	0.9	0.8	**0.91**	0.9	0.89	**0.93**
12	0.33	0.63	**0.83**	0.9	0.69	**0.98**	0.22	0.2	**0.87**	0.79	0.64	**0.9**
13	0.79	0.78	**0.87**	0.97	0.86	**0.98**	0.64	0.6	**0.94**	0.97	0.96	**0.98**
14	0.68	0.54	**0.91**	0.86	0.63	**0.88**	0.9	0.85	**0.91**	0.96	0.76	0.87
15	0.87	0.8	**0.91**	0.85	0.84	**0.95**	0.97	0.96	**0.98**	0.95	0.94	**0.97**
16	0.16	0.42	**0.46**	-0.6	-0.6	**0.8**	0.04	0.05	**0.33**	-0.83	-0.92	-0.8
17	0.48	0.40	**0.9**	0.3	0.25	**0.84**	0.83	0.74	**0.86**	0.9	0.89	**0.94**
18	0.47	0.4	**0.91**	0.52	0.33	**0.77**	0.85	0.81	**0.94**	0.94	0.9	**0.96**
19	0.76	0.71	**0.98**	0.81	0.79	**0.85**	**0.91**	0.79	0.85	0.9	**0.98**	0.94
20	0.81	0.79	**0.98**	0.67	0.61	**0.77**	0.83	0.81	**0.88**	0.78	0.7	**0.8**
Mean	0.61	0.58	**0.87**	0.70	0.67	**0.85**	0.70	0.69	**0.85**	0.81	0.75	**0.83**
SD	0.29	0.24	0.10	0.38	0.35	0.23	0.25	0.26	0.13	0.39	0.40	0.39

*Note. Generally, the strongest (**0.77 ≤ r ≤ 0.99**) (close to perfect + correlation) correlation coefficients were found between O1 and O2; weaker but strong (0.35 ≤ r ≤ 0.98) correlation appeared between CD and O1; the weakest coefficients (0.12 ≤ r ≤ 0.96) occured between CD and O2 for both directions and joints. Correlation coefficients in the case of subjects 9 and 16 showed negative correlation in the comparison of CD-O1 and CD-O2. Since the mean of all coefficients is higher than 0.58 with small SD, torque profiles are regarded object invariant under the given object circumstances.*

The magnitude but not the shape of the torque-time curve depended on the object held in the hand. The magnitude and the amplitude of joint torques were larger for heavier objects than for the lightest one in both the elbow and the shoulder. For lifting movements the joint torques show increasing profiles, though for putting-down they show decreasing profiles (Figure 3.2).

Mean joint torques are depicted as a function of mean elbow and shoulder joint angles to demonstrate the dependence of torque on individual joint angles under all object conditions (Figure 3.3). Mean torque curves were fitted by 4^{th} order polynomials. Note that elbow and shoulder angles are in increasing order and not in order of occurrence during the movement execution. Similar polynomially approximated torque characteristics were observed during putting-down.

DOI:10.15774/PPKE.ITK.2012.004

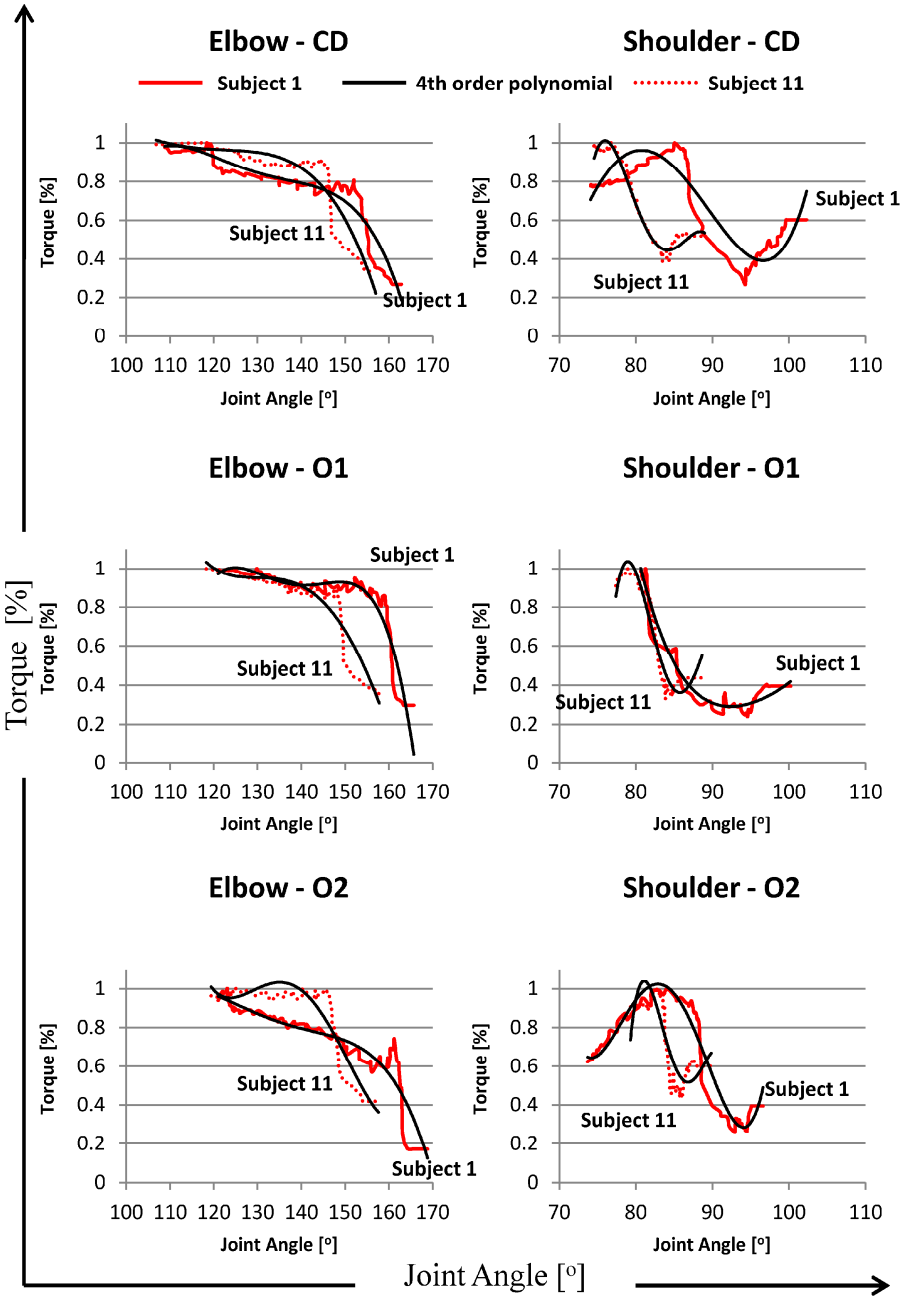

Figure 3.3. Mean joint torque of ten trials under each load condition (CD, O1, O2) of two individuals (number 1 and 11) are depicted as a function of mean elbow and shoulder joint angles during lifting for the entire time of movement execution. Elbow and shoulder joint angles are in increasing order and not in order of occurrence during movement execution. Torque curves were approximated by 4th order polynomial fits. Joint angles may span different angular domains but with similar torque-angle curves. Subject 11 has a smaller angular domain than subject 1. but the torque-angle curves are similar in the sense that the fourth order polinom associated to subject 1 is transformed into a fourth order polinom with a smaller angular domain associated to subject 11. The predicted torque in the elbow slightly increased and then decreased with the extension of the elbow which is in agreement with the findings of Uchiyama et. al., (1998). The torque in the shoulder coincides with the results of the shoulder torque profiles provided by Landin & Thompson (2011). Similar polynomially approximated torque characteristics are present during putting-down.

DOI:10.15774/PPKE.ITK.2012.004

To be competitive with other biomechanical models [28], [89-91], [97] besides the modeling part of the research work (written in Chapter 2) a framework was also developed for displaying the direction and magnitude components of the predicted force vectors on a moving 3D stick figure referring the individual whose joint coordinates were used as the inputs of the model. Furthermore, some other parameters characterizing the movement were added as references of the investigated trial. Such parameters are primarily the angular changes of the shoulder, elbow and wrist joints, 3D angular acceleration, 3D torques generated by the spanning muscles in the rotation center, measured EMG activities of 4 upper limb muscles (BI, TR, DA, DP) (Figure 3.4).

Remark: The brachioradialis muscle was defined in the model geometrically. However its activity was not taken into account either during the simulation of all individuals or in the variance analysis of different movement control levels (see Chapter 4).

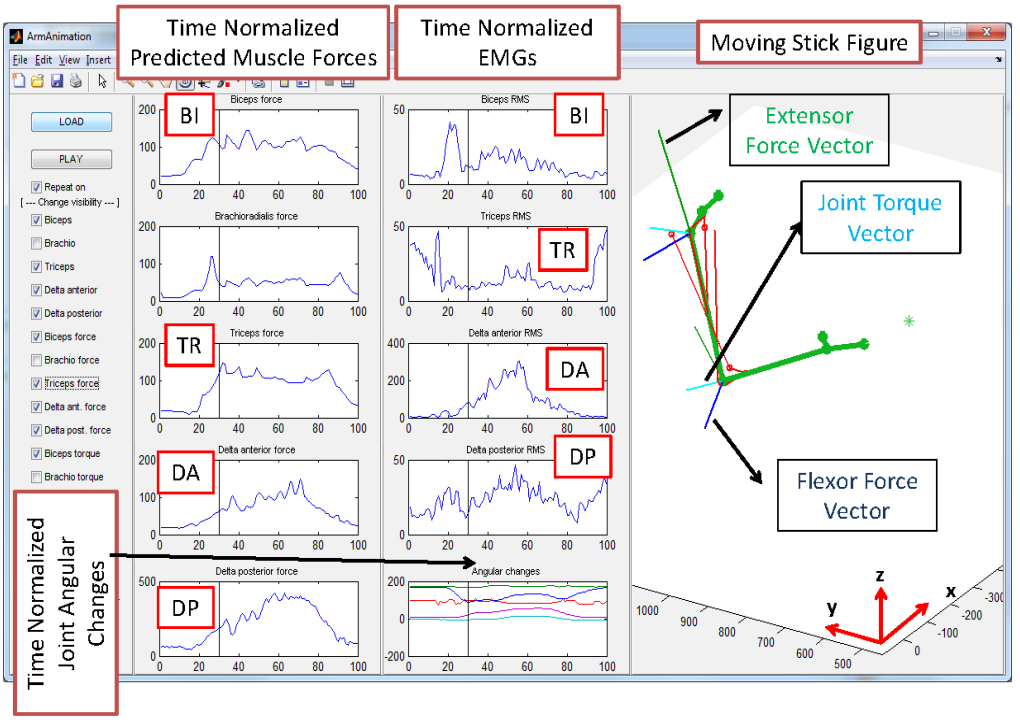

Figure 3.4. A framework for displaying the predicted 3D muscle force and joint torque vectors was developed. It is divided into 3 different parts. From left to the right these are the parts for displaying the magnitude of predicted time normalized muscle force vectors; time normalized filtered and smoothed muscle activities; moving 3D stick figure with given muscle geometry. Light green lines represent the upper limb segments, red lines show personalized muscle geometry, light blue lines are torques in the joint generated by the spanning flexor (green) and extensor (dark blue) muscle forces.

DOI:10.15774/PPKE.ITK.2012.004

Mainly, the framework is divided into 3 different parts. From left to the right these are the parts for displaying the magnitude of predicted time normalized muscle force vectors; time normalized filtered and smoothed muscle activities; moving 3D stick figure with given muscle geometry respectively.

Remark: Basically, the presented 3D biomechanical model can be used for muscle force prediction and for the proper analysis of the motor behavior under changing conditions. In this result section the analysis of the motor control levels under different object conditions was not involved since the results of the variance analysis are summarized in details in the following chapter.

III.3. Discussion

To make a voluntary movement, the motor system must be capable of converting a desired goal (e.g. reaching and grasping an object in front of us) into an action plan and principally into the spinal motoneuron activity that is able to produce the required muscle contractions through innervations of muscle fibers. This involves coupled open-loop feed-forward and closed-loop feedback control mechanisms. Feed-forward processes performed by neurons convert the goal into a motor command that is further transformed by the spinal cord into muscle activity. Proprioceptive and visual feedback closes the motor control loop by sending information to the motor system about the physical consequences of the motor command [98].

Figure 3.5 illustrates different internal models that describe various aspects of the properties of the limb. The inverse kinematics part of the system is able to determine the relationship e.g. between hand position in space and limb joint angles while inverse dynamics gives the relationship between joint angles and muscle force required to establish the desired torque. These parts of the motor system are used to perform feed-forward sensorimotor transformations in order to convert signals on target location and current limb position into motor commands or to transform sensory information and motor-command within feedback pathways into estimates of current behavioral state. Such state estimates can be compared with information about desired behavior to generate on-line error-correction signals.

DOI:10.15774/PPKE.ITK.2012.004

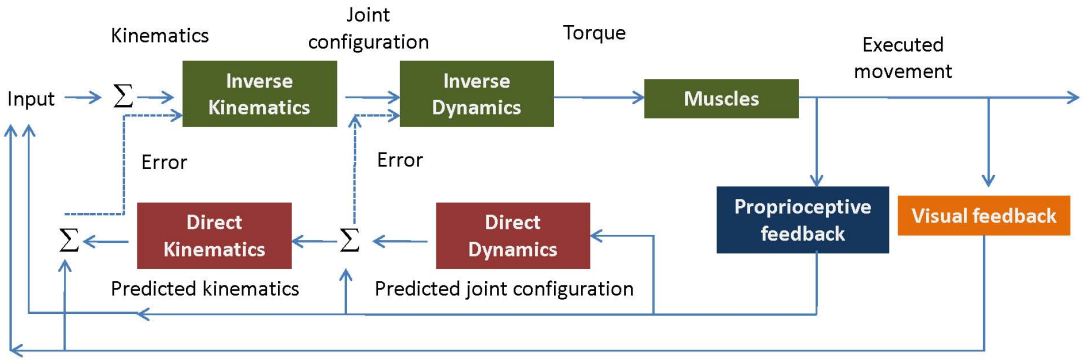

Figure 3.5. Schematic figure of internal models in the central nervous system for executing a movement and for adaptation to different external effects (changing object condition).

In the above presented 3D neuro-biomechanical model the feed-forward part of the system was focused to have proper information on the torques required to be generated through muscle forces so as to execute a desired point to point upper limb movement at a certain amount of angular changes.

An inverse dynamic problem solver in the 3D space was presented to predict joint and muscle activation patterns (joint torque, muscle force). The prediction was made by using previously measured 3D coordinates of anatomical landmarks and anthropometric features of the upper limb during the execution of dynamic, slightly constrained upper limb movements (see Chapter 2).

The presented model has pointed out that the studied movement (lifting and putting-down an object with distinct masses along the sagittal plane) can be executed only by activating the flexor muscles of the elbow and shoulder joints separately considering the time courses of the activation patterns while the gravity might be considered acting as an extensor. This finding is supported by Landin *et al*. [99] and Landin and Thompson [100] who investigated the contribution of the biceps brachii and triceps brachii to the activation of shoulder muscles in different static postures and found that these flexors had only a minimal influence on shoulder muscle activation during the elevation of the arm. Furthermore, Landin and Thompson [100] demonstrated that the torque in the shoulder joint was the greatest at about 80^0 of shoulder elevation and slightly decreased as the shoulder angle moved to higher angular ranges. These findings coincide with the shoulder torque generation profiles that are resulted by the model (Figure 3.3). An important finding is that the torque profile is object invariant (Table 3.1).

DOI:10.15774/PPKE.ITK.2012.004

The same correlation analysis was performed for muscle forces of the biceps and deltoid anterior (Table 6.1). The strongest ($0.21 \leq r \leq 0.99$) correlation coefficients were observed between O1 and O2, weaker correlation ($-0.1 \leq r \leq 0.98$) was present between CD and O1 and the weakest coefficients ($-0.89 \leq r \leq 0.97$) were obtained between CD and O2 in the case of the force exerted by the biceps during lifting. Such correlation patterns were not present either during putting-down in the case of the biceps or in the case of the deltoid anterior muscle considering both directions. Therefore, the object invariant feature observed for the torque profiles is not true for the force profiles.

The results show that under different conditions the joint angles may span different domains but with similar torque-angle curves (Figure 3.3). The predicted torque in the elbow increased and then decreased with the extension of the elbow (Figure 3.3).
Such elbow joint torque behavior was elicited by Uchiyama *et al*. [101] during the investigation of angle - joint torque and angle - EMG relations. In the shoulder the domain of the measured joint angles under O1 condition is smaller than for the other conditions, thus the related 4^{th} order polynom has a smaller domain.
This reflects that there is a general central action pattern that is implemented under different external conditions. This finding can be compared with other observations that presented the dependence of arm movement trajectories on the size of the movement. For instance if the motor task is to draw a figure under the following conditions: on a paper of A4 size, or on a large blackboard then the endpoint trajectory differs in size but the trajectory profile is invariant due to a certain pattern [4].

The applicability and reality of the model was checked by comparing computed moment arm data with experimental results adopted from the literature. It has been shown by many studies that physical features such as inertia and MA vary over a wide range depending on anthropometric properties and muscle path [29], [102], [103]. Thus, from the modeling point of view it is important to have accurate attachments, since MA and torque are sensitive to the location of muscle insertion and origin areas. Furthermore, it is difficult to resolve the inconsistencies on the range of peak MAs because either anatomical or modeling studies have investigated peak magnitudes of MAs under restricted, static conditions.

DOI:10.15774/PPKE.ITK.2012.004

TABLE 3.2.
COMPARISON OF PREDICTED AND MEASURED PEAK MOMENT ARMS ADOPTED FROM THE LITERATURE GIVEN AS A FUNCTION OF JOINT ANGULAR RANGE.

	Peak Magn. (cm)	**Ang. Range (^{o})**	**Peak Magn. (cm)**	**Ang. Range (^{o})**
	Murray et. al.		*Predictive Model*	
BI	3.5-5	>80	2.2-5	110-150
TR	2.5-3.5	0-40	2-3	140-160
	Kuechle et. al.			
DA	3-4	65-80	4-8	80-95
DP	0.4-2.2	20-40	2-2.5	80-85

Note. In the left peak moment arm magnitudes and angular ranges concerning to the peak moment arms are presented based on data adopted from the literature. In the right the same values predicted by the presented biomechanical model are summarized. The presented model predicted similar moment arm ranges for all individuals considering the three object conditions than it had been published for dynamic and static movements by Murray et al. [102] *and Kuechle et al.* [104] *respectively.*

Table 3.2 summarizes the minimum and maximum predicted peak MAs observed in holding under all object conditions. Minimum and maximum were computed across all individuals and all conditions. Moment arm ranges predicted by the model are similar to those published for dynamic and static movements by Murray *et al*. [102] and Kuechle *et al*. [104] respectively for all individuals.

In the future the model will be extended to be capable of predicting the relationship between the generated muscle forces and stimulation frequencies (motor command) applied by the central nervous system. If this relationship is revealed then the model will be capable of predicting movement patterns for reproducing reaching and grasping arm movements artificially by using FES. In that case it would be desirable to take the feed-back part of the motor control system (Figure 3.5) into account by using visual feed-back and error correction in all levels of the system.

Eventually, the 3D biomechanical model described in this chapter is a general model that is applicable for various motor tasks performed by the human arm. It was applied to a task without planar restrictions which was similar to a motor task executed in the real life.

Having the model it is achievable to study the effect of external conditions on muscle forces. Particularly, in the next chapter this model is applied to discern how the mass of an object during holding time interval affected both kinematic and muscle activity patterns.

DOI:10.15774/PPKE.ITK.2012.004

Chapter IV

VARIANCE ANALYSIS OF MOTOR CONTROL LEVELS

IV.1. Introduction

The answer to the question of how the nervous system is able to control multiple muscles and body segments while handling the redundancy problem in choosing a unique action from the set of finite possible actions is still contradictory [105] and has been recently investigated by many studies. In an attempt to make this answer clear, Feldman *et al*. [105], [106] showed that motor actions emerge from central resetting of the threshold position of proper body segments e.g. the virtual position at which muscles are silent but deviations from the muscle are going to evoke activity and resistive forces. Furthermore, the difference between the centrally-set threshold position and the sensory-signaled actual position may be responsible for the activation of neuromuscular elements between them and the environment. These elements tend to decrease the activity level and interactions by minimizing the gap between the actual position and the position determined by a given threshold. However, threshold control the so-called Lambda-model [106], [107] does not solve the redundancy issue, it only limits the set of possible actions coded by the central nervous system. In the study made by Terrier *et al*. [108] the applicability of using a pseudo-inverse and null-space optimization approach in the modeling of the shoulder biomechanics to diminish the effect of multiple spanning muscles on the shoulder joint considered as a spherical joint was investigated. Such frameworks appear to be a useful tool in the explanation of the control and production of different variety of motor actions like reach-to-grasp movements [79], specification of different hand configurations and grip force generation [109-112].

The major issue in the investigation of motor synergies [113], [114] is that there are an infinity number of solutions for a given motor task, due to the high number of DOF of the musculoskeletal system.

In other words in each joint the human body has much more muscles than necessary. An important question to consider is which combinations of muscle activities and which criterion is supposed to be chosen by the human motor control to have the optimal solution. Hence, muscles cooperate in different ways depending on the chosen criterion.

DOI:10.15774/PPKE.ITK.2012.004

This concept is called muscle synergy phenomena and was studied primarily by Bernstein [51] and among others for arm movements by Latash [57] and Prilutsky [58].

The effect of load on arm movement variances has recently been studied by Laczkó and Keresztenyi [115]. Further models using different optimum principles such as minimal jerk [116-118]; minimum torque change [55], [56], [116], [119-121]; or the minimum energy [122] investigate the motor synergy phenomena from different point of view of optimized parameters.

To get the whole arm moved by means of an artificial control method is rather complicated partly because the complexity of the shoulder mechanism and because the high variances of muscle activities [79]. To define proper activation patterns, it is advantageous to model those flexor and extensor muscle groups planned to be stimulated in the shoulder and elbow.

Variances of the movements of a kinematic chain are affected by neuro-motor diseases such as stroke and Parkinson's disease [4], [123]. In the case of the upper limb it was found that both hand position variances and joint configuration variances were higher for Parkinson patients than for healthy individuals. Variance increment was observed between the healthy and patients for both hand position and joint configuration. The rate of increment was the same for both cases. But the effect of external load on motor variances at different levels of movement controlling (hand position, arm configuration, muscle activity) has not yet been compared despite the fact that an object in the hand may have serious effects on either movement execution or the kinematics of the upper limb [79].

IV.2. Results

In the analysis of the whole movement period (A) results (Table 4.1) did not show significant difference at $p<0.05$ between the 2 load conditions either in the case of the endpoint ($F(1,19)=0.073$ $p=0.79$; $F(1,19)=0.005$ $p=0.943$) or in joint configuration ($F(1,19)=0.242$ $p=0.628$; $F(1,19)=0.05$ $p=0.825$) variances in both lifting and putting-down.

DOI:10.15774/PPKE.ITK.2012.004

TABLE 4.1.
R-ANOVA PARAMETERS OF THE WHOLE MOVEMENT PERIOD

		LIFTING				PUTTING-DOWN			
		F		p		F		p	
EP		0.073		0.79		0.005		0.943	
JC		0.242		0.628		0.05		0.825	
		BI	TR	DA	DP	BI	TR	DA	DP
EMG	F	**9.711**	1.124	**6.154**	1.1	**9.053**	1.316	**10.683**	3.276
	p	**0.006**	0.302	**0.023**	0.3	**0.007**	0.266	**0.004**	0.086
		BI	TR	DA	DP	BI	TR	DA	DP
FORCE	F	**10.486**	0.363	**16.909**	0.92	**5.754**	0.026	**17.796**	0.82
	p	**0.004**	0.554	**0.001**	0.349	**0.027**	0.874	**0.001**	0.377

*Note. Values signed by **bold** assign significant differences between the investigated object conditions at p<0.05 significance level. At kinematic levels (EP-JC) the difference was not significant. In muscle activity levels (EMG-FORCE) significant differences were only observed in the case of the flexor muscles.*

At both muscle activity levels (EMG and FORCE) significant differences were found only in the case of the flexor muscles (Table 4.1).

TABLE 4.2.
R-ANOVA PARAMETERS OF THE HOLDING PERIOD

		LIFTING				PUTTING-DOWN			
		F		p		F		p	
EP		1.62		0.21		1.99		0.17	
JC		0.73		0.4		**8.11**		**0.01**	
		BI	TR	DA	DP	BI	TR	DA	DP
EMG	F	**10.724**	**16.791**	**6.385**	**5.979**	**10.775**	**12.853**	**10.945**	**7.87**
	p	**0.004**	**0.001**	**0.021**	**0.024**	**0.004**	**0.002**	**0.004**	**0.011**
		BI	TR	DA	DP	BI	TR	DA	DP
FORCE	F	**30.63**	**17.24**	**32.27**	0.26	**27.15**	**19.63**	**21.73**	1.26
	p	**0.000024**	**0.00054**	**0.000018**	0.61	**0.00005**	**0.00028**	**0.00017**	0.27

*Note: Values signed by **bold** assign significant differences between the investigated object conditions at p<0.05 significance level. At kinematic levels (EP-JC) significant difference was only present in JC during putting-down indicating the enhanced effect of the gravity on joint configuration. Contrary to Table 4.1 at EMG level the difference was significant in all muscles. At FORCE level the difference was not significant only in the case of the DP. The different behavior of the DP compared to the EMG level may be because the main action lines of muscle forces may alter and influence the muscle force variances. The access of DP activity highly depends on the muscle geometry* [78].

In the analysis of the time interval when the object was in the hand (B) of the actual individual endpoint variances did not show significant (Table 4.2) difference between

DOI:10.15774/PPKE.ITK.2012.004

the two object conditions either in lifting ($F(1,19)=1.62$, $p=0.21$) or in putting-down ($F(1,19)=1.99$, $p=0.17$) (Figure 6.1, Table 4.2).

In the case of the joint configuration variances (Figure 6.2) there was no significant difference between the two object conditions during lifting ($F(1,19)=0.73$, $p=0.4$) (Table 4.2) while during the putting-down phase the arm configuration variance was greater if movements were executed with load than without load and this difference was significant ($F(1,19)=8.11$, $p=0.01$) (Table 4.2).

This may caused by the fact that the load had a notably smaller effect on joint configuration variability if the movement was executed against the gravity.
In EMG variances during both lifting and putting-down significant differences were observed in BI, TR, DA, DP (Table 4.2). EMG variances of the elbow flexor and extensor muscles are presented during lifting and putting-down in Figure 6.3 and Figure 6.4 respectively for all participated individuals. The EMG variances of the shoulder muscles are seen in Figure 6.5 and Figure 6.6 for both directions separately. Predicted muscle force variances showed significant difference (Table 4.2) between the two object conditions either during lifting or putting-down for all muscles except DP. Predicted muscle force variances for the elbow and shoulder flexor and extensor muscles are presented in Figure 6.7, Figure 6.8, Figure 6.9, Figure 6.10 respectively for both movement directions.

To compare the effect of a certain object with a distinct mass on different motor control levels, ratios of variances (Table 4.7) were computed by dividing the mean variance of movements executed under the heavier object (O2) by the mean variance of movements performed with the CD case (CD) for 1) the endpoint (Table 4.3); 2) the joint configuration (Table 4.4); 3) the sEMG muscle activities (Table 4.5); 4) the predicted muscle forces (Table 4.6); separately in both directions.

DOI:10.15774/PPKE.ITK.2012.004

TABLE 4.3.
MEAN VARIANCES AND THEIR STANDARD DEVIATION FOR THE ENDPOINT

EP	**UP**		**PD**	
	CD	*O2*	*CD*	*O2*
Mean(mm^2)	**599**	**448**	**501**	**653**
SD (mm)	**477**	**342**	**470**	**447**

Note. Variances were computed for each individual separately considering both directions and both object conditions (Figure 6.1) by using the measured coordinates of marker number 7(Table 2.1, MARKER CHANNEL 7) placed on the little finger Proximal Metacarp. Individual variances (Figure 6.1) were then averaged across all individuals. SD is the standard deviation of mean variances between individuals. Values signed by ***blue*** *represent the mean and SD of the CD while values signed by* ***red*** *represent the mean and SD of the O2 according to the colors used in Figure 6.1.*

TABLE 4.4.
MEAN VARIANCES AND THEIR STANDARD DEVIATION FOR THE JOINT CONFIGURATION

JC	**UP**		**PD**	
	CD	*O2*	*CD*	*O2*
Mean(^{o} ^2)	**49**	**57**	**37**	**53**
SD (^{o})	**22**	**26**	**15**	**24**

Note. Variances were originated for each individual separately considering both directions and both object conditions (Figure 6.2). Individual variances (Figure 6.2) were then averaged across all individuals. SD is the standard deviation of mean variances between individuals. Values signed by ***blue*** *represent the mean and SD of the CD while values signed by* ***red*** *represent the mean and SD of the O2 according to the colors used in Figure 6.2.*

DOI:10.15774/PPKE.ITK.2012.004

TABLE 4.5.
MEAN VARIANCES AND THEIR STANDARD DEVIATION FOR EMG

EMG		Elbow				Shoulder			
		UP		PD		UP		PD	
		CD	*O2*	*CD*	*O2*	*CD*	*O2*	*CD*	*O2*
Mean	FLEXOR	**49**	**193**	**40**	**192**	**1100**	**2137**	**846**	**1898**
(mV^2)	EXTENSOR	**13**	**32**	**7**	**23**	**68**	**193**	**55**	**188**
SD	FLEXOR	**56**	**199**	**41**	**220**	**605**	**1149**	**523**	**1677**
(mV)	EXTENSOR	**11**	**23**	**6**	**18**	**143**	**206**	**61**	**147**

Note. Variances were computed for each individual separately considering both directions and both object conditions (Figure 6.3)-(Figure 6.6). Individual (Figure 6.3)-(Figure 6.6) variances were then averaged across all individuals. SD is the standard deviation of mean variances between individuals. Values signed by ***blue*** *represent the mean and SD of the CD while values signed by* ***red*** *represent the mean and SD of the O2 according to the colors used in Figure 6.3 - Figure 6.6.*

TABLE 4.6.
MEAN VARIANCES AND THEIR STANDARD DEVIATION FOR PREDICTED MUSCLE FORCES

FORCE [N^2]		Elbow				Shoulder			
		UP		PD		UP		PD	
		CD	*O2*	*CD*	*O2*	*CD*	*O2*	*CD*	*O2*
Mean	FLEXOR	**23**	**220**	**32**	**184**	**12**	**64**	**17**	**82**
(N^2)	EXTENSOR	**24**	**55**	**18**	**51**	**679**	**742**	**785**	**886**
SD	FLEXOR	**16**	**168**	**28**	**143**	**8**	**42**	**14**	**70**
(N)	EXTENSOR	**15**	**38**	**14**	**36**	**839**	**604**	**928**	**758**

Note. Variances were computed for each individual separately considering both directions and both object conditions (Figure 6.7)-(Figure 6.10). Individual variances (Figure 6.7)-(Figure 6.10) were then averaged across all individuals. SD is the standard deviation of mean variances between individuals. Values signed by ***blue*** *represent the mean and SD of the CD while values signed by* ***red*** *represent the mean and SD of the O2 according to the colors used in Figure 6.7 – Figure 6.10.*

DOI:10.15774/PPKE.ITK.2012.004

Table 4.7 presents the mean ratios across 20 individuals. The ratio was higher for joint configuration variances than for endpoint variances for both lifting and putting-down. Endpoint variances during lifting with load were smaller than without load (the ratio of endpoint variances was smaller than 1).

For joint configurations ratios remained only in six individuals less than 1 (Figure 6.2).

For EMG variances and for simulated muscle force variances, ratios were much higher than 1 concerning all measured muscles. Hence, muscle activity variances in all muscles except DP in both directions were affected by the given object at a higher rate than kinematic variances. According to the table it is seen that the effect of load on variances was the highest at muscle activity levels (EMG and virtual muscle forces) while it was smaller at joint configuration level and it was the smallest at the level of the endpoint.

TABLE 4.7.
RATIOS OF MEAN VARIANCES (MEANO2/MEANCD)

	UP		**PD**	
EP	0,7		1,3	
JC	1,2		1,4	
EMG	**BI**	**TR**	**BI**	**TR**
	3,9	2,5	4,79	3,05
	DA	**DP**	**DA**	**DP**
	1,9	2,8	2,24	3,43
Force	**BI**	**TR**	**BI**	**TR**
	9,6	2,3	5.75	2,83
	DA	**DP**	**DA**	**DP**
	5,3	1,1	4,82	1,12

Note. In the table the RATIO of movement variances with load (O2) to movement variances without load (CD) is summarized for the studied motor control levels. As a result it can be seen that the RATIO was smaller for endpoint and joint configuration variances than for sEMG and muscle FORCE variances respectively representing that enhanced muscle synergies stabilize the movement at kinematic level by controlling primarely through the hand position and less by the combined joint rotations and not by individual muscle activities.

Results of the muscle motor control levels showed that either in simulated muscle force variances (Figure 6.7 - 6.10, Table 4.7) or in measured muscle activity variances (Figure 6.3 - 6.6, Table 4.7) the larger mass of the object was associated with increased variances

DOI:10.15774/PPKE.ITK.2012.004

in both flexor and extensor activities. The mean variances are presented for both conditions for all levels of motor control (Figure 4.1) summarizing the values presented in tables (4.3 – 4.6).

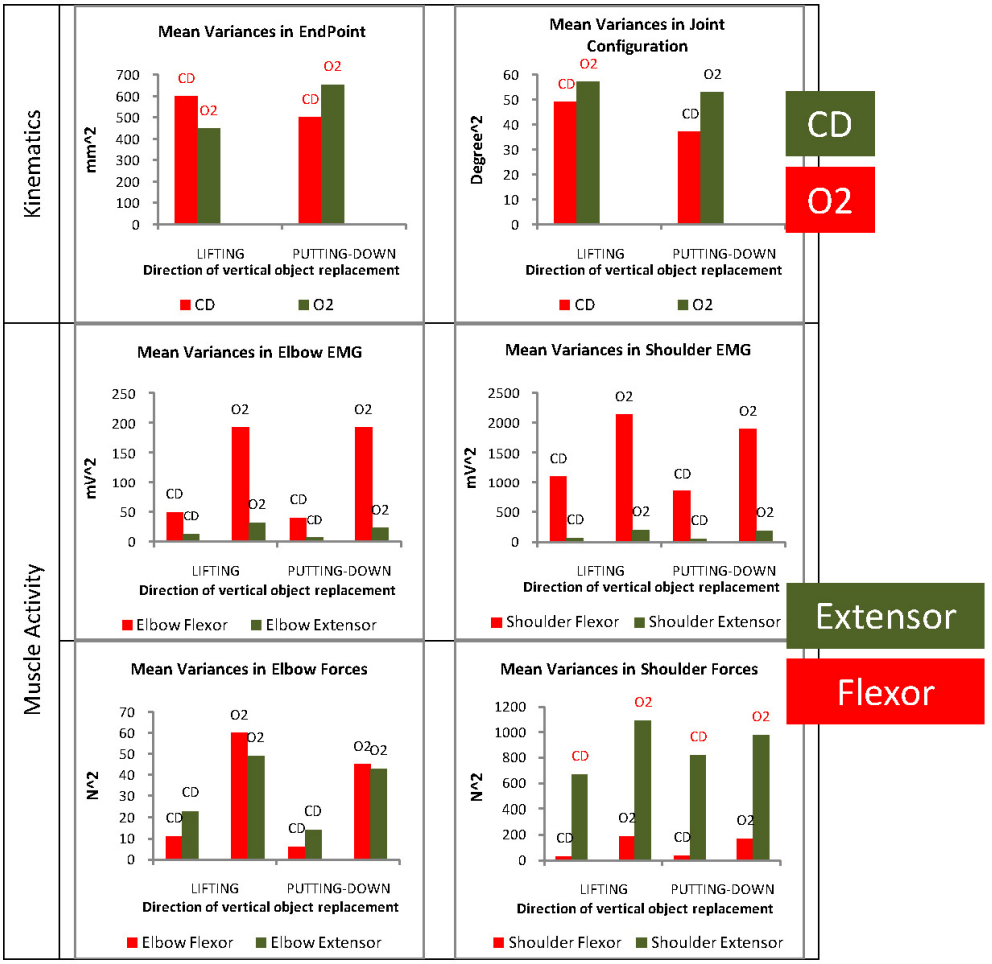

Figure 4.1. The mean variances across individuals (Table 4.3 - 4.6) for both object conditions and for both directions of movement execution considering kinematics (EP-JC) and muscle activities (EMG-FORCE) of motor control levels.CD and O2 sign the cases at certain motor control levels (EP, JC during lifting, FORCE shoulder extensor during either lifting or putting-down) where the mean variances of movements executed under 2 kg was higher but not significantly higher than mean variances of movements performed under CD across all individuals.

The difference between variances of the two conditions was higher for muscle activities than for kinematic variances. The variances of EMGs were higher for flexors than for extensors both for elbow and shoulder muscles. However, the shoulder extensor (DP) behaved differently than the other muscles. The variances of shoulder muscle forces were higher for extensor than for flexor in contrast to EMG variances. Note that only DP

DOI:10.15774/PPKE.ITK.2012.004

muscle force variances were not affected significantly by the load (Table 4.2). This may be because the main action lines of the muscle forces may alter and influence the muscle force variances. The access of DP activity highly depends on the muscle geometry [78]. The increment in muscle force variances for flexors was larger than for extensors when the mass of the object increased (Table 4.7).

As it is presented in tables (4.3 - 4.6) the standard deviations of the variances of kinematic variables and especially muscle activity variables were remarkably high comparing to the mean values. The high predicted muscle force standard deviations across all individuals indicate unique force patterns between individuals exerted by individual muscles under the execution of the same point to point movement. Therefore, the execution of movements under differing object conditions varies individual by individual. To demonstrate the presence of muscle force uniqueness across individuals, standard deviations were computed within subjects (for 10 trials) for both directions (UP, DOWN) under each load condition (CD, O2) to all individuals separately and then averaged across all individuals (Table 4.8, **SD within subjects**).

TABLE 4.8.
WITHIN AND BETWEEN SUBJECTS STANDARD DEVIATIONS OF MUSCLE FORCES

		SD within subjects (N)		SD between subjects (N)	
		CD	O2	CD	O2
UP	BI	2.4	5.5	16	168
	TR	2.7	2.9	15	38
	DA	2	5	8	42
	DP	16	30	839	604
DOWN	BI	3.2	4.7	28	143
	TR	2.5	3	14	36
	DA	2.3	3.6	14	70
	DP	19	16	928	758

Note. ***Between subjects standard deviations of predicted muscle forces*** *(Table 4.6) were remarkably high compared to the mean of predicted muscle forces across subjects indicating different execution patterns between subjects. Furthermore, averaged* ***within subjects standard deviations*** *were significantly smaller than between subjects standard deviations at $p<0.05$ significance level. Thus, generalized activation patterns cannot be applied during rehabilitation procedures. Instead of using generalized action patterns for all patients, personalized movement patterns rather lead to adequate rehabilitation processes of individuals.*

DOI:10.15774/PPKE.ITK.2012.004

Within subjects averaged SDs (Table 4.8, **SD within subjects**) were significantly smaller ($p<0.05$) than between subjects SDs (Table 4.8, **SD between subjects**) for both directions under each object condition.

IV.3. Discussion

The particular aim of this study was to investigate how the variances of arm movements were affected if a load was held in the hand. The variances were analyzed at different levels of the motor apparatus. The central neural control may take responsibility for smaller variances of the most relevant variables for instance the endpoint trajectory and joint configuration at kinematic level while the required mechanical action was distributed between the muscles at the muscular level with higher variances.

The joint configuration variances were averaged during the whole movement interval for all individuals separately. Statistical methods did not prove any significant difference between the two object conditions for these averaged variances. This may be because averaged variances remained high in the pre and post-holding parts (when the individuals didn't hold the object) and reached their top out at about 300 Degree^2 and during holding only at about 100 Degree^2. This was true for lifting and putting-down suggesting that movement performed with an object held in the hand varied less than without an object.

Therefore, the investigation was focused on the holding time interval. The dependence of motor stability on different object conditions can be revealed by analysing variances in external workspace, in internal joint space and in the space of muscle activation patterns. For instance the effect of load was studied to discern muscle synergies while individuals shifted their body weight forward and backward [124], [125].

Here muscle synergies were investigated while individuals moved their whole arm upward and downward holding different loads. Freitas *et al*. [126], [127] investigated whether kinematic synergies are more related to stabilization of the instantaneous anterior-posterior position of the center of mass or the center of pressure in whole-body movements executed in standing. By applying uncontrolled manifold (UCM) analysis they found that more 'good' and less 'bad' joint variance related to stability of the center of mass than to the center of pressure position. It has been recently proven by Gera *et al*. [127] that the orientation constraint does not affect the stability of the hand's spatial path

DOI:10.15774/PPKE.ITK.2012.004

during placing a certain object from one place to another that required either precise or minimal orientation to the target. The effects of learning was studied on muscle activity and kinematic variability by Gabriel [128] during maximal performance task. It was found that at increased limb speed both target error and trajectory (velocity versus position) variability decreased in the case of kinematics of the limb while in EMG of the biceps brachii and the triceps an increase was observed in the absolute measure of total EMG variability. Further studies were performed to investigate the variability of surface EMG during maximum voluntary isometric and anisometric contractions for the upper limb [129] and for the lower limb muscles [130].

As a consequence of the results, generalized movement patterns using predicted muscle forces for FES rehabilitation cannot be generated because it changes between individuals. However, using the musculoskeletal model, personalized movement patterns are to be applicable in FES rehabilitation procedures of handicapped patients.

The muscle force calculation model offers muscle forces for the studied point to point arm movements. As the model shows, these specific movements can be performed activating only one muscle around each joint at any given instant, and it is the flexor for both the elbow and shoulder joint. .

For artificial control of joint rotations this would be a possible solution even for 3D arm movements. This was the motivation of the muscle force computation method proposed in the previous chapter and this may be used to define muscle activity patterns for FES assisted movements. Even if only one muscle group is activated, muscle geometry may ensure that high increment in muscle activity variance is related to a smaller increment in joint and endpoint variances. Additional muscles may be considered for generating neuromorphic muscle activity patterns.

Measured surface EMG variances also showed a higher range of increment for flexors than for extensors in the elbow but the opposite was observed for shoulder muscles while variances of shoulder flexor activity were exceptionally high (Figure 4.1, Table 4.7).

As a main conclusion the enhanced muscle synergies stabilize the movement at kinematic level by controlling mostly through the hand position and less by the joint rotations and not by individual muscle activities. Therefore, peripheral patterns reflect central neural processes (joint or muscle synergies) rather than being separately controlled components of the action. Such findings were suggested for grip force

DOI:10.15774/PPKE.ITK.2012.004

adjustment [131]. This finding supports furthermore the results that external conditions or practice of movements effect joint configuration variances and endpoint variances at a different rate. Practice helps to stabilize the hand position by decreasing those variances of the joint configurations that affect the hand position while giving space to the joint configurations that do not affect the hand position [59], [60].

Here, the effect of load on kinematic variances, on measured muscle activity variances and on virtual muscle activity variances was compared. The analysis of variance suggested that kinematic variability of the studied arm movement was restricted in such a way that enhanced joint synergies helped to stabilize hand position while an object was held in the hand. Reasonable variances of endpoint positions and joint rotations reflected enhanced muscle synergies rather than being directly determined by individual muscle activity variances. Otherwise high muscle activity variances would increase kinematic variances at the same rate. In the dissertation study of the structure of the joint configuration variance was not involved as this was done for other arm movement tasks [126], [131] where higher dimensional joint spaces were applied.

Finally, the results summarized in this chapter are applicable in occupational biomechanics and in medical rehabilitation processes. These kinds of task specific movements are frequent in industrial environment [132]. The research confirms that not only individual muscle performance but the cooperation of muscle groups should also be trained and enhanced for stable and reproducible movement execution.

DOI:10.15774/PPKE.ITK.2012.004

Chapter V

SUMMARY

V.1. New Scientific Results

Thesis I. *Three dimensional model for establishing the direction and magnitude of 3D muscle force vectors and joint torques in general upper limb movements using measured 3D kinematic and anthropometric data.*

Related publications: [Tibold *et al*., 2011; Tibold and Laczkó, 2011; Laczkó and Tibold, 2010; Laczkó *et al*., 2009]

In the case of 3D movement modeling the direction of torques and muscle forces acting in a given joint are not an obvious questions especially not if one would like to consider how muscles (agonists and antagonists) are operating together at a given time instant. Another important issue is the determination of either proper 3D muscle geometry (containing 3D muscle insertions and origins) or the biomechanical characteristics of muscles (the active ($F_a(l)$) and passive ($F_p(l)$) force length relations). In the following groups of theses results of these are summarized.

I.1. **I have given a mathematical algorithm for determining the direction of three dimensional muscle force vectors to generate a desired joint torque during the execution of general, three dimensional point-to-point arm movements. As a part of the algorithm I have elaborated a novel general method to determine three dimensional muscle insertion and origin areas located on the surface of the bone by applying both cadaveric parameters and personal anthropometric values to have accurate muscle geometry.**

If only one muscle is active at a time instant *t*, than the torque generated by the muscle in the spanned joint is computed as the difference of the total torque and the gravitational torque:

$$\overrightarrow{F_m(t)} \times \overrightarrow{R_m(t)} = \overrightarrow{\beta(t)} \cdot {}^{(\mathbf{joint})}I\,(t) - \overrightarrow{T_{g(\mathbf{joint})}(t)} \tag{5.1}$$

DOI:10.15774/PPKE.ITK.2012.004

where $\overrightarrow{F_m(t)}$ is the force generated by the muscle, $\overrightarrow{R_m(t)}$ is the moment arm of the muscle, $\overrightarrow{\beta(t)}$ is the angular acceleration of the joint spanned by the muscle, $I^{(\mathbf{joint})}(t)$ is the moment of inertia , $\overrightarrow{T_{g(\mathbf{joint})}(t)}$ is the gravitational torque due to the rotated body part. Depending on the direction of the required torque either the flexor or the extensor muscle group should be activated at each instant for an artificial control of the joint torque. Such virtual muscle forces (Figure 5.1) were predicted for 4 arm muscles separately (BI, TR, DA, DP) at each time step during the desired movement. The novelty of my computation is that I considered that all parameters (except $I^{(\mathbf{joint})}(t)$) were three dimensional vectors and not only their magnitude but their direction was changing in time throughout the movement. Modeling approaches usually have been elaborated by restricting joint rotations around predefined rotational axes [28], [89], [90], although natural human movements do not comply with such restrictions [133], [134]. I elaborated 3D computation for all of the vectors as the function of time.

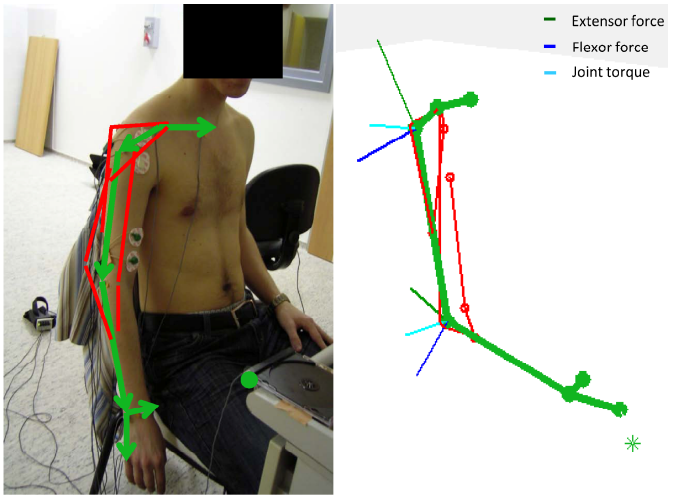

Figure 5.1. Virtual determination of 3D muscle forces for flexor (blue) and extensor (green) muscles needed to generate the 3D joint torque (light blue) in the spanned joint at a discrete time instant.

I determined personalized 3D coordinates of muscle attachments located on the surface of the bone. First, based on the cadaver study of Veeger *et al.* [76] I put the questioned muscle insertion-origin points to the midline of the bone segment containing either the insertion or the origin. But since 1) muscles are located on the bone surface and not on the midline of the bone segment and since 2) Veeger provided data for only fully

DOI:10.15774/PPKE.ITK.2012.004

stretched elbow - which was only the initial posture of the measured movement - I applied the Rodrigues' rotation formula to predict 3D coordinates of muscle attachments (Figure 5.2) for the entire movement interval.

$$\left(\overline{uBII_{t+1}}\right)=\overline{uBII_t}\cos\Theta_{(e)t}+\left(z_t\times\overline{uBII_t}\right)\sin\Theta_{(e)t}+\left(z_t z_t^T*\overline{uBII_t}*(1-\cos\Theta_{(e)t})\right) \tag{5.2}$$

$$\Theta_{(e)t}=\alpha\left(E_{t+1}\right)-\alpha\left(E_t\right) \tag{5.3}$$

$$\overline{E_{t+1}BII_{t+1}}=\left\|E_{t+1}-BII_{t+1}\right\|*\overline{uBII_{t+1}} \tag{5.4}$$

$$OnBoneSurf\_BII_{t+1}=\overline{E_{t+1}BII_{t+1}}+E_{t+1} \tag{5.5}$$

Remark: A mathematical method for computing the biceps insertion. The same method as above was applied by replacing the rotation axis z_t ; the rotated muscle attachment unit vector; the angle of rotation θ_t to particular ones related to the specific muscle.

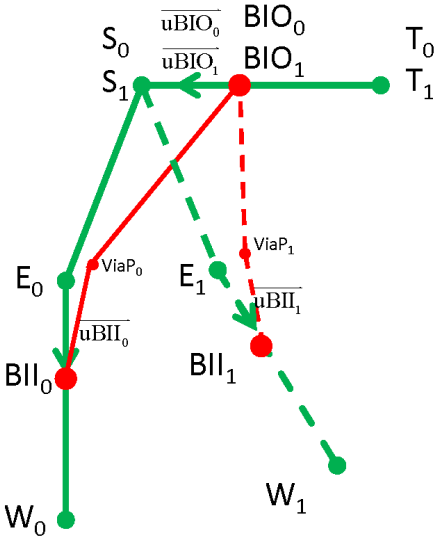

Figure 5.2. Anatomical landmarks (T – thorax; S – shoulder; E – elbow; W - wrist); muscle attachments of the biceps (BIO - origin; BII - insertion); unit muscle attachment vectors ($\overline{uBII}$, $\overline{uBIO}$,) used in the rotation method of Rodrigues during the calculation of the biceps attachments located on the surface of the bone are presented at two successive time instants (t and t+1). The rotation method was applied to determine muscle insertions and origins for not only the initial position (t=0) but for the whole movement interval as well.

DOI:10.15774/PPKE.ITK.2012.004

I.2. I have proven that the elbow and shoulder joint torque profiles predicted by the 3D biomechanical model are invariant to changes of the mass of the object held in the hand. The range but not the shape of the torque-time curve depended on the object held in the hand.

Mean torque profiles of all trials were generated within each subject for the three object conditions during lifting and putting-down separately for the holding movement periods (the actual object is in the hand of the individual). Each subject's ten trials were averaged. Data of one representative subject are shown in (Figure 5.3).

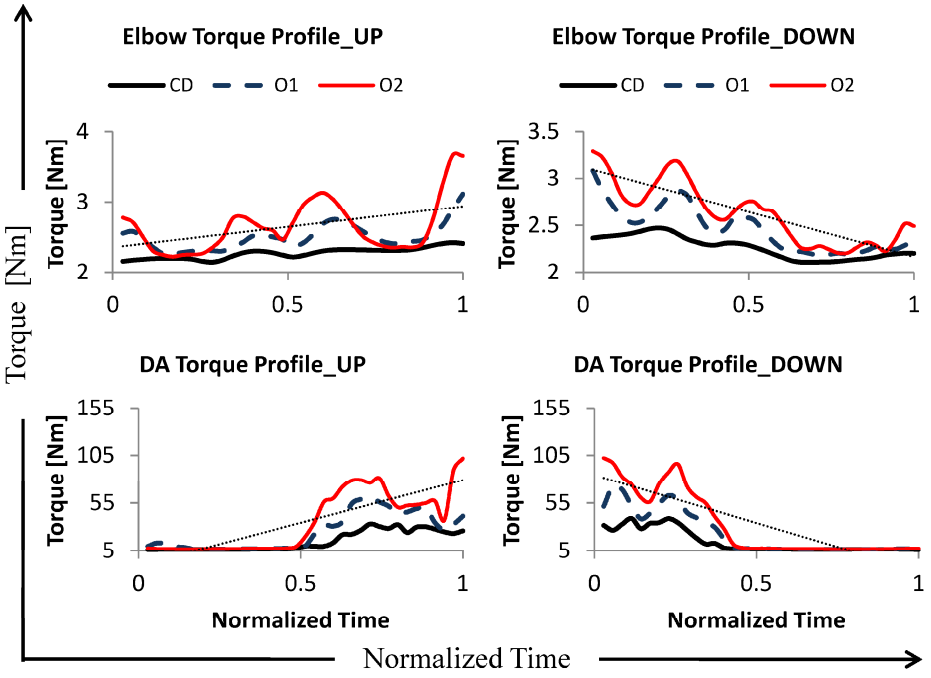

Figure 5.3. Mean predicted torque profiles of ten trials in each object conditions (CD, O1, O2) for both movement directions (UP, DOWN) observed during holding time interval (the period during which the subject was holding the object) for one representative individual (number 1). Dotted lines (linear regression fit) sign the linear increasing or decreasing tendency of the torque during lifting and putting-down respectively. Only the range but not the shape of the torque-time curve depended on the mass of the object held in the hand. The magnitude of joint torques was larger for heavier objects than for the lightest one in both joints. The invariance of the shape is supported by the correlation coefficients performed for all conditions (considering all movement directions and object masses) in both joints (shoulder and elbow) summarized in Table 5.1.

To present the effect of changing object conditions on mean torque profiles correlation analysis was performed for holding time intervals (Table 5.1). The strongest ($0.77 \leq r \leq$

DOI:10.15774/PPKE.ITK.2012.004

0.99) Pearson's coefficients were observed when comparing the linear relation between O1 and O2 torque curves. Weaker ($0.35 \leq r \leq 0.98$), but still strong linear correlation was present between CD and O1 torque profiles while the weakest ($0.12 \leq r \leq 0.96$) correlation was found between CD and O2 conditions. Because mean correlation coefficients (Table 5.1) are higher than 0.58 in all object conditions for both directions indicating high linear connection between separate conditions the torque profile is considered to be object invariant for both directions (Table 5.1). The magnitude but not the shape of the torque-time curve depended on the object held in the hand. The magnitude and the amplitude of joint torques were larger for heavier objects than for the lightest one in both the elbow and shoulder. For lifting movements the joint torques show increasing profiles, though for putting-down they show decreasing profiles (Figure 5.3).

TABLE 5.1.
PEARSON'S R-VALUES OF ALL SUBJECTS FOR THE ELBOW AND SHOULDER JOINT TORQUES OBSERVED DURING HOLDING CONSIDERING ALL OBJECT CONDITIONS.

SUBJID	ELBOW TORQUE						SHOULDER TORQUE					
	UP			DOWN			UP			DOWN		
	CD-O1	CD-O2	O1-O2	CD-O1	CD-O2	O1-O2	CD-O1	CD-O2	O1-O2	CD-O1	CD-O2	O1-O2
1	0.71	0.58	**0.85**	0.89	0.87	**0.97**	0.69	0.79	**0.9**	**0.91**	0.77	0.8
2	0.69	0.51	**0.88**	0.9	0.82	**0.95**	0.75	0.87	**0.9**	0.92	0.87	**0.95**
3	0.89	0.74	**0.92**	0.89	0.87	**0.9**	0.98	0.97	**0.99**	0.95	0.9	**0.97**
4	0.63	0.55	**0.86**	0.87	0.83	**0.94**	0.51	0.71	**0.87**	0.9	0.84	**0.98**
5	0.83	0.66	**0.88**	0.66	0.76	**0.89**	0.79	**0.93**	0.73	**0.97**	0.86	0.87
6	0.86	0.72	**0.91**	0.55	0.72	**0.92**	0.88	0.81	**0.93**	0.92	0.91	**0.97**
7	0.67	0.62	**0.86**	0.97	0.96	**0.98**	0.45	0.5	**0.8**	0.95	0.94	**0.99**
8	0.85	0.74	**0.92**	0.95	0.94	**0.97**	0.82	0.76	**0.83**	0.9	0.75	**0.98**
9	-0.3	-0.01	**0.87**	0.4	**0.72**	-0.08	0.35	0.12	**0.86**	**0.87**	0.75	0.79
10	0.44	0.37	**0.86**	0.9	0.87	**0.97**	0.75	0.74	**0.89**	0.79	0.72	**0.94**
11	0.64	0.58	**0.85**	0.81	0.7	**0.82**	0.9	0.8	**0.91**	0.9	0.89	**0.93**
12	0.33	0.63	**0.83**	0.9	0.69	**0.98**	0.22	0.2	**0.87**	0.79	0.64	**0.9**
13	0.79	0.78	**0.87**	0.97	0.86	**0.98**	0.64	0.6	**0.94**	0.97	0.96	**0.98**
14	0.68	0.54	**0.91**	0.86	0.63	**0.88**	0.9	0.85	**0.91**	0.96	0.76	0.87
15	0.87	0.8	**0.91**	0.85	0.84	**0.95**	0.97	0.96	**0.98**	0.95	0.94	**0.97**
16	0.16	0.42	**0.46**	-0.6	-0.6	**0.8**	0.04	0.05	**0.33**	-0.83	-0.92	-0.8
17	0.48	0.40	**0.9**	0.3	0.25	**0.84**	0.83	0.74	**0.86**	0.9	0.89	**0.94**
18	0.47	0.4	**0.91**	0.52	0.33	**0.77**	0.85	0.81	**0.94**	0.94	0.9	**0.96**
19	0.76	0.71	**0.98**	0.81	0.79	**0.85**	**0.91**	0.79	0.85	0.9	**0.98**	0.94
20	0.81	0.79	**0.98**	0.67	0.61	**0.77**	0.83	0.81	**0.88**	0.78	0.7	**0.8**
Mean	0.61	0.58	**0.87**	0.70	0.67	**0.85**	0.70	0.69	**0.85**	0.81	0.75	**0.83**
SD	0.29	0.24	0.10	0.38	0.35	0.23	0.25	0.26	0.13	0.39	0.40	0.39

*Note. Generally, the strongest (**$0.77 \leq r \leq 0.99$**) (close to perfect + correlation) correlation coefficients were found between O1 and O2; weaker but strong ($0.35 \leq r \leq 0.98$) correlation appeared between CD and O1; the weakest coefficients ($0.12 \leq r \leq 0.96$) occured between CD and O2 for both directions and joints. Correlation coefficients in the case of subjects 9 and 16 showed negative correlation in the comparison of CD-O1 and CD-O2. Since the mean of all coefficients is higher than 0.58 with small SD, torque profiles are regarded object invariant under the given object circumstances.*

DOI:10.15774/PPKE.ITK.2012.004

Thesis II. *The effect of objects with distinct masses on the variances of endpoint (EP), joint configuration (JC), sEMG and simulated muscle forces (FORCE) as levels of the bilogical motor apparatus during holding the object in the hand.*

Related publications: [Tibold *et al*., 2011; Tibold *et al*., 2009; Laczkó and Tibold, 2009]

In order to reproduce complex arm movements artificially first the issue of muscle synergies namely how the CNS chooses its strategy to select proper muscles for optimal solution of a given motor task and what is controlled by the nervous system under changing object conditions must be understood.

The following group of theses summarizes how different levels of motor control and the cooperation of flexor and extensor muscles were affected by a heavier object during the time interval of holding through variance analysis. Variances of the performed movements were computed during holding as functions of normalized time and were averaged across time for both object conditions (CD, O2) within all subjects in lifting and putting-down. These values were computed for the endpoint, joint configuration, sEMG of 4 arm muscles (BI, TR, DA, DP) and for computed muscle forces of the same muscles separately. The mean variance across holding with load was divided by the mean variance across holding without load for 1) all subject separately and for 2) the mean of individual variances (Figure 5.4) across all subjects (*RATIO*), (Table 5.2).

II.1. I have proven that motor stability highly depends on altering load conditions. Movements executed with load (O2) varied in a higher manner than movements executed without load (CD) during holding time interval.

This has been proven by analyzing variances (Figure 5.4) in external workspace, in internal joint space and in the space of muscle activation patterns when an object was in the hand of the actual subject (HOLDING time interval).

In endpoint variances results didn't show significant difference between the two object conditions either in lifting ($F(1,19)=1.62$, $p=0.21$) or in putting-down ($F(1,19)=1.99$, $p=0.17$) at $p<0.05$. In joint configuration there was no significant difference between the object conditions during lifting ($F(1,19)=0.73$, $p=0.4$). However, in putting-down the arm configuration variance was significantly ($F(1,19)=8.11$, $p=0.01$) greater if movements

DOI:10.15774/PPKE.ITK.2012.004

were executed with load proving a less enhanced effect of the gravity on movement execution while acting against the gravity. High significant differences occurred in both surface EMG and virtually computed muscle force levels depicting minimal p values in the ranges of $0.0002 \leq p_{EMG} \leq 0.024$ and $0.00002 \leq p_{FORCE} \leq 0.0005$ respectively. But in computed muscle forces DP showed no difference between the object conditions either in lifting or in putting-down.

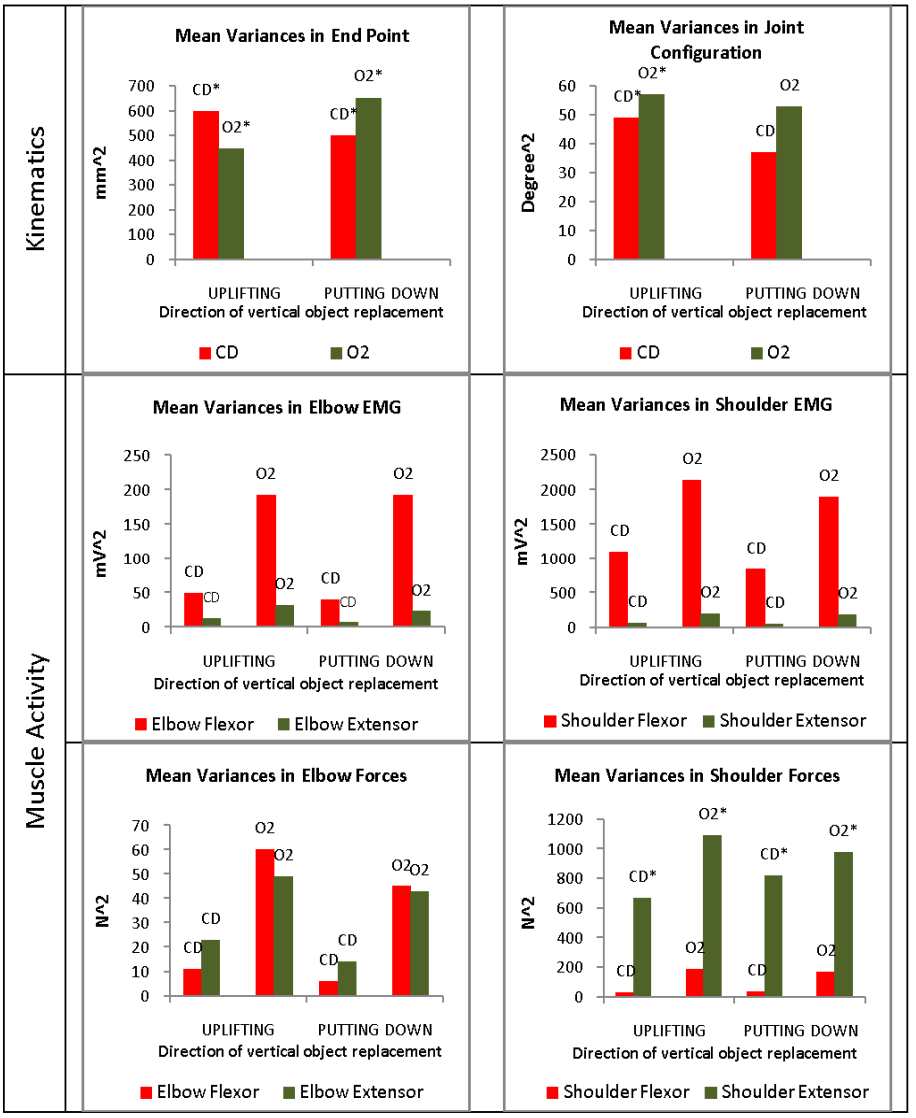

*Figure 5.4. Mean values of variances across 20 subjects for all motor control levels in both directions (UPLIFTING, PUTTING DOWN) under both conditions (CD, O2). In the cases of coherent CD-O2 pairs * means that even though the variance of movements executed with O2 is higher than movements executed with CD but this difference was not significant at $p<0.05$.*

DOI:10.15774/PPKE.ITK.2012.004

II.2. I have shown that RATIO of movement variances with load (O2) to movement variances without load (CD) was smaller for endpoint and joint configuration variances than for sEMG and muscle FORCE variances respectively representing that enhanced muscle synergies stabilize the movement at kinematic level by controlling primarely through the hand position and less by the combined joint rotations and not by individual muscle activities.

To compare the effect of load on different control levels I computed the ratios of mean variances across all subjects by dividing the mean variance of movements with load by the mean variance of movements without load. (*RATIO*)

$RATIO_{JC}>RATIO_{EP}$ for both lifting and putting-down. $RATIO_{EMG}>>1$ and $RATIO_{FORCE}>>1$ concerning all investigated muscles except DP.

Thus, it's obvious that the load effected the muscle variances at a higher rate than kinematic variances (Table 5.2) proving that the effect of the heavier object on variances was the highest at muscle activity level, smaller at joint configuration level and it was the smallest at endpoint level.

TABLE 5.2.
RATIOS OF MEAN VARIANCES

		UP		DOWN
EP		0.7		1.3
JC		1.2		1.4
EMG	**BI**	**TR**	**BI**	**TR**
	3.9	2.5	4.8	3.3
	DA	**DP**	**DA**	**DP**
	1.9	2.83	2.2	3.42
FORCE	**BI**	**TR**	**BI**	**TR**
	9.6	2.3	5.75	2.83
	DA	**DP**	**DA**	**DP**
	5.3	1.1	4,83	1,12

Note. In the table the RATIO of movement variances with load (O2) to movement variances without load (CD) is summarized for the studied motor control levels. As a result it can be seen that the RATIO was smaller for endpoint and joint configuration variances than for sEMG and muscle FORCE variances respectively representing that enhanced muscle

DOI:10.15774/PPKE.ITK.2012.004

The shoulder extensor (DP) had a slightly different behavior than the other muscles because the variances of DP were higher than the variances of DA in contrast to EMG variances (Figure 5.4). A possible reason of this is that the main action lines of muscle forces may alter and influence muscle force variances caused by the complex structure of the deltoid muscle [78].

II.3. I have shown that using virtually predicted muscle forces, generalized muscle activity patterns for rehabilitation of the upper extremity containing the shoulder complex cannot be generated in the cases of the main arm muscles. Instead of using generalized action patterns for all patients, personalized movement patterns rather lead to adequate rehabilitation processes of individuals.

TABLE 5. 3.
BETWEEN SUBJECTS MEAN AND SD OF PREDICTED MUSCLE FORCES

		Mean *(N)*		**SD** *(N)*	
		CD	**O2**	**CD**	**O2**
UP	**BI**	23	220	16	168
	TR	24	55	15	38
	DA	12	64	8	42
	DP	679	742	839	604
DOWN	**BI**	32	184	28	143
	TR	18	51	14	36
	DA	17	82	14	70
	DP	785	886	928	758

Note. Between subjects mean and SD of predicted muscle forces (BI, TR, DA, DP) for all individuals. Standard deviations of predicted muscle forces were remarkably high compared to the mean of predicted muscle forces across subjects indicating different execution patterns between subjects.

Predicted muscle force standard deviations (SD) across all subjects were relatively high compared to the mean across subjects for both object conditions (Table 5.3) indicating distinctive force patterns between subjects exerted by individual muscles under the

DOI:10.15774/PPKE.ITK.2012.004

execution of the same point-to-point movement. Thus, the execution of movements under differing object conditions varies subject by subject. To demonstrate this across subjects, standard deviations were computed within subjects (for 10 trials) for both directions (UP, DOWN) under each load condition (CD, O2) to all subjects separately and then averaged across all subjects (Table 5.4).

TABLE 5. 4.
WITHIN SUBJECTS PREDICTED MUSCLE FORCE SD-S

[N]	**UP**		**DOWN**	
CD	**BI**	**TR**	**BI**	**TR**
	2.4542	2.7512	3.255	2.5224
	DA	**DP**	**DA**	**DP**
	2.0863	16.166	2.3067	19.475
O2	**BI**	**TR**	**BI**	**TR**
	5.5247	2.8967	4.7365	3.0204
	DA	**DP**	**DA**	**DP**
	5.0782	30.423	3.6851	16.128

Note. In the table averaged, within subjects predicted muscle force SD can be seen. Averaged within subjects standard deviations were significantly smaller than between subjects standard deviations (Table 3) at $p<0.05$ significance level. Thus, generalized activation patterns cannot be applied during rehabilitation procedures. Instead of using generalized action patterns for all patients, personalized movement patterns rather lead to adequate rehabilitation processes of individuals.

Within subjects SDs (Table 5.4) were significantly smaller ($p<0.05$) than between subjects SDs for both directions under each object condition.

As a consequence of this fact, generalized movement patterns using predicted muscle forces for FES rehabilitation cannot be generated because it changes between subjects. However, using the presented 3D biomechanical model (Theses I.) personalized movement patterns are applicable in FES rehabilitation procedures of tetraplegic patients.

DOI:10.15774/PPKE.ITK.2012.004

V.2. Possible Applications

In the first theses group I summarized the most important novel results of a personalized biomechanical model.

These results will be useful to generate personalized muscle activity patterns for patients having rehabilitation of their upper extremity. Personalized movement patterns will be created based on anthropometric data to define typical muscle geometries characterizing the subjects anatomical muscle geometries as accurately as possible. Furthermore, in the next step of the research I plan to reveal the relationship between virtually computed muscle forces and stimulation patterns. Such stimulation patterns should be applied by using electrical stimulators in FES applications to activate the main muscles of the upper limb and generate reaching-grasping arm movements artificially in the 3D space. In the second theses group I summarized how the heavier object affected different levels of the motor apparatus thus supporting that enhanced muscle synergy stabilizes the movement at kinematic levels.

This issue is going to be very useful in medical rehabilitation and in occupational therapy by assisting medical doctors in selecting which muscles or body parts should be trained for more efficient motor performance.

My theses contribute to human motor control research by better understanding how the central nervous system (CNS) reacts for changing external conditions.

DOI:10.15774/PPKE.ITK.2012.004

Chapter VI

APPENDICES

VI.1. Endpoint Variances – All Individuals

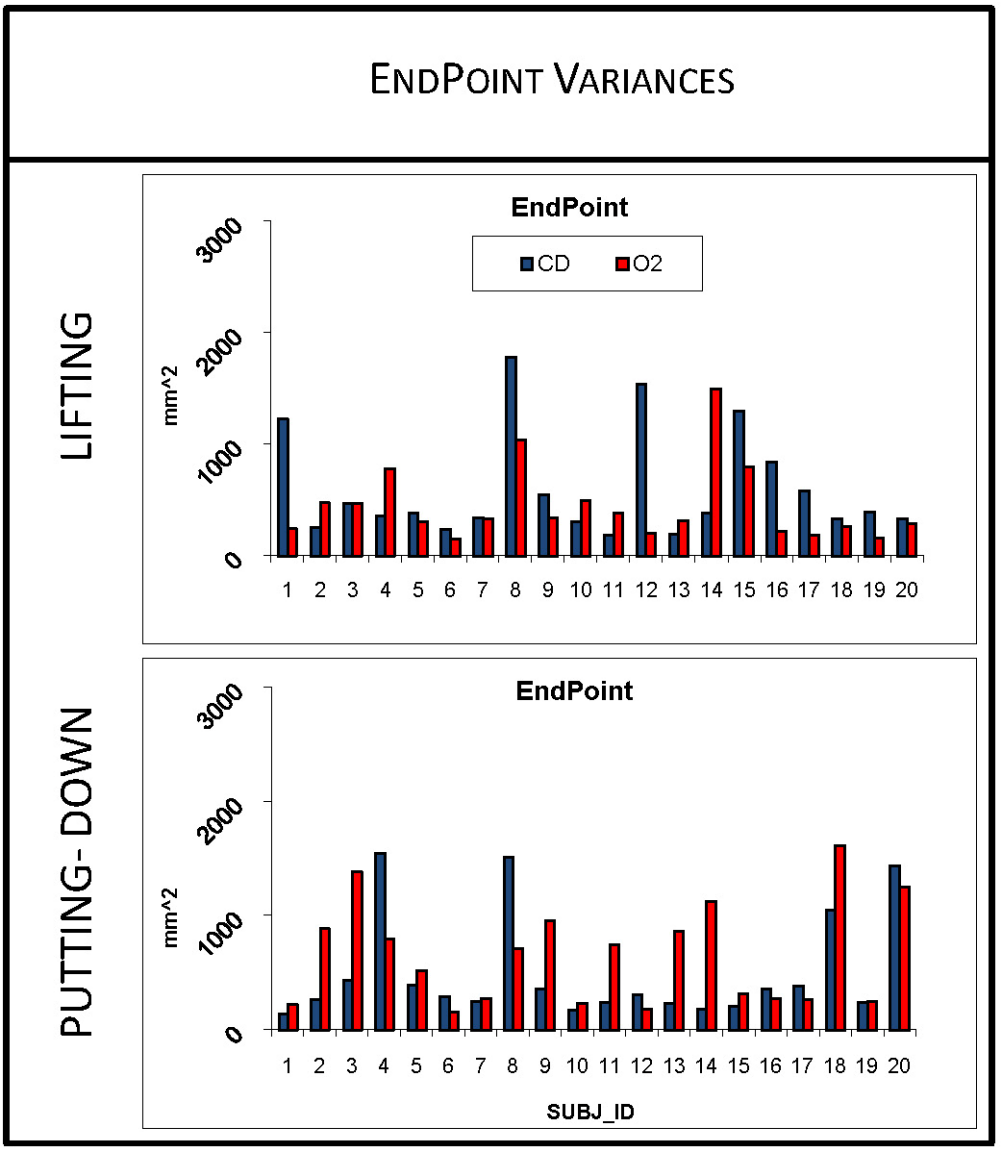

Figure 6.1.Variances of the endpoint during holding movement period for the 20 individuals separately. In the upper panel variances observed during lifting while in the lower panel variances observed during putting-down are presented. Significant difference was not observed between CD and O2 conditions in either cases at $p<0.05$ significance level (Table 4.2). meanCD>meanO2 across individuals occurred only during lifting.

DOI:10.15774/PPKE.ITK.2012.004

VI.2. Joint Configuration Variances – All Individuals

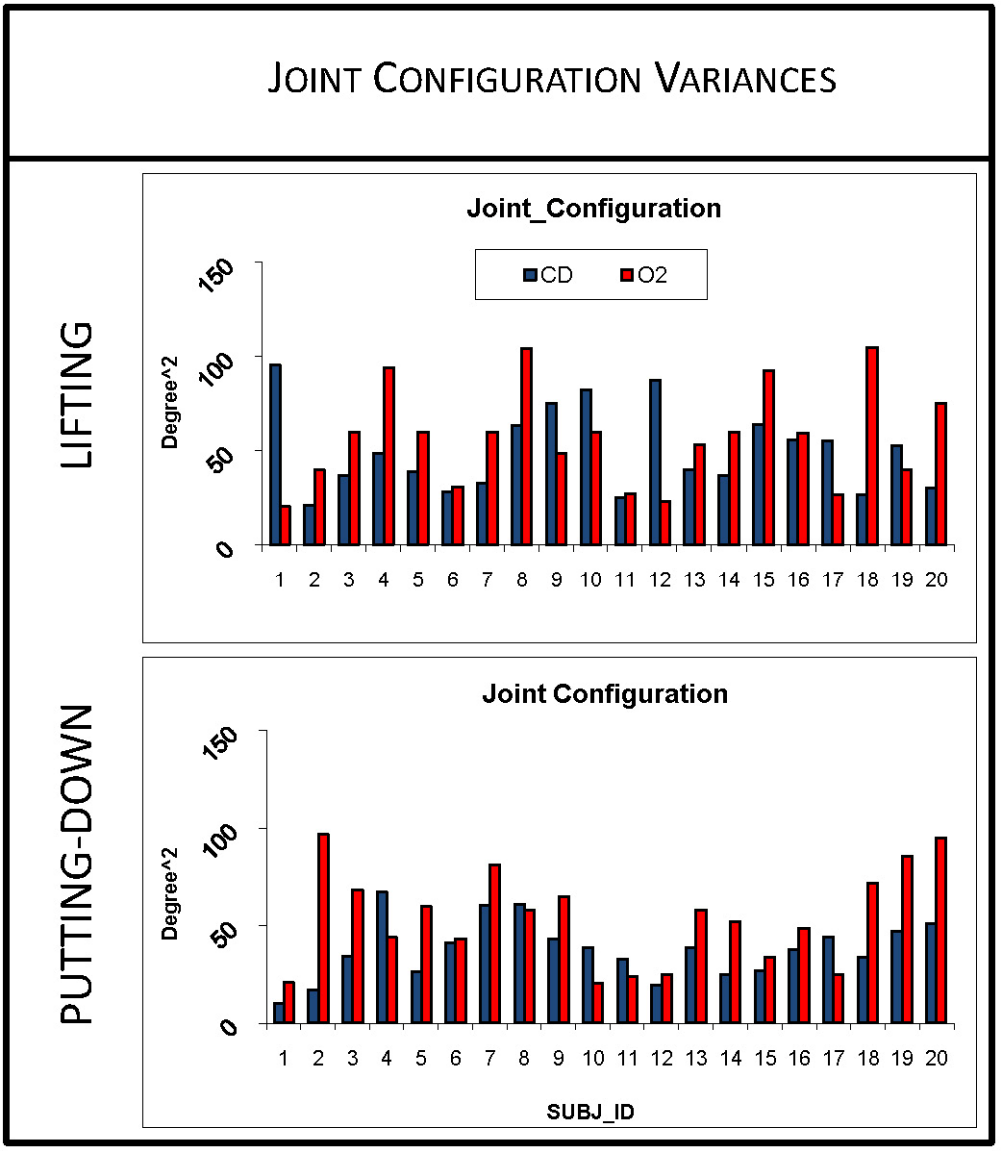

Figure 6.2. Variances of the joint configuration during holding movement period for the 20 individuals separately. In the upper panel variances observed during lifting while in the lower panel variances observed during putting-down are presented. Significant difference was observed at $p<0.05$ significance level between CD and O2 conditions only during putting-down proving the remarkable effect of the gravity on movement execution (Table 4.2). Higher CD variance than O2 variance was observed only in 6 subjects during lifting and only in 5 subjects during putting-down. meanCD<meanO2 across subjects occurred in both directions.

DOI:10.15774/PPKE.ITK.2012.004

VI.3. EMG Variances – All Individuals

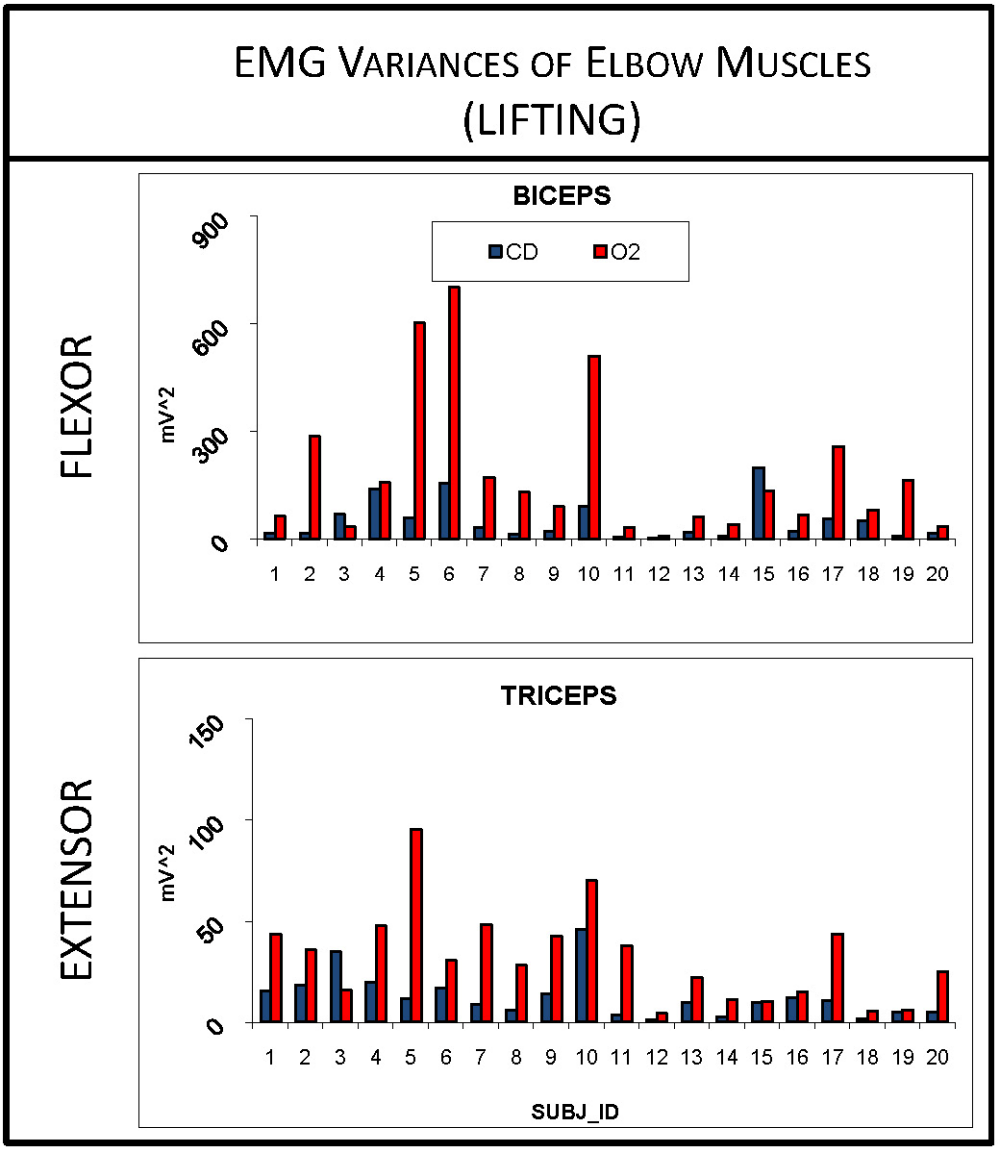

Figure 6.3. Variances of elbow muscle EMGs during holding period in lifting for the 20 individuals separately. In the upper panel variances observed in the flexor while in the lower panel variances observed in the extensor are presented. Significant difference was observed at $p<0.05$ significance level between CD and O2 conditions either for flexor or extensor (Table 4.2). Higher CD variance than O2 variance was observed only in 2 individuals for flexor and only in 1 individual for extensor activity. meanCD<meanO2 occurred across individuals.

DOI:10.15774/PPKE.ITK.2012.004

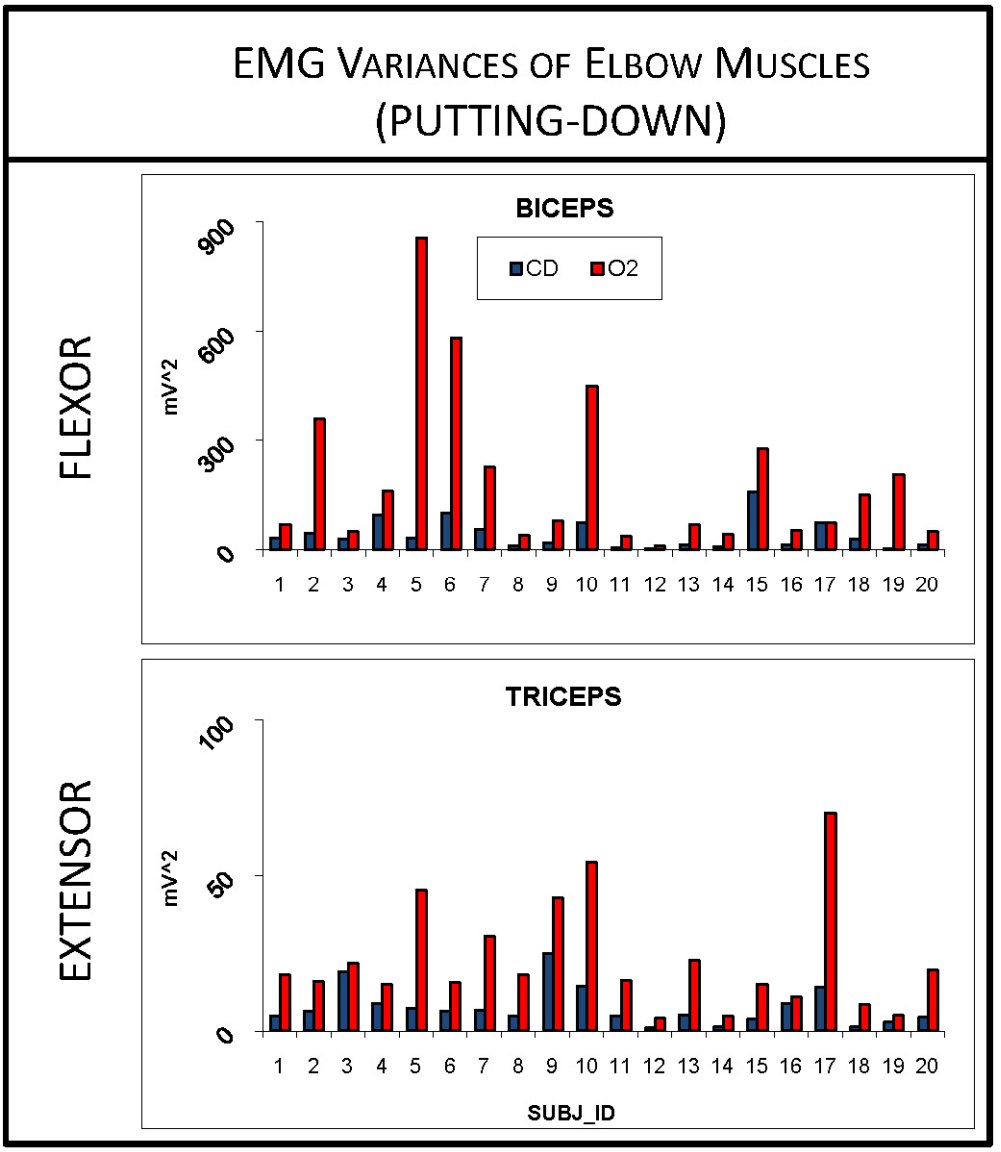

Figure 6.4. Variances of elbow muscle EMGs during holding period in putting-down for the 20 individuals separately. In the upper panel variances observed in the flexor while in the lower panel variances observed in the extensor are presented. Significant difference was observed at $p<0.05$ significance level between CD and O2 conditions either for flexor or extensor (Table 4.2). Higher CD variance than O2 variance was not observed in either muscle types. meanCD<meanO2 occured across individuals.

DOI:10.15774/PPKE.ITK.2012.004

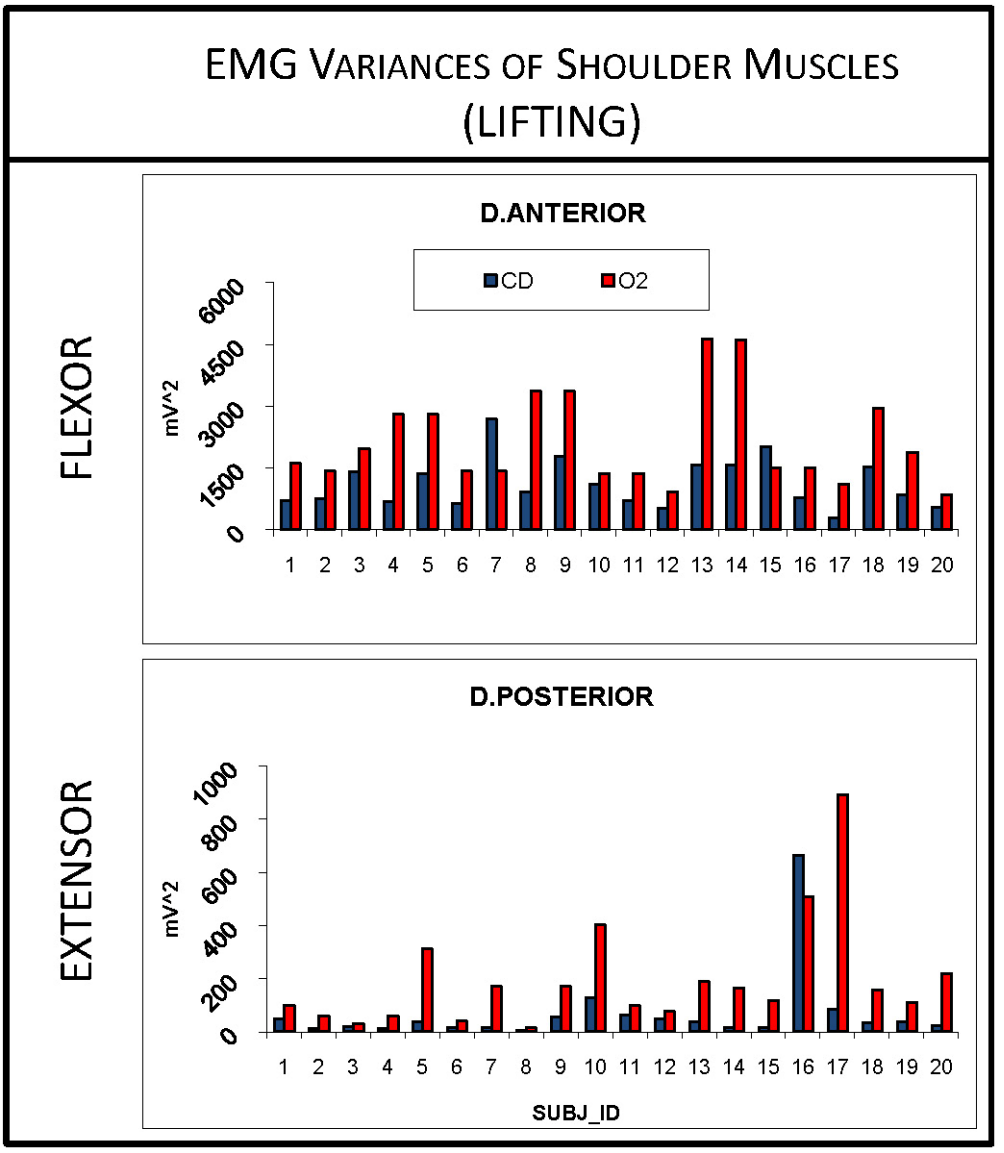

Figure 6.5. Variances of shoulder muscle EMGs during holding period in lifting for the 20 individuals separately. In the upper panel variances observed in the flexor while in the lower panel variances observed in the extensor are presented. Significant difference was observed at $p<0.05$ significance level between CD and O2 conditions either for flexor or extensor (Table 4.2). Higher CD variance than O2 variance was observed only in 2 individuals for flexor and only in 1 individual for extensor activity. meanCD<meanO2 occurred across individuals.

DOI:10.15774/PPKE.ITK.2012.004

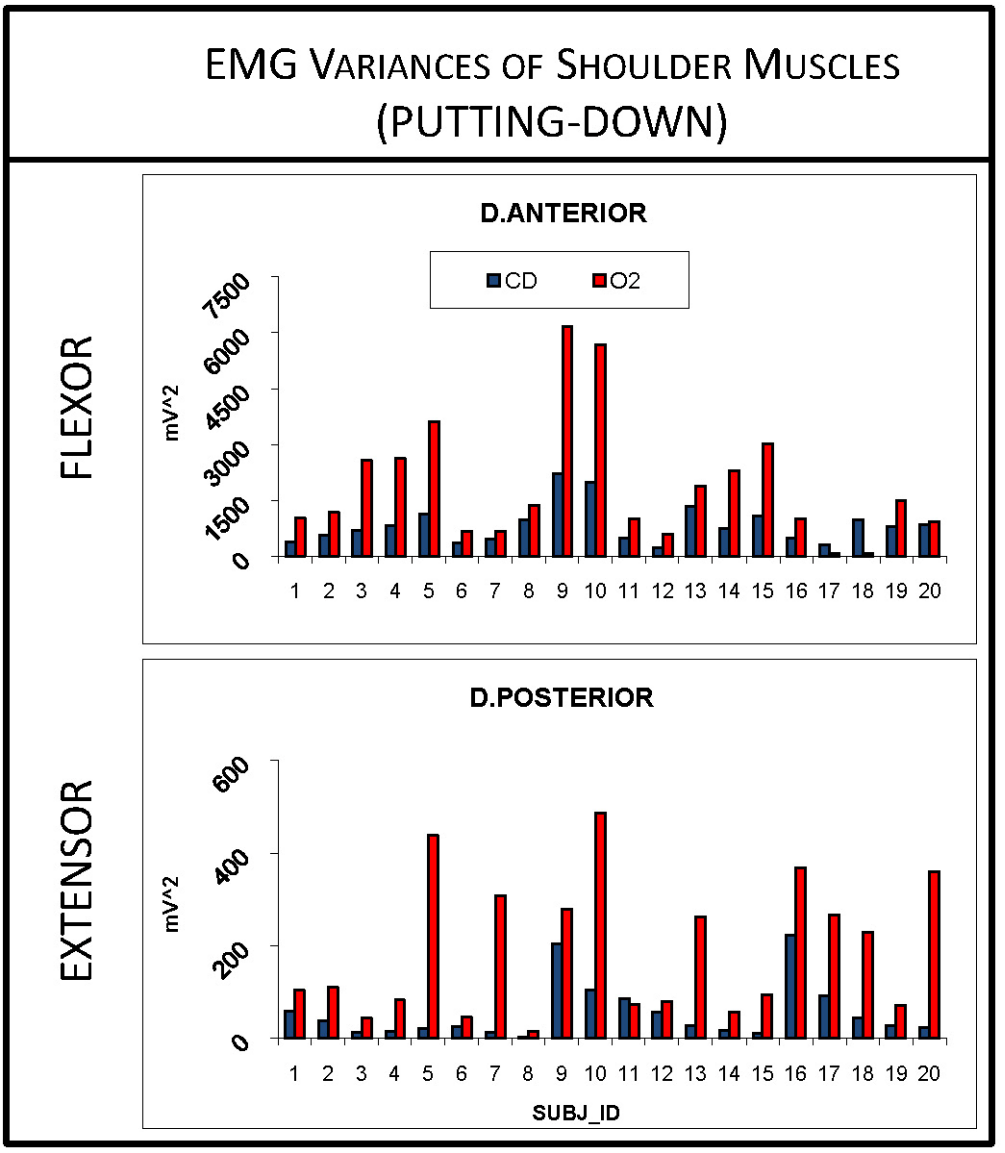

Figure 6.6. Variances of shoulder muscle EMGs during holding period in putting-down for the 20 individuals separately. In the upper panel variances observed in the flexor while in the lower panel variances observed in the extensor are presented. Significant difference was observed at $p<0.05$ significance level between CD and O2 conditions either for flexor or extensor (Table 4.2). Higher CD variance than O2 variance was observed only in 2 individuals for flexor and only in 1 individual for extensor activity. meanCD<meanO2 occurred across individuals.

DOI:10.15774/PPKE.ITK.2012.004

VI.4. Predicted Muscle Force Variances – All Individuals

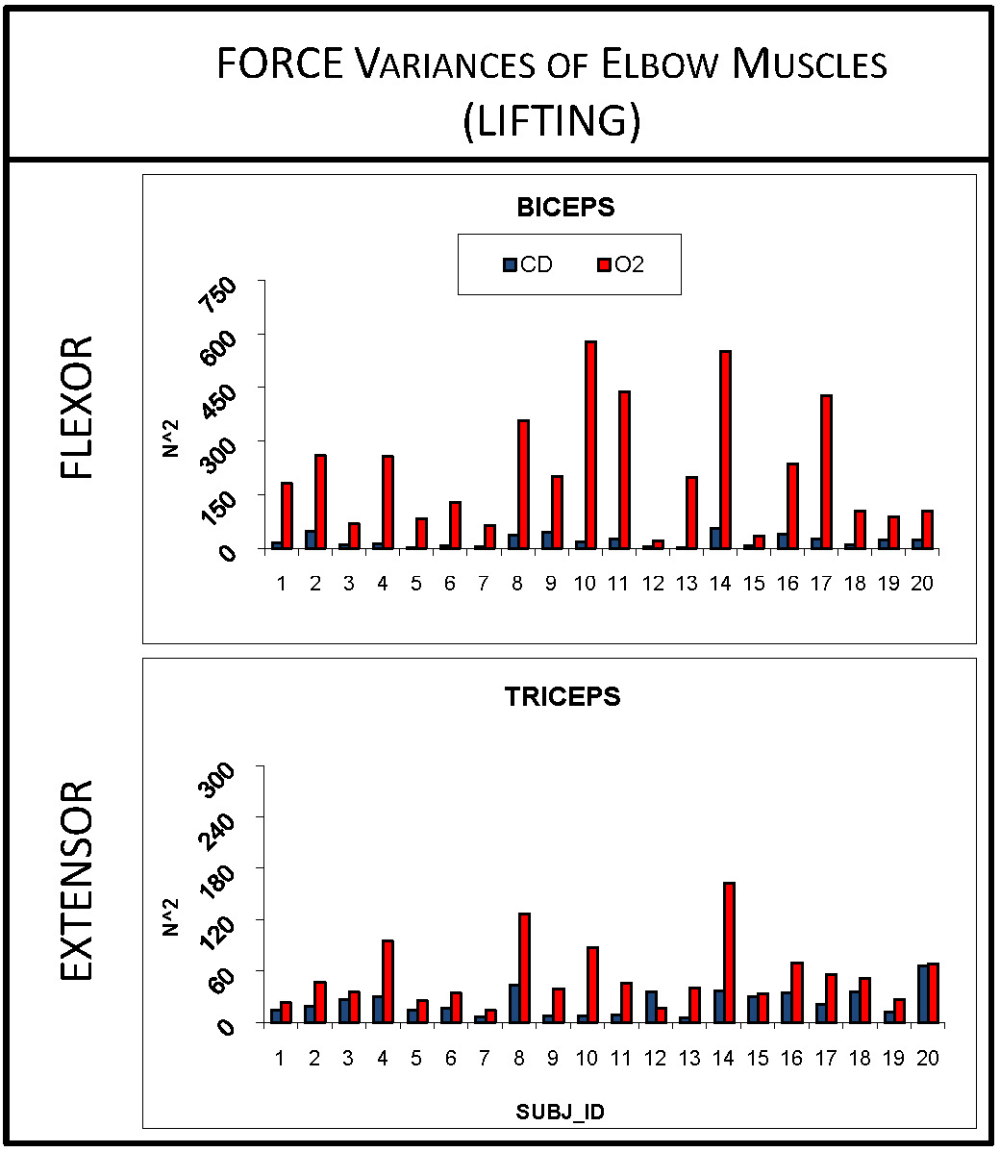

Figure 6.7. Variances of elbow muscle FORCEs during holding period in lifting for the 20 individuals separately. In the upper panel variances observed in the flexor while in the lower panel variances observed in the extensor are presented. Significant difference was observed at $p<0.05$ significance level between CD and O2 conditions either for flexor or extensor (Table 4.2). Higher CD variance than O2 variance was not observed for flexor and only in 1 individual for extensor activity. meanCD<meanO2 occurred across individuals.

DOI:10.15774/PPKE.ITK.2012.004

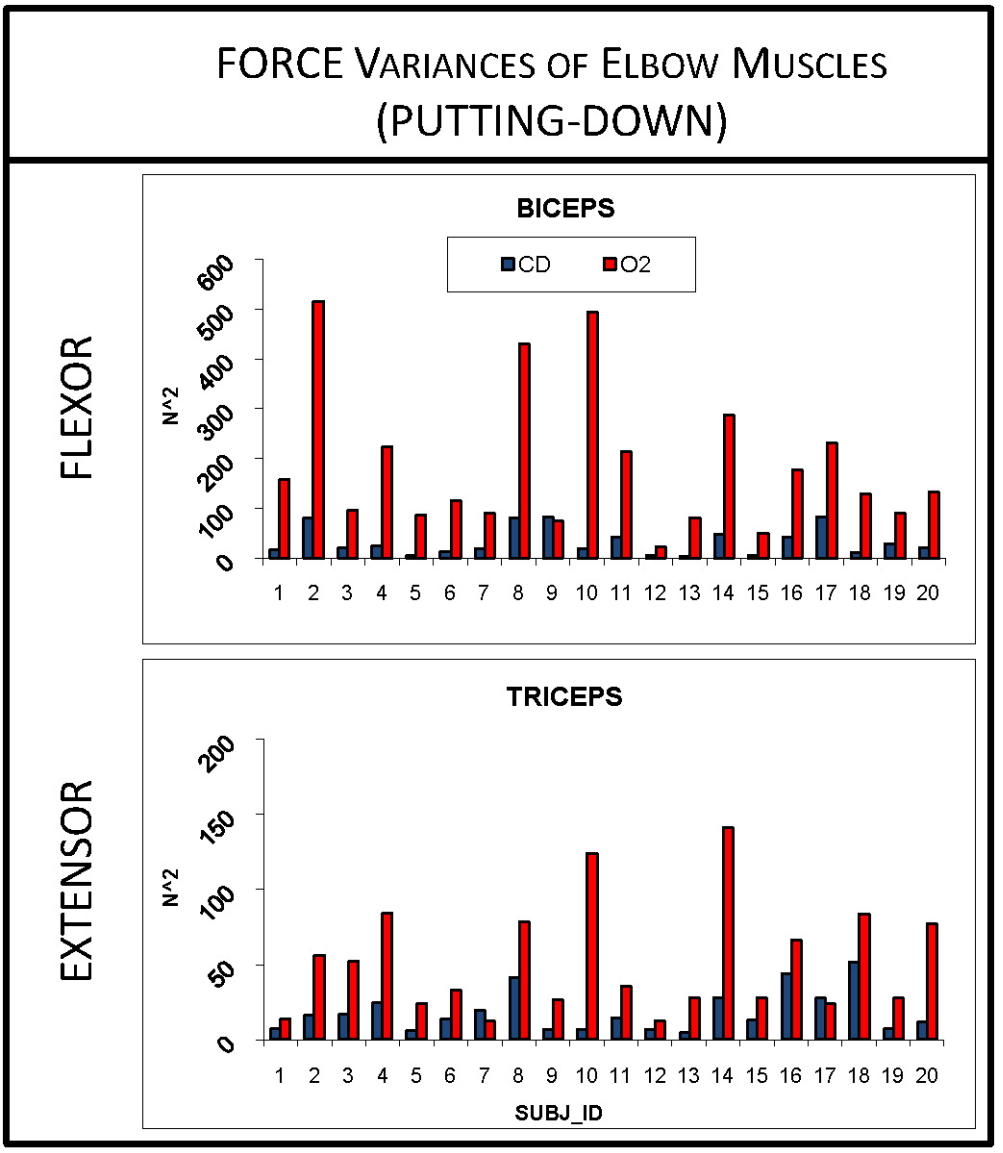

Figure 6.8. Variances of elbow muscle FORCEs during holding period in putting-down for the 20 individuals separately. In the upper panel variances observed in the flexor while in the lower panel variances observed in the extensor are presented. Significant difference was observed at $p<0.05$ significance level between CD and O2 conditions either muscle types (Table 4.2). Higher CD variance than O2 variance was observed only in 1 individual for both flexor and extensor activity. meanCD<meanO2 occurred across individuals.

DOI:10.15774/PPKE.ITK.2012.004

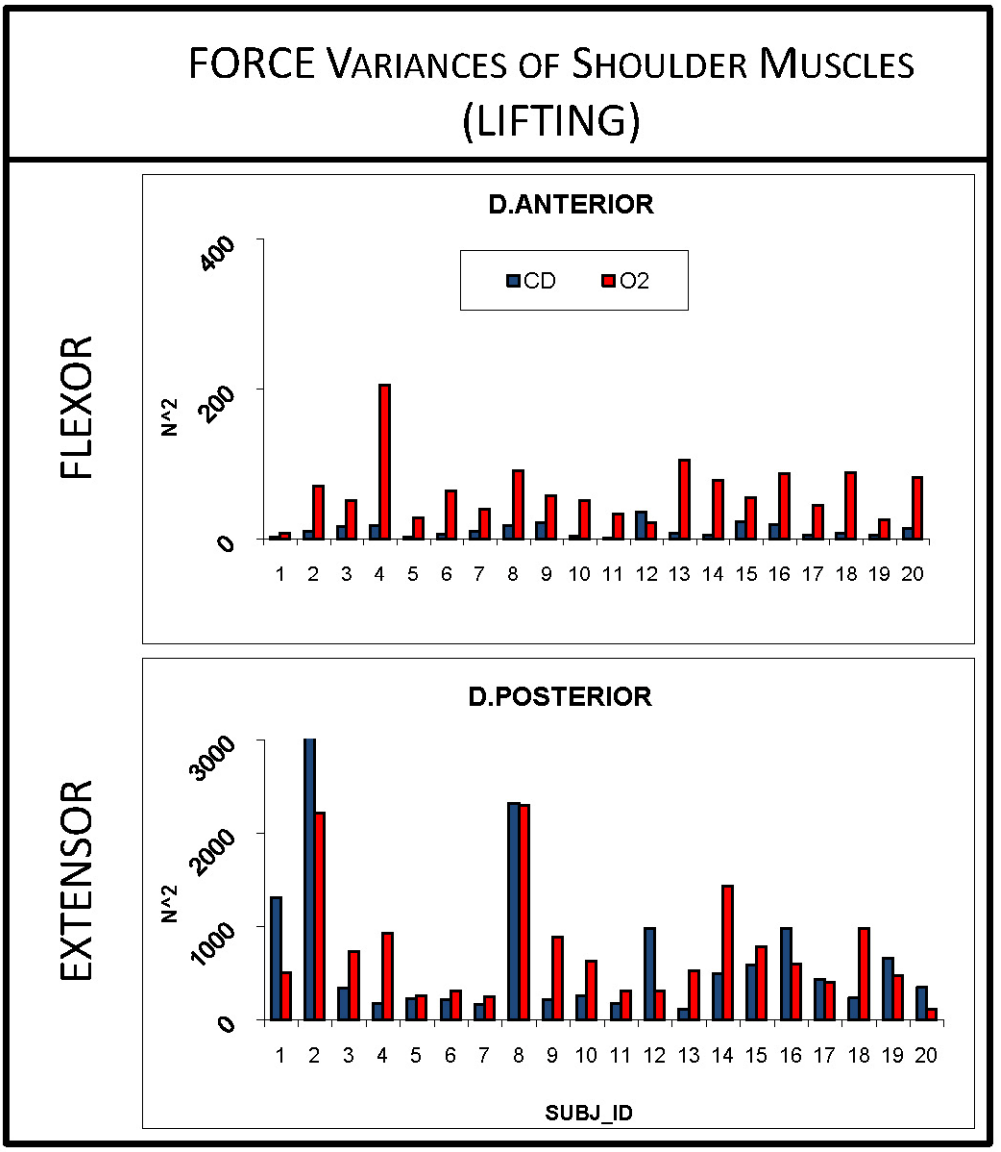

Figure 6.9. Variances of shoulder muscle FORCEs during holding period in lifting for the 20 individuals separately. In the upper panel variances observed in the flexor while in the lower panel variances observed in the extensor are presented. Significant difference was observed at $p<0.05$ significance level between CD and O2 conditions only for the flexor muscle (Table 4.2). Higher CD variance than O2 variance was observed only in 1 individual for flexor and in 7 individuals for extensor activity. meanCD<meanO2 occurred across individuals.

DOI:10.15774/PPKE.ITK.2012.004

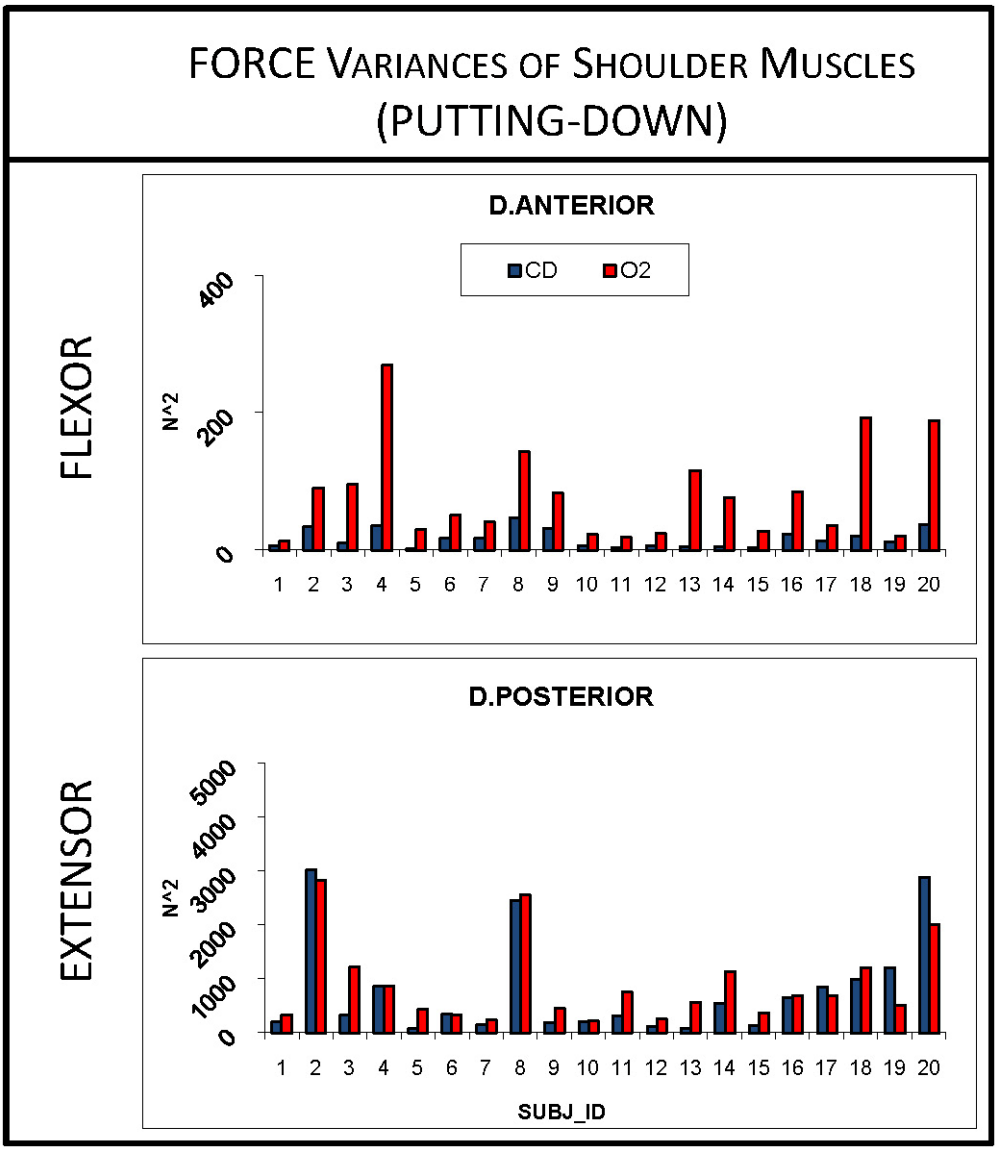

Figure 6.10. Variances of shoulder muscle FORCEs during holding period in putting-down for the 20 individuals separately. In the upper panel variances observed in the flexor while in the lower panel variances observed in the extensor are presented. Significant difference was observed at $p<0.05$ significance level between CD and O2 conditions only for the flexor muscle (Table 4.2). Higher CD variance than O2 variance was not observed for flexor and in 4 individuals for extensor activity. meanCD<meanO2 occurred across individuals.

DOI:10.15774/PPKE.ITK.2012.004

TABLE 6.1.
PEARSON'S R-VALUES OF ALL SUBJECTS FOR THE BI AND DA MUSCLE FORCES OBSERVED DURING HOLDING CONSIDERING ALL OBJECT CONDITIONS.

SubjID	BI FORCE						DA FORCE					
	UP			DOWN			UP			DOWN		
	CDO1	*CDO2*	*O1O2*	*CDO1*	*CDO2*	*O1O2*	*CDO1*	*CDO2*	*O1O2*	*CDO1*	*CDO2*	*O1O2*
1	0.38	0.3	**0.83**	0.69	0.8	**0.91**	-0.1	-0.1	**0.9**	**0.88**	0.68	0.7
2	0.27	-0.2	**0.63**	0.9	0.87	**0.94**	-0.1	0.01	**0.61**	0.82	0.8	**0.83**
3	0.53	0.43	**0.88**	0.98	0.97	**0.99**	-0.1	0.01	**0.61**	**0.98**	0.93	0.92
4	-0.2	0.03	**0.63**	0.83	0.77	**0.86**	0.04	0.15	**0.77**	**0.87**	0.52	0.7
5	0.4	0.39	**0.86**	0.86	0.98	0.85	0.47	0.68	**0.82**	**0.98**	0.95	0.94
6	0.75	0.71	**0.9**	0.9	0.84	**0.93**	0.17	0.47	**0.89**	0.95	0.96	**0.98**
7	**0.6**	-0.04	0.24	0.89	0.85	**0.94**	0.41	**0.71**	0.52	**0.89**	0.88	0.86
8	0.54	0.45	**0.55**	0.81	0.56	0.67	-0.44	-0.67	**0.7**	0.63	0.6	**0.89**
9	**0.21**	-0.02	-0.25	0.76	-0.01	0.1	-0.53	-0.89	**0.8**	**0.93**	0.72	0.73
10	-0.4	-0.3	**0.87**	0.75	0.47	**0.85**	0.18	-0.04	**0.87**	0.9	0.86	**0.95**
11	0.6	0.32	**0.76**	0.98	0.89	0.91	0.86	0.72	**0.87**	**0.96**	0.94	0.94
12	0.72	0.68	**0.95**	0.98	0.96	**0.98**	**0.83**	0.47	0.7	**0.98**	0.95	0.97
13	0.33	0.35	**0.88**	0.73	**0.85**	0.67	-0.12	-0.08	**0.81**	**0.82**	0.64	0.8
14	0.15	0.08	**0.88**	**0.97**	0.9	0.95	0.29	0.07	**0.84**	**0.96**	0.84	0.93
15	0.78	0.65	**0.92**	**0.93**	0.8	0.92	0.7	0.57	**0.81**	0.99	0.95	**0.99**
16	0.41	0.26	**0.55**	-0.8	**0.87**	-0.67	0.29	0.46	**0.51**	-0.8	**0.96**	-0.71
17	0.29	0.11	**0.89**	**0.91**	0.3	0.85	0	-0.2	**0.75**	0.83	0.9	**0.92**
18	0.38	0.39	**0.87**	0.86	0.9	**0.96**	-0.01	0.001	**0.71**	0.87	0.81	**0.94**
19	0.65	0.64	**0.98**	**0.94**	0.8	0.87	0.62	0.74	**0.81**	**0.94**	0.89	0.92
20	0.57	0.51	**0.94**	**0.95**	0.84	0.86	0.49	0.14	**0.88**	0.88	0.84	**0.96**
Mean	0.38	0.28	**0.73**	**0.79**	0.76	0.76	0.19	0.16	**0.75**	0.81	**0.83**	0.80
SD	0.30	0.29	0.29	0.38	0.24	0.39	0.39	0.44	0.11	0.38	0.13	0.36

*Note. The strongest ($0.21 \leq r \leq 0.99$) correlation coefficients were observed between O1 and O2; weaker correlation ($-0.1 \leq r \leq 0.98$) was present between CD and O1; the weakest coefficients ($-0.89 \leq r \leq 0.97$) were obtained between CD and O2 in the case of the force exerted by the biceps during lifting (**strongest correlation**; strong, but weaker correlation; the weakest correlation). Such correlation patterns were not present either during putting-down in the case of the biceps or in the case of the deltoid anterior muscle considering both directions. Therefore, the object invariant feature observed for the torque profiles is NOT true for the force profiles.*

DOI:10.15774/PPKE.ITK.2012.004

BIBLIOGRAPHY

PUBLICATIONS OF THE AUTHOR

Journal papers

R. **Tibold**, G. Fazekas, J. Laczkó, „Three-dimensional model to predict muscle forces and their relation to motor variances in reaching arm movements", *Journal of Applied Biomechanics* (in press), 2011

R. **Tibold**, J. Laczkó, „The effect of load on torques in point to point arm movements, a 3D model", *Journal of Motor Behavior* (submitted), 2011

J. Laczkó, **R**. **Tibold**, „Implications on Upper Extremity FES – A systematic review", *Ideggyógyászati Szemle/Clinical Neuroscience* (submitted), 2011

Conference papers

R. **Tibold**, A. Poka, B. Borbely, J. Laczkó, „The effect of load on joint- and muscle synergies in reaching arm movements". *Accepted at VII. Conference on Progress in Motor Control*, Marseille, France 2009. July, 2009

J. Laczkó, **R**. **Tibold**, G. Fazekas, „Neuromuscular synergy ensures kinematic stability during 3D reaching arm movements with load". *Program No. 272.2 2009 Neuroscience Meeting*. Chicago, IL: Soc. for Neuroscience, 2009. Online, 2009.

J. Laczkó, **R**. **Tibold**, „3D analysis to reveal muscle activity timing in object replacing arm movements", *11th International Symposium on the 3D Analysis of Human Movement*, San Francisco, 2010

J. Laczkó, T. Pilissy, **R**. **Tibold**, „Neuro-mechanical Modeling and Controlling of Human Limb Movements of Spinal Cord Injured Patients". *Proc. of the 2nd International Symposium on Applied Sciences in Biomedical and Communication Technologies*. ISBN 978-80-227-3216-1, 2009

DOI:10.15774/PPKE.ITK.2012.004

CITED PUBLICATIONS

[1] J. Sanyal, D. P. Chakraborty, and V. R. Rao, “Environmental and familial risk factors of Parkinsons disease: case-control study.,” *The Canadian journal of neurological sciences. Le journal canadien des sciences neurologiques*, vol. 37, no. 5, pp. 637-642, 2010.

[2] C. Fazekas, T. Vörös, Z. Kereszténvi, G. Kozmann, and J. Laczkó, “Computer aided interactive remote diagnosis of Parkinsonians.,” *Studies In Health Technology And Informatics*, vol. 90, pp. 572-576, 2002.

[3] Z. Kereszténvi, J. Laczkó, and K. Bötzel, “The time course of the return of upper limb bradykinesia after cessation of subthalamic stimulation in Parkinson’s disease.,” *Parkinsonism related disorders*, vol. 13, no. 7, pp. 438-442, 2007.

[4] Z. Kereszténvi, P. Cesari, G. Fazekas, and J. Laczkó, “The relation of hand and arm configuration variances while tracking geometric figures in Parkinson’s disease: aspects for rehabilitation.,” *International journal of rehabilitation research Internationale Zeitschrift fur Rehabilitationsforschung Revue internationale de recherches de readaptation*, vol. 32, no. 1, pp. 53-63, 2009.

[5] S. Judd, *Genetic Disorder Sourcebook*, Fourth Edi. Omnigraphics.

[6] S. Meunier, S. Lehéricy, L. Garnero, and M. Vidailhet, “Dystonia: lessons from brain mapping.,” *The Neuroscientist a review journal bringing neurobiology neurology and psychiatry*, vol. 9, no. 1, pp. 76-81, 2003.

[7] P. Czobor, J. Vitrai, S. Marosfi, and I. Toth, “Steady-state visual evoked-potential tests in Sclerosis Multiplex.,” *Electroencephalography and Clinical Neurophysiology*, vol. 50, no. 3-4, p. 117, 1980.

[8] J. Czopf, K. Hegedus, M. Kissantal, and G. Karmos, “Statistical-analysis of EEG and clinical data in multiple-sclerosis - significance of visual evoked-response in diagnosis of multiple-sclerosis.,” *Electroencephalography and Clinical Neurophysiology*, vol. 41, no. 2, p. 210, 1976.

[9] C. Bowen, A. MacLehose, and J. G. Beaumont, “Advanced multiple sclerosis and the psychosocial impact on families.,” *Psychology health*, vol. 26, no. 1, pp. 113-127, 2011.

[10] R. I. Spain, M. H. Cameron, and D. Bourdette, “Recent developments in multiple sclerosis therapeutics.,” *BMC Medicine*, vol. 7, no. 1, p. 74, 2009.

[11] T. Pilissy, K. Pad, G. Fazekas, M. Horvath, G. Stefanik, and J. Laczkó, “The role of ankle-joint during cycling movement task.,” *International Journal of Rehabilitation Research*, vol. 30, pp. 58-59, 2007.

[12] J. Szecsi, C. Krewer, F. Müller, and A. Straube, “Functional electrical stimulation assisted cycling of patients with subacute stroke: kinetic and kinematic analysis.,” *Clinical Biomechanics*, vol. 23, no. 8, pp. 1086-1094, 2008.

[13] A. Frotzler, S. Coupaud, and P. Eser, “High-volume FES-cycling partially reverses bone loss in people with chronic spinal cord injury.,” *Bone*, vol. 43, no. 1, pp. 169-176, 2008.

[14] E. Ambrosini, S. Ferrante, T. Schauer, G. Ferrigno, F. Molteni, and A. Pedrocchi, “Design of a symmetry controller for cycling induced by electrical stimulation: preliminary results on post-acute stroke patients.,” *Artificial Organs*, vol. 34, no. 8, pp. 663-667, 2010.

[15] E. Ambrosini, S. Ferrante, and T. Schauer, “Simulation and experimental design of a symmetry controller for fes cycling optimised on stroke patients.,” *Technology*, pp. 245-250, 2007.

[16] L. A. Johnson and A. J. Fuglevand, “Mimicking muscle activity with electrical stimulation.,” *Journal of Neural Engineering*, vol. 8, no. 1, pp. 9-16, 2011.

[17] P. F. Li, Y. Hong, and J. Zhang, “An FES cycling control system based on CPG.,” *Conference Proceedings of the International Conference of IEEE Engineering in Medicine and Biology Society*, vol. 2009, pp. 1569-1572, 2009.

[18] A. Szentgyorgyi, “Muscle research.,” *Scientific American*, vol. 180, no. 6, pp. 22-25, 1949.

[19] J. Szecsi, S. Krafczyk, J. Quintern, M. Fiegel, A. Straube, and T. Brandt, “Paraplegic cycling using functional electrical stimulation. Experimental and model-based study of power output,” *Der Nervenarzt*, vol. 75, no. 12, pp. 1209-1216, 2004.

[20] A. J. Van Soest, M. Gföhler, and L. J. R. Casius, “Consequences of ankle joint fixation on FES cycling power output: a simulation study.,” *Medicine & Science in Sports & Exercise*, vol. 37, no. 5, pp. 797-806, 2005.

[21] J. Szecsi, C. Schlick, M. Schiller, W. Pöllmann, N. Koenig, and A. Straube, “Functional electrical stimulation-assisted cycling of patients with multiple sclerosis: biomechanical and functional outcome--a pilot study.,” *Journal of rehabilitation medicine official journal of the UEMS European Board of Physical and Rehabilitation Medicine*, vol. 41, no. 8, pp. 674-680, 2009.

[22] L. Comolli, S. Ferrante, A. Pedrocchi, M. Bocciolone, G. Ferrigno, and F. Molteni, “Metrological characterization of a cycle-ergometer to optimize the

DOI:10.15774/PPKE.ITK.2012.004

cycling induced by functional electrical stimulation on patients with stroke.," *Medical Engineering & Physics*, vol. 32, no. 4, pp. 339-348, 2010.

[23] P. N. Taylor, J. Esnouf, and J. Hobby, "Pattern of use and user satisfaction of Neuro Control Freehand system.," *Spinal cord the official journal of the International Medical Society of Paraplegia*, vol. 39, no. 3, pp. 156-160, 2001.

[24] P. N. Taylor, J. Esnouf, and J. Hobby, "The functional impact of the Freehand system on tetraplegic hand function - Clinical results.," *Spinal cord the official journal of the International Medical Society of Paraplegia*, vol. 40, no. 11, pp. 560-566, 2002.

[25] A. Naito, M. Yajima, H. Fukamachi, and Y. Shimizu, "Functional electrical stimulation (FES) to the biceps brachii for controlling forearm supination in the paralyzed upper extremity.," *The Tohoku journal of experimental medicine*, vol. 173, no. 2, pp. 269-273, 1994.

[26] R. Raikova, "A general approach for modelling and mathematical investigation of the human upper limb.," *Journal of Biomechanics*, vol. 25, no. 8, pp. 857-867, 1992.

[27] J. Langenderfer, S. A. Jerabek, V. B. Thangamani, J. E. Kuhn, and R. E. Hughes, "Musculoskeletal parameters of muscles crossing the shoulder and elbow and the effect of sarcomere length sample size on estimation of optimal muscle length.," *Clinical Biomechanics*, vol. 19, no. 7, pp. 664-670, 2004.

[28] K. R. S. Holzbaur, S. L. Delp, G. E. Gold, and W. M. Murray, "Moment-generating capacity of upper limb muscles in healthy adults.," *Journal of Biomechanics*, vol. 40, no. 11, pp. 2442-2449, 2007.

[29] A. A. Amis, D. Dowson, V. Wright, and J. H. Miller, "The derivation of elbow joint forces, and their relation to prosthesis design.," *Journal of medical engineering technology*, vol. 3, no. 5, pp. 229-234, 1979.

[30] A. A. Amis, D. Dowson, and V. Wright, "Analysis of elbow forces due to high-speed forearm movements.," *Journal of Biomechanics*, vol. 13, no. 10, pp. 825-831, 1980.

[31] A. A. Amis, J. H. Miller, D. Dowson, and V. Wright, "Elbow joint forces – Basic data for prosthesis designers.," *Journal of Bone and Joint Surgery-British*, vol. 62, no. 2, pp. 251-252, 1980.

[32] K. N. An, F. C. Hui, B. F. Morrey, R. L. Linscheid, and E. Y. Chao, "Muscles across the elbow joint: A biomechanical analysis.," *Journal of Biomechanics*, vol. 14, no. 10, pp. 659-669, 1981.

[33] K. N. An, K. R. Kaufman, and E. Y. Chao, “Physiological considerations of muscle force through the elbow joint.,” *Journal of Biomechanics*, vol. 22, no. 11-12, pp. 1249-1256, 1989.

[34] S. I. Backus, J. D. Mabry, M. A. Kroll, R. F. Warren, and J. C. Otis, “Torque production in the shoulder of the normal young-adult male.,” *Physical Therapy*, vol. 65, no. 5, p. 715, 1985.

[35] J. T. London, “Kinematics of the elbow.,” *The Journal of Bone and Joint Surgery*, vol. 63, no. 4, pp. 529-535, 1981.

[36] J. C. Otis, R. F. Warren, S. I. Backus, T. J. Santner, and J. D. Mabrey, “Torque production in the shoulder of the normal young adult male. The interaction of function, dominance, joint angle, and angular velocity.,” *The American Journal of Sports Medicine*, vol. 18, no. 2, pp. 119-123, 1990.

[37] F. E. Zajac and M. E. Gordon, “Determining muscle’s force and action in multi-articular movement.,” *Exercise and Sport Sciences Reviews*, vol. 17, no. 1, pp. 187-230, 1989.

[38] E. Pennestrì, R. Stefanelli, P. P. Valentini, and L. Vita, “Virtual musculo-skeletal model for the biomechanical analysis of the upper limb.,” *Journal of Biomechanics*, vol. 40, no. 6, pp. 1350-1361, 2007.

[39] Q. Shao, D. N. Bassett, K. Manal, and T. S. Buchanan, “An EMG-driven model to estimate muscle forces and joint moments in stroke patients.,” *Computers in Biology and Medicine*, vol. 39, no. 12, pp. 1083-1088, 2009.

[40] Q. Shao and T. S. Buchanan, “A biomechanical model to estimate corrective changes in muscle activation patterns for stroke patients.,” *Journal of Biomechanics*, vol. 41, no. 14, pp. 3097-3100, 2008.

[41] G. Fazekas, M. Horvath, T. Troznai, and A. Toth, “Robot-mediated upper limb physiotherapy for patients with spastic hemiparesis: a preliminary study.,” *Journal of rehabilitation medicine official journal of the UEMS European Board of Physical and Rehabilitation Medicine*, vol. 39, no. 7, pp. 580-582, 2007.

[42] H. A. Abdullah, C. Tarry, R. Datta, G. S. Mittal, and M. Abderrahim, “Dynamic biomechanical model for assessing and monitoring robot-assisted upper-limb therapy.,” *Journal Of Rehabilitation Research And Development*, vol. 44, no. 1, pp. 43-62, 2007.

[43] H. Abdullah, C. Tarry, and G. Mittal, “A biomechanical model to aid robot-assisted therapy of upper limb impairment,” in *IECON 200632nd*, 2006, no. 519, pp. 4107-4112.

[44] “Stroke Center,” 2011. [Online]. Available: http://www.strokecenter.org/patients/stats.htm.

DOI:10.15774/PPKE.ITK.2012.004

[45] J. Laczkó, A. J. Pellionisz, B. W. Peterson, and T. S. Buchanan, "Multidimensional sensorimotor 'patterns' arising from a graphics-based tensorial model of the neck-motor system.," *Society for Neuroscience Abstracts*, vol. 13, no. 1, p. 372, 1987.

[46] J. Laczkó, A. Pellionisz, H. Jongen, and S. C. A. M. Gielen, "Computer modeling of human forelimb muscle activation in multidimensional Intrinsic coordinate frames.," *Society fot Neuroscience. Abstract*, vol. 14, no. 2, p. 955, 1988.

[47] J. Laczkó, "Modeling of limb movements as a function of motoneuron activities.," *Kalokagathia*, vol. 43, no. 3, pp. 24-34, 2005.

[48] J. Laczkó, K. Walton, and R. Llinas, "A neuro-mechanical transducer model for controlling joint rotations and limb movements.," *Ideggyogyaszati Szemle*, vol. 59, no. 1-2, pp. 32-43, 2006.

[49] J. Laczkó, T. Pilissy, and A. Klauber, "Modeling of limb movements for controlling functional electrical stimulation of paraplegics.," *Proc. of the Third Hungarian Conference on Biomechanics*, pp. 151-157, 2008.

[50] J. Laczkó, "Modeling of multi-joint movements.," *Kalokagathia 2001, Spec. Issue*, pp. 91-96, 2001.

[51] N. Bernstein, "The co-ordination and regulation of movements.," *Neuropsychologia*, vol. 6, no. 1, p. 215, 1967.

[52] I. M. Gelfand, M. L. Tsetlin, V. S. Gurfinkel, and S. V. Fomin, "Mathematical modeling of the mechanisms of the central nervous system," *Models of the structuralfunctional organization of certain biological systems*, pp. 1-22, 1971.

[53] T. Flash and N. Hogan, "The coordination of arm movements: an experimentally confirmed mathematical model.," *Journal of Neuroscience*, vol. 5, no. 7, pp. 1688-1703, 1985.

[54] J. Laczkó, S. Jaric, J. Tihanyi, V. M. Zatsiorsky, and M. L. Latash, "Components of the end-effector jerk during voluntary arm movements.," *Journal of Applied Biomechanics*, no. 16, pp. 14-26, 2000.

[55] M. Kawato, Y. Maeda, Y. Uno, and R. Suzuki, "Trajectory formation of arm movement by cascade neural network model based on minimum torque-change criterion.," *Biological Cybernetics*, vol. 62, no. 4, pp. 275-288, 1990.

[56] Y. Uno, M. Kawato, and R. Suzuki, "Formation and control of optimal trajectory in human multijoint arm movement," *Biological Cybernetics*, vol. 61, no. 2, pp. 89-101, 1989.

[57] M. L. Latash, *Control of human movement*. Human Kinetics, 1993.

[58] B. I. Prilutsky, “Coordination of two- and one-joint muscles: functional consequences and implications for motor control.,” *Motor Control*, vol. 4, no. 1, pp. 1-44, 2000.

[59] D. Domkin, J. Laczkó, S. Jaric, H. Johansson, and M. L. Latash, “Structure of joint variability in bimanual pointing tasks.,” *Experimental Brain Research*, vol. 143, no. 1, pp. 11-23, 2002.

[60] D. Domkin, J. Laczkó, M. Djupsjöbacka, S. Jaric, and M. L. Latash, “Joint angle variability in 3D bimanual pointing: uncontrolled manifold analysis.,” *Experimental Brain Research*, vol. 163, no. 1, pp. 44-57, 2005.

[61] M. L. Latash, J. K. Shim, and V. M. Zatsiorsky, “Is there a timing synergy during multi-finger production of quick force pulses?,” *Psychopharmacology*, vol. 177, no. 1-2, pp. 217-223, 2004.

[62] M. L. Latash, V. Krishnamoorthy, J. P. Scholz, and V. M. Zatsiorsky, “Postural synergies and their development.,” *Neural Plasticity*, vol. 12, no. 2-3, pp. 119-30; discussion 263-72, 2005.

[63] G. Torres-Oviedo, J. M. Macpherson, and L. H. Ting, “Muscle synergy organization is robust across a variety of postural perturbations.,” *Journal of Neurophysiology*, vol. 96, no. 3, pp. 1530-1546, 2006.

[64] E. Kellis and A. Katis, “Hamstring antagonist moment estimation using clinically applicable models: Muscle dependency and synergy effects.,” *Journal of Electromyography and Kinesiology*, vol. 18, no. 1, pp. 144-153, 2008.

[65] J. Laczkó, K. Walton, and R. Llinas, “Modeling study of the relationship between spinal motoneuron pool firing rate and hindlimb posture during locomotion: consideration of the effects of alerting gravity during development.,” in *Program No. 448.5. 2006 Abstract Viewer. Society for Neuroscience.*, 2006.

[66] T. Schaaf, J. Hartmann, and E. J. Seidel, “Comparison of measurement devices Zebris (R) CMS 70 P and Varilux Essilor VisionPrint System (TM) for identification of neuro-muscular patterns ‘head-or-eye-mover’,” *Physikalische Medizin Rehabilitationsmedizin Kurortmedizin*, vol. 20, no. 1, pp. 20-26, 2010.

[67] E.-M. Malmström, M. Karlberg, A. Melander, and M. Magnusson, “Zebris versus Myrin: a comparative study between a three-dimensional ultrasound movement analysis and an inclinometer/compass method: intradevice reliability, concurrent validity, intertester comparison, intratester reliability, and intraindividual variab,” *Spine*, vol. 28, no. 21, p. E433-E440, 2003.

[68] L. D. Loukopoulos, S. F. Engelbrecht, and N. E. Berthier, “Planning of reach-and-grasp movements: effects of validity and type of object information.,” *Journal of Motor Behavior*, vol. 33, no. 3, pp. 255-264, 2001.

DOI:10.15774/PPKE.ITK.2012.004

[69] J. Szentágothai and M. Réthelyi, *A felső végtag izmai, Funckionális anatómiai I.* Medicina, 2002, pp. 583-607.

[70] J. Szentágothai and M. Réthelyi, *A felső végtag csontjai és ízületei, Funckionális anatómiai I.* Medicina, 2002, pp. 412-433.

[71] K. S. Erer, "Adaptive usage of the Butterworth digital filter.," *Journal of Biomechanics*, vol. 40, no. 13, pp. 2934-2943, 2007.

[72] M. Horvath and G. Fazekas, "Assessment of motor impairment with electromyography--the kinesiological EMG.," *Ideggyogyaszati Szemle*, vol. 56, no. 11-12. pp. 360-369, 2003.

[73] J. Becher, J. Harlaar, T. W. Vogelaar, and H. Bakker, "Assessment of muscle function in hemiplegic and healthy-subjects by kinesiological emg-registration during repetitive movements.," *Electrophysiological Kinesiology*, vol. 804, pp. 357-360, 1988.

[74] D. H. Sutherland, "The evolution of clinical gait analysis part l: kinesiological EMG.," *Gait & Posture*, vol. 14, no. 1, pp. 61-70, 2001.

[75] V. M. Zatsiorsky, *Kinematics of Human Motion*. Champaign IL: Human Kinetics, 2008.

[76] H. E. J. Veeger, B. Yu, K. N. An, and R. H. Rozendal, "Parameters for modeling the upper extremity.," *Journal of Biomechanics*, vol. 30, no. 6, pp. 647-652, 1997.

[77] K. N. An, M. Jacobsen, L. Berglund, and E. Chao, "Application of a magnetic tracking device to kinesiologic studies," *Journal of Biomechanics*, vol. 21, no. 7, pp. 613–615, 1988.

[78] J. B. Wickham and J. M. Brown, "Muscles within muscles: the neuromotor control of intra-muscular segments.," *European Journal Of Applied Physiology And Occupational Physiology*, vol. 78, no. 3, pp. 219-225, 1998.

[79] R. Tibold, G. Fazekas, and J. Laczkó, "Three-dimensional model to predict muscle forces and their relation to motor variances in reaching arm movements.," *Journal of Applied Biomechanics*, p. (in press), 2011.

[80] J. M. Brown, J. B. Wickham, D. J. McAndrew, and X. F. Huang, "Muscles within muscles: Coordination of 19 muscle segments within three shoulder muscles during isometric motor tasks.," *Journal of Electromyography and Kinesiology*, vol. 17, no. 1, pp. 57-73, 2007.

[81] A. V. Hill, "The heat of shortening and the dynamic constants of muscle.," *Proceedings of the Royal Society B Biological Sciences*, vol. 126, no. 843, pp. 136-195, 1938.

[82] R. D. Woittiez, P. A. Huijing, and R. H. Rozendal, “Influence of muscle architecture on the length-force diagram a model and its verification.,” *Pfliigers Arch*, vol. 397, pp. 73-74, 1983.

[83] R. D. Woittiez, P. A. Huijing, H. B. Boom, and R. H. Rozendal, “A three-dimensional muscle model: a quantified relation between form and function of skeletal muscles.,” *Journal of Morphology*, vol. 182, no. 1, pp. 95-113, 1984.

[84] P. A. Huijing and R. D. Woittiez, “The effect of architecture on skeletal muscle performance: a simple planimetric model.,” *Netherlands Journal of Zoology*, vol. 34, no. 1, pp. 21-32, 1984.

[85] Y. W. Chang, F. C. Su, H. W. Wu, and K. N. An, “Optimum length of muscle contraction.,” *Clinical Biomechanics*, vol. 14, no. 8, pp. 537-542, 1999.

[86] J. Fridén and R. L. Lieber, “Quantitative evaluation of the posterior deltoid to triceps tendon transfer based on muscle architectural properties.,” *The Journal of hand surgery*, vol. 26, no. 1, pp. 147-155, 2001.

[87] L. De Wilde, E. Audenaert, E. Barbaix, A. Audenaert, and K. Soudan, “Consequences of deltoid muscle elongation on deltoid muscle performance: a computerised study.,” *Clinical Biomechanics*, vol. 17, no. 7, pp. 499-505, 2002.

[88] G. L. Gottlieb, “A computational model of the simplest motor program.,” *Journal of Motor Behavior*, vol. 25, pp. 153-161, 1993.

[89] K. R. S. Holzbaur, W. M. Murray, and S. L. Delp, “A model of the upper extremity for simulating musculoskeletal surgery and analyzing neuromuscular control.,” *Annals of Biomedical Engineering*, vol. 33, no. 6, pp. 829-840, 2005.

[90] S. L. Delp, J. P. Loan, M. G. Hoy, F. E. Zajac, E. L. Topp, and J. M. Rosen, “An interactive graphics-based model of the lower extremity to study orthopaedic surgical procedures.,” *IEEE Transactions on Biomedical Engineering*, vol. 37, no. 8, pp. 757-767, 1990.

[91] S. L. Delp and J. P. Loan, “A graphics-based software system to develop and analyze models of musculoskeletal structures.,” *Computers in Biology and Medicine*, vol. 25, no. 1, pp. 21-34, 1995.

[92] J. Vaughan, D. A. Rosenbaum, C. J. Harp, L. D. Loukopoulos, and S. F. Engelbrecht, “Finding final postures.,” *Journal of Motor Behavior*, vol. 30, no. 3, pp. 273-284, 1998.

[93] M. A. Lemay, P. E. Crago, M. Katorgi, and G. J. Chapman, “Automated tuning of a closed-loop hand grasp neuroprosthesis.,” *IEEE Transactions on Biomedical Engineering*, vol. 40, no. 7, pp. 675-685, 1993.

DOI:10.15774/PPKE.ITK.2012.004

[94] M. A. Lemay and P. E. Crago, “A dynamic model for simulating movements of the elbow, forearm, and wrist.,” *Journal of Biomechanics*, vol. 29, no. 10, pp. 1319-1330, 1996.

[95] F. E. Zajac, “Muscle and tendon: properties, models, scaling, and application to biomechanics and motor control.,” *Critical Reviews in Biomedical Engineering*, vol. 17, no. 4, pp. 359-411, 1989.

[96] C. Fleischer and G. Hommel, “Calibration of an EMG-based body model with six muscles to control a leg exoskeleton.,” *Proceedings 2007 IEEE International Conference on Robotics and Automation*, no. April, pp. 2514-2519, 2007.

[97] E. M. Arnold, S. R. Ward, R. L. Lieber, and S. L. Delp, “A model of the lower limb for analysis of human movement.,” *Annals of Biomedical Engineering*, vol. 38, no. 2, pp. 269-279, 2010.

[98] A. M. Green and J. F. Kalaska, “Learning to move machines with the mind.,” *Trends in Neurosciences*, vol. 34, no. 2, pp. 61-75, 2011.

[99] D. Landin, J. Myers, M. Thompson, R. Castle, and J. Porter, “The role of the biceps brachii in shoulder elevation.,” *Journal of Electromyography and Kinesiology*, vol. 18, no. 2, pp. 270-275, 2008.

[100] D. Landin and M. Thompson, “The shoulder extension function of the triceps brachii.,” *Journal of Electromyography and Kinesiology*, vol. 21, no. 1, pp. 161-165, 2011.

[101] T. Uchiyama, T. Bessho, and K. Akazawa, “Static torque-angle relation of human elbow joint estimated with artificial neural network technique.,” *Journal of Biomechanics*, vol. 31, no. 6, pp. 545-554, 1998.

[102] W. M. Murray, S. L. Delp, and T. S. Buchanan, “Variation of muscle moment arms with elbow and forearm position.,” *Journal of Biomechanics*, vol. 28, no. 5, pp. 513-525, 1995.

[103] J. M. Winters and D. G. Kleweno, “Effect of initial upper-limb alignment on muscle contributions to isometric strength curves.,” *Journal of Biomechanics*, vol. 26, no. 2, pp. 143-153, 1993.

[104] D. K. Kuechle, S. R. Newman, E. Itoi, G. L. Niebur, B. F. Morrey, and K. N. An, “The relevance of the moment arm of shoulder muscles with respect to axial rotation of the glenohumeral joint in four positions.,” *Clinical Biomechanics*, vol. 15, no. 5, pp. 322-329, 2000.

[105] A. G. Feldman, V. Goussev, A. Sangole, and M. F. Levin, “Threshold position control and the principle of minimal interaction in motor actions,” *Brain*, vol. 165, pp. 267-281, 2007.

[106] A. G. Feldman, “Once more on the equilibrium-point hypothesis (l model) for motor control,” *Journal of Motor Behavior*, vol. 18, no. 1, pp. 17-54, 1986.

[107] M. F. Levin and A. G. Feldman, “The lambda-model for motor control - more than meets the eye - authors response,” *Behavioral and Brain Sciences*, vol. 18, no. 4, p. 786, 1995.

[108] A. Terrier, M. Aeberhard, and D. P. Pioletti, “A musculoskeletal shoulder model based on pseudo-inverse and null-space optimization.,” *Medical Engineering & Physics*, vol. 32, no. 9, pp. 1050-1056, 2010.

[109] F. Gao, M. L. Latash, and V. M. Zatsiorsky, “Similar motion of a hand-held object may trigger nonsimilar grip force adjustments.,” *Journal of hand therapy official journal of the American Society of Hand Therapists*, vol. 20, no. 4, pp. 300-307, 2007.

[110] F. Danion and V. K. Jirsa, “Motor prediction at the edge of instability: alteration of grip force control during changes in bimanual coordination.,” *Journal of Experimental Psychology: Human Perception and Performance*, vol. 36, no. 6, pp. 1684-1692, 2010.

[111] T. H. Falk, C. Tam, H. Schwellnus, and T. Chau, “Grip force variability and its effects on children’s handwriting legibility, form, and strokes.,” *Journal of Biomechanical Engineering*, vol. 132, no. 11, pp. 1145-1150, 2010.

[112] J. Valvano, J. Davis, N. Denniston, and T. Nicklas, “Grip force production linked to upper extremity kinematics describes impairments in bimanual motor control in children with hemiplegic cerebral palsy.,” *Journal of Sport & Exercise Psychology*, vol. 32, pp. 133-134, 2010.

[113] J. Jacquier-Bret, N. Rezzoug, and P. Gorce, “Adaptation of joint flexibility during a reach-to-grasp movement.,” *Motor Control*, vol. 13, no. 3, pp. 342-361, 2009.

[114] J. Nishii and Y. Taniai, “Evaluation of trajectory planning models for arm-reaching movements based on energy cost.,” *Neural Computation*, vol. 21, no. 9, pp. 2634-2647, 2009.

[115] J. Laczkó and Z. Keresztényi, “Variances of hand positions and arm configurations during arm movements under external load and without external load.,” *Motor Control*, no. 11, p. 127, 2007.

[116] M. D. Klein Breteler, R. G. J. Meulenbroek, and S. C. A. M. Gielen, “An evaluation of the minimum-jerk and minimum torque-change principles at the path, trajectory, and movement-cost levels.,” *Motor Control*, vol. 6, no. 1, pp. 69-83, 2002.

DOI:10.15774/PPKE.ITK.2012.004

[117] A. Piazzi and A. Visioli, “Global minimum-jerk trajectory planning of robot manipulators.,” *IEEE Transactions on Industrial Electronics*, vol. 47, no. 1, pp. 140-149, 2000.

[118] M. Suzuki, K. Matsunami, Y. Yamazaki, and N. Mizuno, “Application of the minimum jerk model to formation of the trajectory of the centre of mass during multijoint limb movements.,” *Folia primatologica international journal of primatology*, vol. 66, no. 1-4, pp. 240-252, 1996.

[119] E. Nakano, H. Imamizu, Y. Uno, and M. Kawato, “Quantitative examinations of internal representations for arm trajectory planning: minimum commanded torque change model.,” *Journal of Neurophysiology*, vol. 81, no. 5, pp. 2140-2155, 1999.

[120] T. Matsui, M. Honda, and N. Nakazawa, “A new optimal control model for reproducing human arm’s two-point reaching movements: A modified minimum torque change model,” *2006 IEEE International Conference on Robotics and Biomimetics*, pp. 1541-1546, 2006.

[121] T. Matsui, “A new optimal control model for reproducing two-point reaching movements of human three-joint arm with wrist joint’s freezing mechanism.,” *2008 IEEE International Conference on Robotics and Biomimetics*, pp. 383-388, 2009.

[122] M. Ackermann and A. J. Van Den Bogert, “Optimality principles for model-based prediction of human gait.,” *Journal of Biomechanics*, vol. 43, no. 6, pp. 1055-1060, 2010.

[123] M. F. Levin, “Interjoint coordination during pointing movements is disrupted in spastic hemiparesis.,” *Brain: A journal of neurology*, vol. 119, no. 1, pp. 281-293, 1996.

[124] V. Krishnamoorthy, M. L. Latash, J. P. Scholz, and V. M. Zatsiorsky, “Muscle synergies during shifts of the center of pressure by standing persons.,” *Experimental Brain Research*, vol. 152, no. 3, pp. 281-292, 2003.

[125] V. Krishnamoorthy, S. Goodman, V. Zatsiorsky, and M. L. Latash, “Muscle synergies during shifts of the center of pressure by standing persons: identification of muscle modes.,” *Biological Cybernetics*, vol. 89, no. 2, pp. 152-161, 2003.

[126] S. Freitas, J. P. Scholz, and M. L. Latash, “Analyses of joint variance related to voluntary whole-body movements performed in standing.,” *Journal of Neuroscience Methods*, vol. 188, no. 1, pp. 89-96, 2010.

[127] G. Gera, S. Freitas, M. Latash, K. Monahan, G. Schöner, and J. Scholz, “Motor abundance contributes to resolving multiple kinematic task constraints.,” *Motor Control*, vol. 14, no. 1, pp. 83-115, 2010.

[128] D. A. Gabriel, “Changes in kinematic and EMG variability while practicing a maximal performance task.,” *Journal of Electromyography and Kinesiology*, vol. 12, no. 5, pp. 407-412, 2002.

[129] J. E. Kasprisin and M. D. Grabiner, “EMG variability during maximum voluntary isometric and anisometric contractions is reduced using spatial averaging.,” *Journal of Electromyography and Kinesiology*, vol. 8, no. 1, pp. 45-50, 1998.

[130] M. M. Bamman, S. G. Ingram, J. F. Caruso, and M. C. Greenisen, “Evaluation of surface electromyography during maximal voluntary contraction.,” *Journal of Strength and Conditioning Research*, vol. 11, no. 2, pp. 68-72, 1997.

[131] J. P. Scholz and M. L. Latash, “A study of a bimanual synergy associated with holding an object.,” *Human Movement Science*, vol. 17, pp. 753-779, 1998.

[132] S. E. Mathiassen, T. Möller, and M. Forsman, “Variability in mechanical exposure within and between individuals performing a highly constrained industrial work task.,” *Ergonomics*, vol. 46, no. 8, pp. 800-824, 2003.

[133] J. Laczkó, J. Quintern, and S. Krafczyk, “Modeling of joint-rotations during line tracking arm movements” *In: Neuroprosthetics. From basic research to clinical application,* Eds. A. Pedotti, M. Ferrarin, J. Quintern, Publ. Springer-Verlag, pp. 305-314, 1996.

[134] J. Laczkó, J. Quintern, I. Kovacs, and J. Tihanyi, “Simulation of joint-rotations during human arm-movement control.,” in *Proc. of the 9th. International Conference on Mechanics in Medicine and Biology*, 1996, pp. 383-386.